Winter 2014

DJ-1 AND ATP13A2: TWO PROTEINS INVOLVED IN PARKINSON'S DISEASE

Josephat M Asiago
Purdue University

Graduate School Form 30
(Revised 08/14)

PURDUE UNIVERSITY
GRADUATE SCHOOL
Thesis/Dissertation Acceptance

This is to certify that the thesis/dissertation prepared

By Josephat M. Asiago

Entitled
DJ-1 AND ATP13A2: TWO PROTEINS INVOLVED IN PARKINSON'S DISEASE

For the degree of Doctor of Philosophy

Is approved by the final examining committee:

Dr. Jean-Christophe Rochet

Dr. Laurie L. Parker

Dr. Kevin Otto

Dr. W. Andy Tao

To the best of my knowledge and as understood by the student in the Thesis/Dissertation Agreement, Publication Delay, and Certification/Disclaimer (Graduate School Form 32), this thesis/dissertation adheres to the provisions of Purdue University's "Policy on Integrity in Research" and the use of copyrighted material.

Dr. Jean-Christophe Rochet

Approved by Major Professor(s): _____

_____

Approved by: Dr. Jean-Christophe Rochet 12/05/2014

Head of the Department Graduate Program Date

DJ-1 AND ATP13A2: TWO PROTEINS INVOLVED IN PARKINSON'S DISEASE

A Dissertation

Submitted to the Faculty

of

Purdue University

by

Josephat M. Asiago

In Partial Fulfillment of the

Requirements for the Degree

of

Doctor of Philosophy

December 2014

Purdue University

West Lafayette, Indiana

ACKNOWLEDGMENTS

First, I would like to thank God for good health and strength. “I can do all things through Christ who strengthens me.” Phillipians 4:13. (New King James Version (NJKV).

I would like to thank my family members, my Father, Zachariah Asiago Ogoti, my mother Josephine Nyanchama Asiago, my sisters Irene Asiago, Alice Asiago, my brothers, Alex Asiago, Geoffrey Asiago and Vincent Asiago for their continued love, support and encouragement.

I would like to thank my wife, Edith Nyaboke Nyakundi for her love and patience.

I would like to thank my boss and mentor, Dr. Rochet; through his guidance and counsel, I am a better scientist today than I was yesterday.

I would like to thank my committee members for all the advice throughout my graduate school.

Lastly, I would like to thank my dearest friends, Vartika Mishra, Mitali Tambe, Daniel Ysselstein, Aurélie De Rus Jacquet , Paola Montenegro and Rosemary Onjiko for always reminding me, “you can do it!”

TABLE OF CONTENTS

Page

Page

Page

Page

Page

Page

Page

ABBREVIATIONS

2ME	2-mercaptoethanol
6-OHDA	6-Hydroxydopamine
ADP	adenosine diphosphate
ALP	autophagy lysosomal pathway
AO	acridine orange
AR	androgen receptor
ARE	antioxidant response element
ASK	apoptosis signal-regulating kinase
aSyn	Alpha-synuclein
ATP	adenosine triphosphate
AUC	analytical ultra-centrifugation
COMT	catechol-o-methyl-transferase
CTP	cytosine triphosphate
DA	dopamine
DBS	deep brain stimulation
DNA	deoxyribonucleic acid
ER	endoplasmic reticulum
ERK	extracellular signal regulated protein kinase
GBA	glucocerebrosidase

GFP	green fluorescence protein
GST	glutathione s-transferase
GTP	guanosine triphosphate
H_2O_2	hydrogen peroxide
HCL	hydrochloric acid
KD	knockdown
LB	luria-Bertani broth
LBs	lewy bodies
LC3	microtubule associated protein light chain 3
LMP	lysosomal membrane permeability
METH	methamphetamine
mRNA	messenger ribonucleic acid
Mt	mitochondria
MW	molecular weight
NF-κB	nuclear factor kappa-light-chain-enhancer of activated B cells
NMS	non motor symptoms
PCR	polymerase chain reaction
PD	Parkinson’s disease
PDB	protein data bank
Psi	pound-force per square inch
PVDF	polyvinylidene fluoride
RFP	red fluorescence protein
ROS	reactive oxygen species

SDS PAGE	sodium dodecyl sulfate polyacrylamide gel electrophoresis
SEC-MALS	size-exclusion chromatography with multi-angle light scattering
SNARE	soluble NSF (N-Ethylmaleimide-sensitive factor) attachment protein receptor
SNc	*substantia nigra pars compacta*
SOD	superoxide dismutase
SRBP-2	sterol regulatory binding protein 2
TEM	transmission electron microscope
TRIS	tris (hydroxymethyl) aminomethane
TTP	thymidine triphosphate
UPS	ubiquitin-proteasome system

ABSTRACT

Asiago, Josephat M. Ph.D., Purdue University, December, 2014. DJ-1 and ATP13A2: Two Proteins Involved In Parkinson's Disease. Major Professor: Jean-Christophe Rochet.

Parkinson's disease (PD) is the second most common neurodegenerative disorder after Alzheimer's disease, affecting approximately 0.3% of the total U.S. population, and its prevalence increases with age. Two neuropathological hallmarks of PD are the loss of dopaminergic neurons in the *substantia nigra pars compacta*, a region in the midbrain involved in initiating and sustaining movement, and the presence of cytosolic inclusions called Lewy bodies (LBs) in various brain regions. LBs are enriched with fibrillar forms of the presynaptic protein α-synuclein (aSyn). Two autosomal recessive genes implicated in familial PD are PARK9, encoding the P-type ATPase ATP13A2, a lysosomal ATPase; and PARK7, encoding DJ-1, a protein with proposed antioxidant and chaperone activities. Understanding the biochemical mechanisms underlying the neuroprotective functions of DJ-1 and mechanistic details accounting for functional overlap between ATP13A2 and DJ-1 can provide insight into the cellular pathways relevant to PD pathogenesis.

DJ-1 belongs to the DJ-1/ThiJ/PfpI superfamily, consisting of proteins that typically function as proteases and chaperones. Most members of this

superfamily have shared characteristics including a conserved cysteine residue, a catalytic triad, and the ability to form oligomers. Whereas PH1704, a bacterial protease and a member of the DJ-1/ThiJ/PfpI superfamily, adopts a hexameric structure that is necessary for the formation of a catalytic triad, DJ-1 exists as a homodimer and apparently has a catalytic diad rather than a catalytic triad. A recent study has shown that DJ-1Δ15, a truncated form of DJ-1 (15 amino acids cleaved at the C terminus, resulting in the removal of helix H8, has a much greater protease activity compared to full length DJ-1. The structure of DJ-1Δ15 is similar to that of PH1704, which lacks a C-terminal helix corresponding to helix H8 of full-length DJ-1. We chose to focus on DJ-1Δ15 because it was not known whether this variant has the ability to form a hexamer, or whether such a hexameric structure is responsible for the observed protease activity (similar to PH1704). We analyzed DJ-1Δ15 via computer modelling using PyMOL to determine whether it can form a hexamer with favorable intersubunit interactions. In addition, we prepared recombinant DJ-1Δ15 and analyzed the protein via analytical ultra-centrifugation (AUC), native PAGE electrophoresis, and size exclusion chromatography coupled with multi-angle light scattering. Our PyMOL results showed that (i) DJ-1Δ15 can from a hexamer which may be stabilized by two inter-subunit interfaces, referred to as patch 1' and patch 2 and, (ii) hexamer formation may lead to the formation of a catalytic triad involving residues C106 and H126 from one subunit and E84 from another subunit. The full length DJ-1 was unable to form the hexamer because helix H8 caused steric hindrances. Data from AUC and size exclusion analysis of DJ-1Δ15 showed peaks

representing species with different assembly states. There was evidence of a species with a molecular weight greater than that of the DJ-1Δ15 dimer. In addition the native gel data of DJ-1Δ15 showed a higher molecular weight species. Taken together, our results suggest that the DJ-1Δ15 protease activity may be due to the formation of an oligomer that is larger than the homodimer – potentially a hexamer.

Analysis of the DJ-1 crystal structure revealed a previously undescribed potential ATP binding site that included two arginine residues, Arg 28 and Arg 48, near the oxidizable Cys106 residue. We therefore focused on elucidating whether DJ-1 binds and hydrolyzes ATP. We found that our preparations of recombinant, human WT DJ-1 had ATPase activity that was lost upon filtration or ultracentrifugation. Analysis of our protein samples via sucrose gradient sedimentation coupled with immunoblotting revealed the presence of high molecular weight (high-MW) species immunoreactive with a DJ-1 antibody in our DJ-1 preparations. Additional studies revealed that the high-MW protein fraction of our DJ-1 preparations had ATPase activity and consisted of ring-like structures that could be visualized by electron microscopy. Furthermore, a DJ-1-positive high-MW complex isolated from these preparations by sucrose gradient sedimentation was shown via mass spectrometry analysis to contain F_1 ATPase subunits, which are also known to assemble into ring-like structures, suggesting that the ATPase activity in our high molecular weight fraction might be associated with assembled F_1 ATPase. Consistent with this idea, the ATPase activity in our high molecular weight protein fraction was abolished in the presence of sodium

azide or piceatannol, classical F_1 ATPase inhibitors. Furthermore, we obtained evidence that dimeric DJ-1 may interact with purified *E-coli* F_1 ATP synthase, and this interaction was apparently dependent on the presence of a reduced cysteine residue at position 106. These results imply that (i) F_1 ATP synthase (in mitochondria) may be a target of the DJ-1 chaperone activity, and (ii) this interaction may be modulated by DJ-1 oxidation.

Loss-of-function mutations in the ATP13A2 or DJ-1 gene have been shown to disrupt lysosomal autophagy and interfere with mitochondrial function and quality control. We hypothesized that dysfunction of either protein elicits neurotoxicity by triggering defects in autophagy coupled with an accumulation of dysfunctional mitochondria. To address this hypothesis, we investigated the functional interplay between ATP13A2 and DJ-1 in terms of their ability to protect neuronal cells against a PD related stress, methamphetamine (METH), an abused drug that disrupts autophagy in N27 dopaminergic neuronal cells. Our results showed that knocking down ATP13A2 or DJ-1 results in a buildup of LC3 II, an autophagic marker, whereas ATP13A2 over-expression reduces the accumulation of autophagic vesicles, termed autophagosomes. In addition, ATP13A2 or DJ-1 KD N27 cells showed a decreased rate of O_2 consumption. Strikingly, the level of ATP13A2 mRNA was increased in DJ-1 knockdown in primary midbrain cultures; in contrast the level of DJ-1 mRNA was decreased in ATP13A2 knockdown in the same cultures. These results suggest DJ-1 and ATP13A2 interact functionally in regulating lysosomal degradation and mitochondrial function.

Overall, these studies have yielded insights into biochemical mechanisms of DJ-1-mediated neuroprotection and of the functional interplay between DJ-1 and ATP13A2. Not only do these findings advance our understanding of neuroprotective mechanisms relevant to PD, but they also suggest new strategies to treat this devastating syndrome.

CHAPTER 1: INTRODUCTION

1.1. Parkinson's disease: an irreversible, progressive, neurodegenerative disease

Parkinson's disease (PD) is an irreversible neurodegenerative disease that was discovered in 1817 by a scientist named Dr. James Parkinson. In his "essay on shaking palsy", Dr. Parkinson described the disease as characterized by involuntary tremulous movement and decreased muscular power[1]. Two neuropathological hallmark of PD is the loss of dopaminergic neurons in *substantia nigra pars compacta*, a region in the brain involved in initiating and sustaining movement and, the presence of cytosolic inclusions called Lewy bodies (LBs) in various brain regions [2, 3]. PD is the second most common neurodegenerative disease affecting approximately 0.3% of the total U.S. population and its prevalence increases with age, affecting up to 2% of the population over 65 years [4] and 5% of the population over 85 years old [5]. The U.S. government spent over $14 billion on persons with PD in 2010 [6]. It is estimated that the number of people suffering from PD is likely to double by 2040 [6], and, concurrently, the cost of diagnosis and treatment will continue to rise. With the increase in lifespan due to improved health care, there is a need to understand the disease etiology at the molecular level and develop alternative therapies. The research described herein will provide insight into PD

pathogenesis by analyzing two PD related recessive gene products, DJ-1 and ATP13A2.

1.2. Symptoms, pathology, diagnosis and treatment of PD

1.2.1. Symptoms and pathology

Dr. James Parkinson designated the clinical symptoms of PD as difficulty initiating movements, resting tremor and rigidity [1]. Besides the typical parkinsonian motor dysfunction, PD patients present non-motor symptoms (NMS) including neuropsychiatric, sensory, autonomic, and sleep disorders [7]. These symptoms can lead to disability and a poor quality of life [8, 9]. Two neuropathological hallmark of PD are the loss of dopaminergic neurons in *substantia nigra pars compacta* (SNc), a region in the brain involved in initiating and sustaining movement and, the presence of cytosolic inclusions called Lewy bodies (LBs) [2, 3]. LB have been observed in different regions of the brain, including locus coeruleus, dorsal vagal, nucleus and anterior cingulate gyrus [10]. LBs are granular or globular inclusions present in the soma of affected neurons. Lewy neurites are diseased neurons containing granular material majorly aSyn filaments. PD progression is classified into 6 stages based on the regions of the brain affected by Lewy neurites and LBs [11]. Stage 1-2, medulla and pons, stage 3, *substantia nigra (*SN), stages 4-6, hippocampus and neocortex [11]. LBs are mainly composed of fibrillar forms of the presynaptic protein, aSyn [12-14].

1.2.2. Diagnosis and treatment of PD

The presence of LBs at autopsy is considered a confirmatory of a PD diagnosis [15]. Other diagnoses are based on the typical loss of motor functions, NMS, and

response to levodopa [16]. Levodopa (L-DOPA) is a drug that slows down PD pathogenesis by controlling PD motor related symptoms, particularly bradykinesia [17]. L-DOPA penetrates the central nervous system via the blood brain barrier where it is converted to dopamine via decarboxylation by aromatic amino acid decarboxylase (AADC) [18]

Other alternatives in the management of PD include catechol-o-methyl-transferase (COMT) inhibitors, dopamine receptor agonists and non-dopaminergic therapy (for example adenosine A2A antagonists) which may be used in conjunction with levodopa [19]. The above mentioned PD management therapies generally lose their therapeutic efficacy over time. Some of the reported side effects include recurrence of motor symptoms and dyskinesia [20]. In addition, although surgical intervention of patients with motor dysfunction, (e.g. via deep brain stimulation (DBS)) can have many benefits, it is costly and can cause complications such as infections [21]. None of the aforementioned therapies halts the underlying neurodegeneration, therefore there is a need to develop alternative strategies. Understanding cellular mechanisms that slow neurodegeneration in the brains of PD patients may suggest new therapeutic strategies.

1.3. Idiopathic PD

PD can be classified into two categories: (i) idiopathic PD, also known as sporadic PD; and (ii) familial PD. Idiopathic PD accounts for 90-95% of all PD cases and is caused by non-genetic factors that include aging (the greatest risk factor), exposure to herbicides or pesticides or organic solvents, industrialization,

living in a rural environment, and drinking well water [22-24]. A number of toxic mechanisms have been proposed to play a role in PD pathogenesis, including mitochondrial dysfunction, oxidative stress, and accumulation of misfolded protein and damaged organelles due to dysregulation of proteasomal and lysosomal degradation pathways [25-28]. The focus of this thesis is on the role of mitochondrial dysfunction and dysregulation of lysosomal degradation (autophagy).

1.3.1. Mitochondrial dysfunction and oxidative stress

Analysis of the SNc and frontal cortex regions of post-mortem PD brains shows a decreased activity of complex I, an enzyme of the mitochondria electron transport chain [29-31]. In addition complex I subunits in PD brains show evidence of increased oxidative damage as a result of accumulation of protein carbonyls [32]. Complex I inhibition decreases mitochondrial adenosine triphosphate (ATP) and may cause a 'leakage' of electrons from the electron transport chain, leading to formation of reactive oxygen species (ROS), that damage mitochondrial DNA (mt DNA) and cause further mitochondrial impairment [33-35]. Oxidative stress occurs under conditions that lead to an imbalance between ROS production and antioxidant activity [22]. Dopaminergic neurons contain high level of ROS due to the presence of dopamine. Similar to other catecholamines, dopamine undergoes auto-oxidation to form the *o*-quinone form (Fig 1.1), a reaction that involves the generation of superoxide radicals [36]. In addition, dopamine readily is metabolized by tyrosinase and monoamine oxidase, two ROS-generating enzymes [18, 22]. Free radicals formed as a result of dopamine auto-oxidation or

metabolism can damage mitochondrial electron transport subunits, thereby leading to further oxidative stress associated with mitochondrial dysfunction as part of a vicious cycle [37]. Because dopaminergic neurons have higher basal levels of oxidative stress than other types of neurons, they are more susceptible to pathogenic mechanism that further up-regulate ROS, including mitochondrial dysfunction. ROS are thought to elicit toxicity through oxidative modification of macromolecules and organelles [38-40]. As one example, ROS cause lysosomal destabilization, by disrupting membrane integrity, a process referred to as lysosomal membrane permeabilization (LMP).

1.3.2. Lysosomal involvement in PD

Lysosomes are involved in the clearance of long-lived proteins, including aggregated forms of aSyn, and the removal of old or dysfunctional organelles like mitochondria [41, 42]. Previous studies have shown impaired lysosomal clearance in dopaminergic neurons in both sporadic and genetic PD patients, suggesting that lysosomal impairment may contribute to pathogenesis of PD [43] [44]. Mutations in lysosomal proteins such as glucocerebrosidase (GBA) and ATP13A2, a lysosomal ATPase are associated with PD [45]. These findings suggest that restoring lysosomal function could be a reasonable therapy for PD.

1.3.3. Autophagy in PD

Autophagy has been referred to classically as a process induced in cells to enable the degradation of intracellular components under starvation conditions [46, 47]. There are three types of mammalian autophagy: (i) microautophagy, a process by which the lysosomal membrane surrounds and engulfs cytoplasmic

components for degradation; (ii) chaperone mediated autophagy (CMA), involving the targeting of proteins with a specific sequence motif for uptake into lysosomes with the assistance of the molecular chaperone, Hsc70 [48]; and (iii) macroautophagy (referred to herein as 'autophagy'), a multi-step process that involves the sequestration of organelles and cytoplasmic components via the formation of a double-membrane-bound organelle called an autophagosome [48, 49]. Autophagosomes fuse with lysosomes to form autolysosomes, wherein the intra-lumenal components are degraded by lysosomal hydrolases [50] (Fig. 1.2). In mammalian cells, the microtubule associated protein light chain 3 (LC3) is modified via a ubiquitylation-like system [51, 52] to form LC3-I and LC3-II. LC3-I is a soluble form generated upon carboxyl terminal cleavage of pro-LC3 [53, 54]. LC3-I is modified to a membrane-bound form, LC3-II, by conjugation to phosphatidylethanolamine [54, 55]. Importantly, LC3-II localizes to the autophagosome and autolysosomes and is thus a characteristic marker of these vesicular structures [56] (Fig. 1.2). Defects in autophagy are associated with various diseases including PD [47]. Aggregated proteins and dysfunctional organelles that cannot be degraded via the ubiquitin-proteasome pathway are cleared from the cell via lysosomal autophagy [57]. Accordingly, dysregulation of autophagy leads to the accumulation of protein aggregates and dysfunctional organelles in PD [58].

1.4. Familial PD

To date, there are 28 distinct chromosomal regions that have been identified as being related to familial PD or parkinsonism [59]. Familial PD cases account for

5 % of total PD cases. Eighteen specific chromosomal loci, (referred to as PARK loci) have been identified. These loci are classified chronologically (PARK 1-18) (Table 1.1) depending on when they were identified [59].

1.4.1. Alpha-synuclein (PARK1, 4)

1.4.1.1. Genetics

As mentioned above, aSyn is a major component of Lewy pathology in patients with sporadic form of PD [14]. Missense mutations in the aSyn gene have been linked to familial PD. The following familial substitutions have been identified; alanine to threonine at residue 53 (A53T) [60], alanine to proline at residue 30 (A30P) [61], glutamate to lysine at residue 46 (E46K) [62], histidine to glutamine at residue 50 (H50Q) [63], glycine to aspartate at residue 51 (G51D) [64] (Fig 1.3). Duplication and triplication mutations increase the copy number of the wild type aSyn gene [65, 66]. Although some substitution mutants e.g. A53T form fibrils more rapidly than wild type aSyn, overall the neurotoxic effects of familial PD mutants appears to result from the formation of protofibrils rather than accelerated fibrillization [67]. Some of the substitution mutants appear to favor oligomerization though not necessarily fibril formation [63, 64] Duplication and triplication mutations favor aggregation of the protein via mass action [68]. In addition there is an increased level of cytoplasmic aSyn in aging human brain [69].

1.4.1.2. aSyn function

aSyn is a 140 amino acid protein that localizes to presynaptic terminals [70]. The aSyn sequence is subdivided into three domains: (i) an N-terminal domain (residues 1-67), consisting of seven imperfect repeats, six of which contain the conserved hexamer sequence KTK(E/Q)GV (Fig 1.3), this conserved sequence plays a critical role in the association of aSyn with phospholipid membranes [71, 72]; (ii) the non-amyloid-β-component of Alzheimer's disease (NAC) domain (residues 61-95), consisting primarily of hydrophobic residues that initiate aggregation [73]; and (iii) the carboxy-terminal (C-terminal) region (residues 96-140), enriched with negatively charged residues (aspartate, glutamate) and proline residues (Fig 1.3). Truncation of C-terminal accelerates rates of aggregation [74-76], and truncated forms of aSyn are present in LBs [77].

In addition, aSyn may be involved in regulating synaptic vesicle release [78-80], and the protein modulates synaptic transmission [81-83], dopamine (DA) uptake [84, 85], and assembly of the SNARE complex [86].

1.4.1.3 aSyn degradation in PD

Abnormal aSyn expression causes defects in cellular protein degradation pathways [42]. The ubiquitin-proteasome system (UPS) [87-90] and lysosomal autophagy [91-94] are involved in the degradation of aSyn. Phosphorylated aSyn (pS129) has been shown to be degraded via the proteasome [95, 96]. In addition, *in vivo* studies have shown that at high expression levels aSyn is cleared via macroautophagy in transgenic mouse brains, whereas at lower expression, (i.e.

nontransgenic mouse) aSyn is eliminated via proteasomal degradation [97]. In contrast, other studies have reported that overexpression of aSyn disrupts macroautophagy [98]. Accordingly, disruption of the UPS and lysosomal autophagy is predicted to cause accumulation of aSyn, leading to the formation of toxic aSyn oligomeric species involved in neurodegeneration. Targeting degradation pathways may be a reasonable therapeutic strategy for PD.

1.4.2. DJ-1 (PARK7)

1.4.2.1. Genetics

Deletions and point mutations resulting in a loss of functional DJ-1 protein are involved in autosomal recessive PD [99]. A six exon deletion has been reported in a Dutch family, and a missense mutation resulting in the substitution of proline for leucine at residue 166 (L166P) has been found in an Italian family [99]. Additional homozygous recessive, substitution mutations include M26I [100], E64D [101], E163K [102], A104T [103]. Other studies revealed a mutation in the DJ-1 promoter [102]. In addition, two polymorphisms encoding the substitutions R98Q [103] D149A [100], have been identified in the DJ-1 gene.

1.4.2.2. Protein structure

DJ-1 is a protein composed of 189 amino acids that is encoded by the PARK7 gene. Data from gel filtration, sedimentation and x-ray crystallographic analysis indicate that purified recombinant DJ-1 exists as a homodimer [104-108]. Monomeric DJ-1 has eight alpha helices and eleven beta strands [107] (Fig 1.4). DJ-1 belongs to the ThiJ/PfpI family, consisting of proteins that typically function

as proteases and chaperones [109], and its amino-acid sequence is conserved among many species [110, 111]. Shared features of proteins in this superfamily include a conserved cysteine residue in a “nucleophile elbow” strand-loop-helix motif [106], a catalytic triad (cysteine, histidine and glutamate/aspartic acid) in some (but not all) members, and the ability to form oligomers [106]. The oligomeric state of these proteins varies widely ranging from dimers to hexamers [106].

The structure of the monomeric subunit of DJ-1 is highly homologous to that of the monomeric subunit of PH 1704, an intracellular cysteine protease from *Pyrococcus horikishii*, forms a hexamer stabilized by two types of inter-subunit interfaces, referred to as patch 1’ and patch 2 [105, 112, 113]. Patch 1’ is analogous to the interface between the two monomeric subunits of homodimeric DJ-1 (referred to as patch 1), although the two interfaces are rotated ~90°with respect to each other. The structural features that lead to the presence of a patch 1 interface in the DJ-1 dimer but a patch 1’ interface in the PH1704 hexamer are poorly understood.

1.4.2.3. Functions of DJ-1

Since its initial discovery as an oncogene [114], DJ-1 has been reported to have many other functions (reviewed in [115, 116]). Here we review functions of DJ-1 related to its ability to act as an antioxidant, molecular chaperone, transcriptional regulator, modulator of mitochondrial function, modulator of autophagy and a protease.

1.4.2.4. Antioxidant function of DJ-1

Rotenone and 6-hydroxydopamine (6-OHDA), two known PD-related oxidative stressors, have been shown to up-regulate endogenous DJ-1 mRNA and protein levels and to induce translocation from the cytoplasm to mitochondria [117]. Oxidation of a cysteine residue at position 106 (C106) to the sulfinic acid (SO_2H) facilitates translocation of DJ-1 from the cytoplasm to mitochondria [118-120]. Oxidized DJ-1 enhances cell proliferation by binding and inhibiting apoptosis signal-regulating kinase (ASK1) [121, 122]. Over expression of wild type DJ-1, but not familial mutant forms of the protein, protects neuronal cells from reactive oxygen species (ROS) [123], whereas down-regulation of DJ-1 sensitizes cells to oxidative stress [124]. DJ-1 protects against toxicity elicited by hydrogen peroxide (H_2O_2), 6-OHDA and rotenone by up-regulating the antioxidant molecule glutathione, whereas it induces an increase in levels of the heat shock protein 70 (HSP 70) in neuronal cultures expressing mutant aSyn [125, 126]. These results suggest that DJ-1 protects against various PD-related insults, and the mechanism of DJ-1 neuroprotection depends on the type of stress.

1.4.2.5. A role for DJ-1 as at transcription regulator

Under conditions of oxidative stress, DJ-1 has been found to regulate various genes at the transcriptional level [125, 127]. DJ-1 knockdown in the mouse NIH3T3 cell lines induce a decrease in the level of extracellular superoxide dismutase (SOD3), an enzyme that scavenges ROS [127]. DJ-1 regulates cholesterol synthesis by activating on the promoter region of the low-density

lipoprotein receptor (LDLR) gene [128]. In the cells exposed to oxidative stress, DJ-1 forms a complex with the sterol regulatory binding protein 2 (SREBP2), a transcription factor involved in cholesterol synthesis, and binds to the sterol regulating element (SRE) to stimulate the LDLR promoter activity [128]. DJ-1 positively regulates of the androgen receptor (AR) transcription factor through binding to the same promoter region as PIAS-alpha, a repressor that inhibits androgen receptor transcription activity [129, 130]. Studies in yeast have shown that DJ-1 can directly bind to AR [131]. In addition, DJ-1 stabilizes nuclear factor (erythroid-derived 2)-like 2 (Nrf2), a redox-sensitive transcription factor that regulates the expression of antioxidant and detoxifying genes in response to oxidative stress via the antioxidant response element (ARE) [132]. Although DJ-1 averts the formation of a complex between Nrf2 and Kelch-like erythroid cell-derived protein-1 (Keap1), a negative regulator of Nrf2 [133], there is currently no evidence that DJ-1 binds directly to Nrf2 or Keap1, and thus the mechanism by which DJ-1 stabilizes Nrf2 has yet to be elucidated [134]. In contrast, other studies have reported that Nrf2-ARE is activated in DJ-1 knock out (KO) mice [135]. Two more transcription factors regulated by DJ-1 are p53 and nuclear factor-κβ (NF-κB). p53 is involved in many cellular functions including apoptosis and the maintenance of mitochondrial homeostasis during oxidative stress [136]. DJ-1 has been reported to be both a positive regulator of p53 [136] and an inhibitor of p53 transcriptional activity under normal conditions [137] and conditions of oxidative stress [138]. Interactions between DJ-1 and Cezanne, an inhibitor of the transcriptional activity of NF-κB, allow for the activation of NF-κB.

NF-κB is involvement in many cellular roles including cell survival [139] and the regulation autophagy [140]. These studies suggest that DJ-1 is an upstream regulator of various transcription factors.

1.4.2.6. A role for DJ-1 as a redox-sensitive molecular chaperone

The structures of DJ-1 and HSP 31, an *Escherichia coli* chaperone that is a member of the DJ-1/ThiJ/PfpI superfamily, are conserved [108]. Analysis of the DJ-1 crystal structure revealed hydrophobic patches with the necessary chemical and geometric features to bind non-native protein substrates [108]. DJ-1 acts as a redox-dependent molecular chaperone that inhibits aSyn oligomerization and fibrillization [141, 142]. One group reported that mutation of cysteine 53 abrogates a low isoelectric point variant of the protein and abolishes the chaperone and protective function of DJ-1 [141]. In addition, two separate groups have reported that cysteine 106 oxidation is critical for DJ-1 to function as a chaperone against aSyn misfolding [142, 143]. Furthermore, DJ-1 has been reported to impede the aggregation of citrate synthase (CS) and luciferase [108].

1.4.2.7. Role of DJ-1 in regulating mitochondrial homeostasis

Mitochondrial dysfunction and oxidative damage are characteristic features of neurodegenerative diseases, including PD [144]. Mutations in genes directly linked to mitochondrial function, i.e. Parkin, PINK1, and DJ-1, have been identified in familial forms of PD [144]. Parkin is an E2-dependent E3 ubiquitin ligase [145, 146], plays a role in bioenergetics and mitochondrial quality control pathways [147]. Notably, Parkin is recruited to depolarized mitochondria to

enhance its elimination by autophagy and regulates the levels of PGC-1α, an important regulator of mitochondrial biogenesis [148, 149]. PINK1 (PTEN-induced putative kinase 1) regulates mitochondrial homeostasis via HtrA2, a mitochondrial protease [150], regulates mitochondrial morphology in mammalian cells [151], and plays a role in recruiting Parkin to mitochondria of immortalized cells [152-154]. Loss or mutation of DJ-1 induces an increase in ROS levels, a decrease in respiration rates and mitochondrial membrane potential (MMP), and a disruption of the critical balance between mitochondrial fusion and fission [144]. Oxidative stress in M17 human neuroblastoma cells results in DJ-1 re-localization to mitochondria, a phenomenon associated with protection against cytotoxicity [117, 118]. DJ-1 has also been shown to protect neurons from rotenone-induced oxidative stress and cell death [155-157]. Mitochondrial defects caused by deficiency or mutation of these three genes can be rescued by trio of the enzymes [158]. Mitochondrial fragmentation triggered by aSyn overexpression can be rescued by overexpression of wild-type Parkin, PINK1, or DJ-1, but not their functionally deficient mutants [159]. Recruitment of Parkin to depolarized mitochondria is influenced by oxidative stress of wild-type DJ-1 and not its mutant, C106A [160]. Elucidating the structure and function of this trio of enzymes will provide new avenues for developing therapies in PD.

1.4.2.8. Role of DJ-1 as a protease

As mentioned above, the *Pyrococcus horikoshii* 1704 gene product PH1704 exists as a hexamer [53]. This quaternary structure is thought to be essential for

the assembly of a catalytic triad at one of the subunit interfaces (referred to as patch 2 above). DJ-1 has an additional α helix (helix H8) at the C-terminus compared to PH1704. A recent study has shown that a truncated form of DJ-1 (15 amino acids cleaved at the C terminus, resulting in the removal of helix H8) has much greater protease activity compared to full length DJ-1 [46]. In this study DJ-1 was proposed to act as a cysteine protease with C106 and H126 forming a catalytic diad. The C-terminally truncated form of DJ-1 (DJ-1Δ15) was found to accumulate in dopaminergic cells exposed to oxidative stress, leading to conclude that full-length WT DJ-1 is in fact a zymogen that becomes activated via a redox-sensitive mechanism [46].

1.4.2.9. Impact of DJ-1 on lysosomal function

Cells lacking DJ-1 exhibit an increase in dysfunctional mitochondria and mitochondria-derived ROS [144]. In turn, ROS accumulation can induce permeabilization of lysosomal membranes thereby leading to impaired autophagic clearance and recycling of cytoplasmic constituents, termed basal autophagy [144, 161]. DJ-1 is thought to indirectly regulate autophagy through the extracellular signal regulated protein kinase 1/2 (ERK1/2), a kinase involved in stimulating lysosomal degradation and inducing autophagy [144, 162]. A disruption in the autophagic mitochondrial clearance (mitophagy) results in a build-up of defective mitochondria. Accordingly, a loss of DJ-1 activity leads to a vicious cycle of mitochondrial dysfunction and defects in lysosomal autophagy.

1.4.3. ATP13A2 (PARK 9)

1.4.3.1. Genetics

ATP13A2 is a P type ATPase encoded by the *PARK 9* gene. It is located at chromosome 1p36 between two other PARK loci, PARK6 and PARK7 [163, 164]. ATP13A2 is a 1,180-residue protein that contains ten transmembrane spanning helices [165] and is hypothesized to be localized to the lysosome. P-type ATPases are characterized by their ability to undergo large conformational changes while pumping ions across biological membranes via a process involving ATP hydrolysis. Mutations in the PARK9 gene result in autosomal recessive PD, suggesting a role for the lysosome in neurodegeneration [166, 167]. There are three genetic lesions that have been identified at this locus: (i) heterozygous mutations leading to truncation or in-frame deletion, identified in patients with Kufor-Rakeb syndrome, (KRS) [164]; (ii) a homozygous mutation encoding the substitution G504R [168]; and (iii) heterozygous mutations encoding T12M and G533R[168].

1.4.3.2. Expression and localization

ATP13A2 is mainly expressed in the dopaminergic neurons of the *substantia nigra* in the brain [164]. Other studies have reported that ATP13A2 expression peaks during neurogenesis [169]. Hypoxic conditions increase the transcription of ATP13A2, in HEK 293 and MN9D, dopaminergic cells [170]. Furthermore, high levels of manganese (II) and Zinc elevates expression of ATP13A2 [171, 172]. ATP13A2 is hypothesized to be localized to the late endosomes and lysosomes.

There are three ATP13A2 splice variants [173]. Variant 3 is retained in the endoplasmic reticulum (ER) where it is rapidly degraded [173]. ATP13A2 has recently been reported to localize to the outer membrane of amphisomes [174].

1.4.3.3. Protein structure

There are three alternatively spliced ATP13A2 isoforms expressed in humans [173]. Isoform 1 encodes a protein with 1180 amino acids consisting of 10 transmembrane domains. Isoform 2 encodes a protein of 1175 amino acids [173]. The loss of 5 residues in isoform 2 compared to isoform 1 is the results of an in-frame deletion near the N-terminus [173]. Isoform 3 encodes a protein with 1158 amino acids; compared to isoform 1, this variant has an in-frame deletion of 117 bases, generating a highly diverse C-terminus [173]. My study will focus on isoform-1 of ATP13A2.

1.4.3.4. Protein function

1.4.3.4.1. Role of ATP13A2 in autophagy and mitochondrial clearance

ATP13A2 is involved in the ATP-dependent transport of cations across lysosomal membranes [164]. The localization of ATP13A2 to lysosomal membranes may play a key role in modulating autophagy. A loss of ATP13A2 function has been shown to compromise lysosomal acidification, decrease proteolytic processing of lysosomal enzymes, and reduce the degradation of lysosomal substrates [175]. Because dysfunctional mitochondria are degraded via autophagy [144], impairment of autophagy resulting from ATP13A2 depletion is thought to trigger a buildup of defective mitochondria that produce increased ROS [144, 176].

Expression of ATP13A2 protects mammalian cells from oxidative stress and dysfunctional mitochondria [177]. In addition, loss of ATP13A2 function in human fibroblast decreases ATP production rates, mitochondrial DNA lesions, increased maximum respiration and mitochondrial fragmentation [178]. Previous studies have shown that the yeast homolog of human ATP13A2 suppresses aSyn toxicity in yeast and that it can also protect yeast cells from manganese toxicity [179, 180]. These studies suggest a relationship between genetics and the environment as the cause of neurodegeneration [179]. ATP13A2 regulates lysosomal functions and thus suggesting that it might control lysosomal aSyn degradation and buildup of aSyn aggregation [175, 181, 182]. ATP13A2 is involved in trafficking aSyn to the lysosome via macro-autophagy [175, 181]. Other studies have reported that ATP13A2 enhances removal of aSyn from the cell via exosomes [174].

1.4.3.4.2. Role of ATP13A2 in aSyn clearance

ATP13A2 has been reported to protect both yeast and mammalian cells against aSyn toxicity [179]. ATP13A2 may control aSyn degradation via lysosomal macroautophagy, thus preventing the accumulation of aSyn aggregates [175, 181, 182]. Overexpression of ATP13A2 protects cells from mitochondrial fragmentation induced by aSyn [176, 178, 183]. In addition, ATP13A2 enhances the elimination of aSyn out of the cell via an exosome-mediated pathway [174].

1.4.3.4.3. P-type ATPase Ion transporter

ATP13A2 shares sequence homology with P-type ATPases, a large family of ion pumps that utilizes ATP to transport ions across membranes in eukaryotes and prokaryotes [164] (Table 1.2). P-type ATPases are characterized by their ability to undergo large conformational changes while pumping ions across biological membranes via a process involving ATP hydrolysis. P-type ATPase is classified into five subfamilies; ATP13A2 is a type-5- P type ATPase, a sub family of P-type ATPase expressed only in eukaryotes. Although ATP13A2 is homologous to members of the P-type ATPase family, its ion specificity and biological function are unknown (Table 1.2). Dysfunction of ATP13A2 may lead to accumulation of misfolded or damaged polypeptides.

1.5 Objectives of this thesis

The above sections highlight advances in our understanding of DJ-1 and ATP13A2 neuroprotective activities. However, a number of key questions about the function of these two proteins remain unanswered: (i) what are biochemical mechanisms underlying the neuroprotective function of DJ-1? (ii) How does DJ-1 suppress mitochondrial dysfunction? (iii) Do DJ-1 and ATP13A2 interact on a functional level to modulate mitochondrial and lysosomal function?

This thesis addresses these questions by studying the formation of high-order oligomers by a C-terminally truncated form of DJ-1 in a cell-free system. We also explore a potential mechanism for DJ-1 protective effects against mitochondrial dysfunction through the characterization of an interaction between DJ-1 and E. coli F_1 ATPase, an enzyme that is highly conserved relative to F_1 ATPase in

mammalian mitochondria. Lastly, we examine the interplay between DJ-1 and ATP13A2 in modulating mitochondrial and lysosomal functions in neuronal cells exposed to PD-related insults. These studies will provide insight into molecular phenomena underlying PD pathogenesis, and they may suggest new neuroprotective strategies.

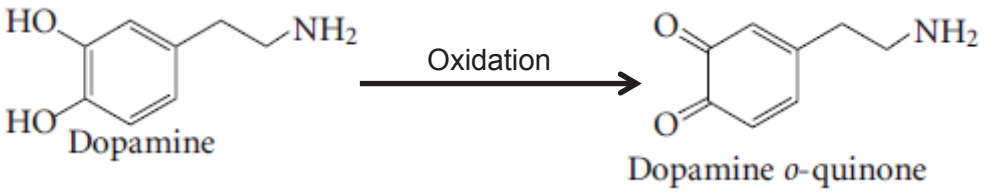

Figure 1.1 Dopamine undergoes auto-oxidation to form dopamine *o*-quinone

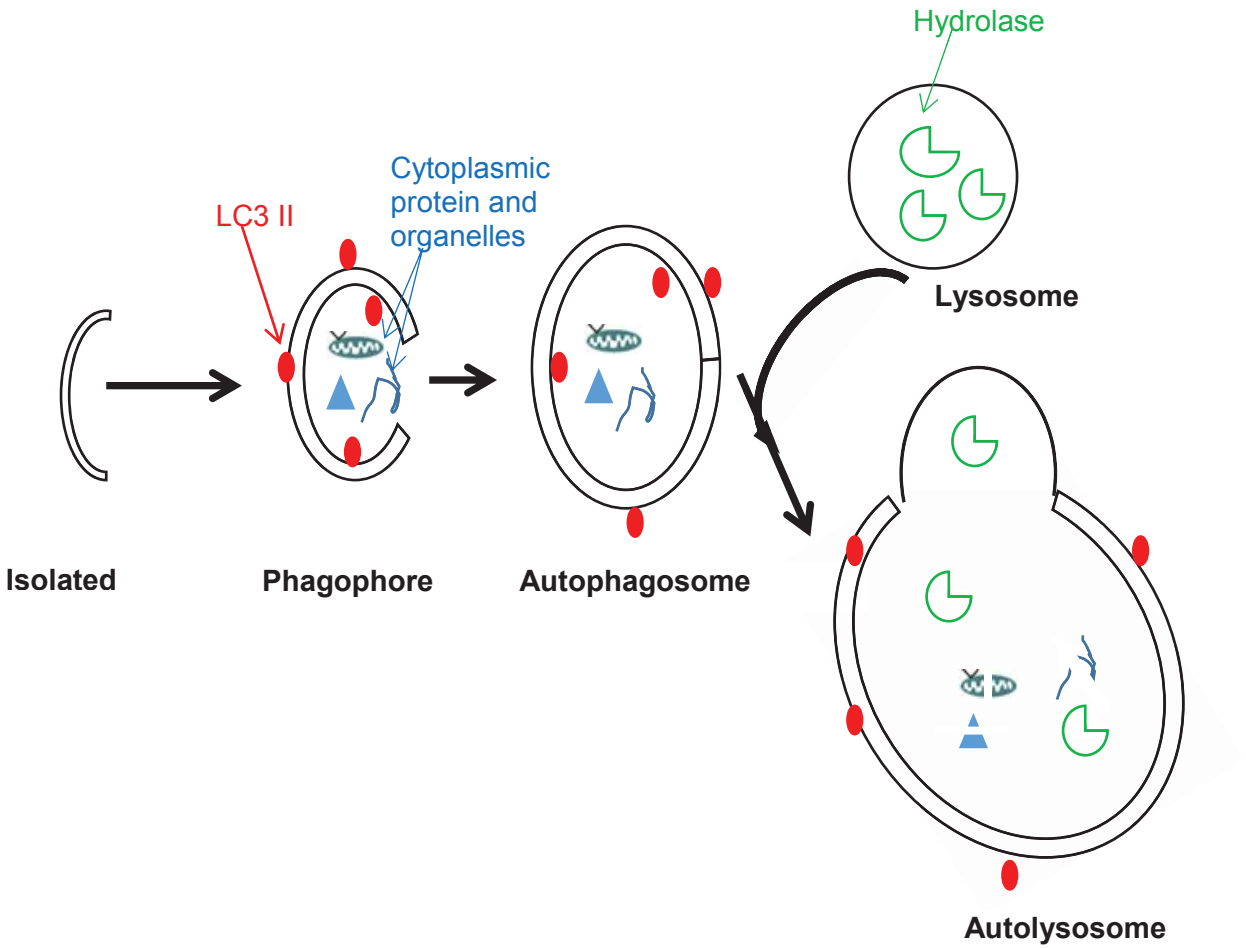

Figure 1.2 Macroautophagy
Macroautophagy starts by the formation of a cup-shaped isolated double membrane that engulfs cytoplasmic protein and organelles. LC3 II (an autophagic marker), is bound to the membrane of the phagophore and autophagosomes and is present in autolysosomes that result from autophagosome-lysosome fusion. The cytoplasmic proteins and organelles are degraded by lysosomal hydrolases.

A

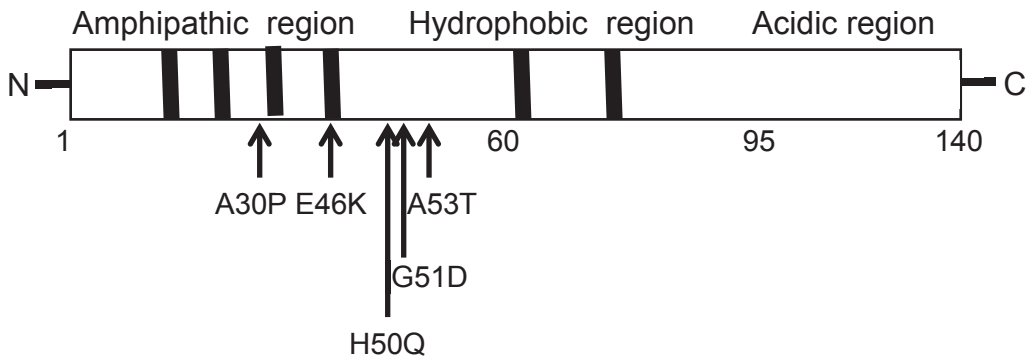

B

1 MDVFMKGLSKAKEGVVAAAEKTKQGVAEAAGKTKEGVLYVGSKTKEGVVH 50

51 GVATVAEKTKEQVTNVGGAVVTGVTAVAQKTVEGAGSIAAATGFVKKDQL 100

101 GKNEEGAPQEGILEDMPVDPDNEAYEMPSEEGYQDYEPEA 140

Figure 1.3 The domain and amino acid sequence of human WT aSyn.
(A) aSyn contains 140 amino acids composed of three regions: (i) the amphipathic N-terminal region spanning residues 1-67, (ii) the hydrophobic NAC region, spanning residues 61-95, and (iii) the acidic C-terminal region, spanning residues 96-140. Six of the imperfect repeats contain the conserved hexamer sequence KTK(E/Q)GV (boxed region). The arrows point to the familial mutants. **(B)** Amino acid sequence of human WT aSyn. Familial mutants are indicated by blue asterixes. Adapted from Dr. Strathearn's (former lab member) thesis.

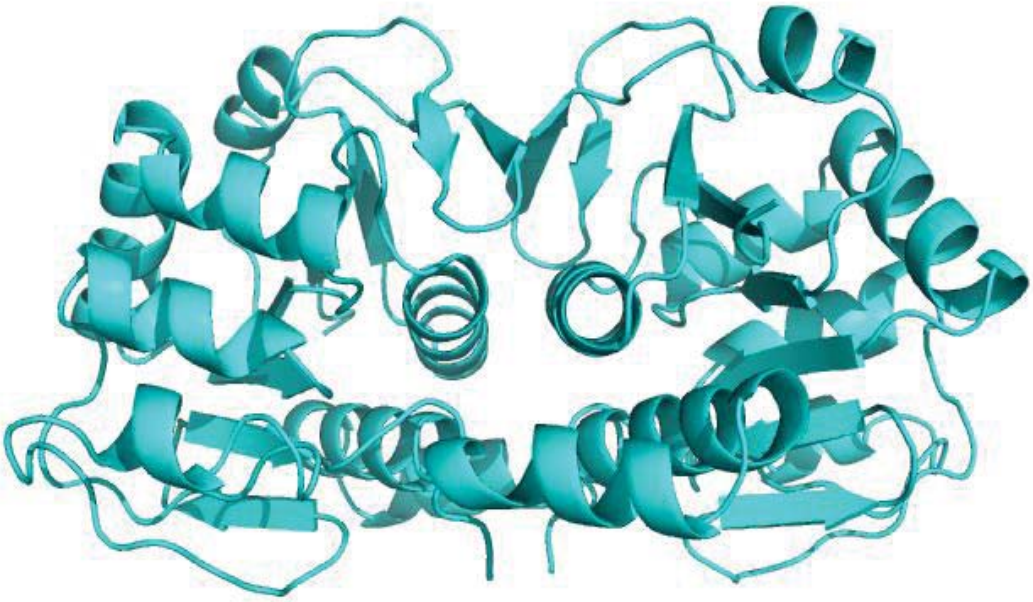

Figure 1.4 Structural model of the human DJ-1 homodimer. The structure was generated via PyMOL.

Table 1.1 Familial PD-related genes. AD, Autosomal dominant; AR, Autosomal recessive.

Symbol	Gene Locus	Gene	Inheritance
PARK1	4q21-22	*aSyn*	AD
PARK 2	6q25.2-q27	*Parkin*	AR
PARK 3	2p13	Unknown	AD
PARK 4	4q21-q23	*aSyn*/triplication	AD
PARK 5	4p23	*UHCL1*	AD
PARK 6	1p35-p36	*PINK1*	AR
PARK 7	1p36	*DJ-1*	AR
PARK 8	12q12	*LRRK2*	AD
PARK 9	1p36	*ATP13A2*	AR
PARK 10	1p32	Unknown	Risk factor
PARK 11	2q36-27	Unknown	AD
PARK 12	Xq21-225	Unknown	Risk factor
PARK 13	2p12	*HTRA2*	AD/Risk factor
PARK 14	22q13.1	*PLA2G6*	AR
PARK 15	22q12-q13	*FBX07*	AR
PARK 16	1p32	Unknown	Risk factor
PARK 17	16q11.2	*VPS35*	AD
PARK 18	3p27.1	*EIF4G1*	AD

Table 1.2 A list of the P-type ATPase's

P-type	Gene	Substrate	Disorder
P1B	ATP7A	Cu2+	Menkes disease (MD), Occipital horn Syndrome (OHS), Spinal muscular atrophy, distal, X-linked 3 (SMAX3)
P1B	ATP7B	CU2+	Wilson disease (WD), Possible genetic risk factor for Alzheimer's disease (AD)and parkinsonism
P2B	ATP2B3	Ca2+	Early onset X-linked spinocerebellarataxia1
P2C	ATP1A2	Na+/K+	Familial hemiplegic migraine type2(FHM2), Alternating hemiplegia of childhood1(AHC1)
P2C	ATP1A3	Na+/K+	Rapid-onset dystonia parkinsonism (DYT12,RDP) Alternating hemiplegia of childhood 2 (AHC2)
P4	ATP8A2	PS	Cerebellar ataxia, mental retardation and disequilibrium syndrome 4 (CAMRQ4)
P4	ATP10A2	?	Angelman syndrome (AS)
P5B	ATP13A2	?	Kufor-Rakeb syndrome (KRS) Neuronal ceroid lipofuscinosis (NCL)
P5B	ATP13A4	?	Specific language impairment (SLI), autism spectrum disorders (ASD)

CHAPTER 2: QUATERNARY STRUCTURE OF A C-TERMINALLY TRUNCATED, PROTEOLYTICALLY ACTIVE FORM OF DJ-1

2.1 Introduction

DJ-1 belongs to the DJ-1/ThiJ/PfpI superfamily of proteins, members of which often have chaperone and/or protease activity. Shared features of proteins in this superfamily include a conserved cysteine residue in a “nucleophile elbow” strand-loop-helix motif [106], a catalytic triad (cysteine, histidine and glutamate/aspartic acid) in some (but not all) members, and the ability to form oligomers [106]. The oligomeric state of these proteins varies widely ranging from dimers to trimers and hexamers [106]. Data from gel filtration, sedimentation, and x-ray crystallographic analysis indicate that purified recombinant DJ-1 exists primarily as a homodimer [184, 185]. The monomeric subunit of DJ-1 is highly homologous to the *Pyrococcus horikoshii* 1704 gene product (PH1704), a bacterial cysteine protease which forms hexamers. DJ-1 has an additional α helix (helix 8) at the C-terminus compared to PH1704. A recent study has shown that a truncated form of DJ-1 (15 amino acids cleaved at the C terminus, resulting in the removal of helix 8 has much greater protease activity compared to full-length DJ-1 [46]. This C-terminally truncated form of DJ-1 (DJ-1Δ15) was found to accumulate in dopaminergic cells exposed to oxidative stress, leading Chen et al. to conclude that full-length WT DJ-1 is in fact a zymogen that becomes activated

via a redox-sensitive mechanism [46]. Importantly, however, it is not known whether DJ-1Δ15 has the ability to form a hexamer, or whether such a hexameric structure is responsible for the observed protease activity.

We hypothesized that human DJ-1Δ15 adopts a hexameric structure similar to that of PH1704. To address this hypothesis, we analyzed the quaternary structure of DJ-1Δ15 using PyMOL, Western blotting, analytical ultracentrifugation (AUC) and native PAGE gel electrophoresis. Our results suggest that DJ-1Δ15 can form an oligomeric species that is larger than a homodimer (potentially a hexamer), whereas full-length DJ-1 does not form a hexamer because helix 8 prevents a conformational change that is required for hexamer assembly.

2.2 Materials and Methods

2.2.1 Materials

The bicinchoninic acid (BCA) protein assay kit was obtained from Pierce Biotechnology (Rockford, IL). The ECF substrate was purchased from GE Healthcare (Piscataway, NJ). Coomassie brilliant blue R250 and SDS were obtained from Amresco (Solon, OH). Trizma base, 2-Mercapto ethanol, ammonium persulfate (APS) and glycine were purchased from Sigma-Aldrich (St. Louis, MO). Isopropyl-β-D-thiogalactopyranoside (IPTG) and ampicillin were purchased from Gold Biotechnology (St. Louis, MO).

2.2.2 Antibodies

The following antibodies were used in these studies: mouse anti human DJ-1 (3E8) (Enzo Life Sciences, Farmingdale, NY. Clone), secondary anti mouse IgG conjugated with alkaline phosphatase (Promega, Madison, WI, USA).

2.2.3 Preparation of the WT DJ-1 and DJ-1Δ15 constructs

A cDNA encoding wild-type (WT) DJ-1 was amplified by PCR and subcloned as a BamHI – Xho I fragment into the vector pGEX-6P-1, yielding the construct, pGEX-6P-1 GST DJ-1, which encodes an N-terminal GSH S-transferase (GST) fusion with DJ-1 (GST DJ-1), by Dr. John Hulleman, a former graduate student in the Rochet lab. A cDNA encoding DJ-1Δ15 was generated via PCR using a reverse primer that included a stop codon after codon 174 and subcloned as a BamHI – Xho I fragment into pGEX-6P-1, yielding the construct, pGEX-6P-1 GST DJ-1Δ15. To develop a system for generating DJ-1Δ15 without the GST tag, cDNA encoding DJ-1Δ15 was amplified by PCR using the reverse primer referred to above and subcloned as an Xba I – Hind III fragment into the vector pT7-7, yielding the construct pT7-7 DJ-1Δ15. The sequence of the aSyn-encoding insert in each construct was verified using an Applied Biosystems (ABI 3700) DNA sequencer (Purdue University).

2.2.4 Purification of recombinant human WT DJ-1 and DJ-1Δ15 constructs

Cells of the BL21 (DE3) strain of *Escherichia coli* were transformed with DJ-1 expression constructs by electroporation. To prepare GST-WT DJ-1 and GST-DJ-1Δ15, the cells were grown to an OD_{600} of 0.4 - 0.6 in LB plus ampicillin (100

μg/mL) at 37 °C, and IPTG was added to a final concentration of 1 mM. The cells were grown under inducing conditions for 18 h at 18°C, harvested by centrifugation, and resuspended in buffer A (25 mM KPi, pH 7.0, 200 mM KCl, 15 mM 2-mercaptoethanol (2-ME)). The cells were lysed by the addition of lysozyme (1 mg/mL), incubated on ice for 30 min, and run through a French 86 pressure cell (p.s.i. > 1000) (Thermo Electron Corporation, Waltham, MA). After centrifugation (20,000 *g*, 20 min), the supernatant was applied to a GSTPrep FF column (GE Healthcare). GST DJ-1 was eluted in 250 mM Tris HCl, pH 8.0, 500 mM NaCl, and 0.3% [w/v] reduced GSH. Fractions most highly enriched with GST DJ-1 were identified by measuring the OD_{280} and pooled. The pooled fractions were dialyzed against buffer A plus 2-ME (0.25 mM) to remove excess GSH. The overall protein concentration was determined with a BCA protein assay, and the fusion protein was cleaved with PreScission™ Protease (GEHealthcare, 16 h, 4°C, 1 unit protease:133 μg DJ-1). Untagged DJ-1 was separated from free GST and residual protease (which contains an uncleavable GST tag) by elution from a GSTPrep FF column equilibrated with buffer A. Fractions most highly enriched with DJ-1 were identified by sodium dodecyl sulfate polyacrylamide gel electrophoresis (SDS PAGE) with Coomassie blue (R-250) staining and pooled. The purity of the final protein sample was estimated to be approximately 95% by Coomassie Blue staining.

To prepare pT7-7-WT DJ-1and pT7-7-DJ-1Δ15, the cells were grown to an OD600 of 0.6 - 0.8 in LB plus ampicillin (100 μg/mL) at 37 °C, and expression of the DJ-1 gene was induced by adding isopropyl-β-D-thiogalactopyranoside

(IPTG, 1 mM). The cells were grown under inducing conditions for 4 h at 37 °C, harvested by centrifugation, resuspended in buffer B (50 mM tris(hydroxymethyl)aminomethane (Tris) HCl, pH 7.4, 100 mM NaCl, 5 mM 2ME), and lysed with a French pressure cell (p.s.i. > 1000) (Thermo Electron Corporation, Waltham, MA). After centrifugation, DJ-1 was partially purified from the supernatant by successive ammonium sulfate precipitations (70% saturation followed by 90% saturation). The pellet from the second ammonium sulfate precipitation was resuspended in buffer B, and the protein solution was applied to a diethylaminoethyl (DEAE) Sepharose (GE Healthcare, Piscataway, NJ) anion exchange column equilibrated with buffer B. Fractions in the flow-through containing DJ-1 were identified by SDS PAGE with Coomassie Blue staining.

All purified DJ-1 samples were supplemented with glycerol (5%, [v/v]) and 2ME (2 mM), and aliquots (1-2 mg/ml) were flash-frozen and stored at -80 °C. DJ-1 proteins were subsequently prepared for analysis by thawing followed by buffer exchange or dialysis (there was no additional freezing or storage of the protein at 4 °C unless otherwise specified). The concentration of dialyzed DJ-1 samples was estimated using the BCA assay.

2.2.5 PDB Files used for PyMOL analysis

PyMOL analyses were carried out using the following Protein Data Bank (PDB) files: 1P5F, human WT DJ-1 [106]; 1G2I, PH1704 [112].

2.2.6 Analytical ultracentrifugation

DJ-1Δ15 (purified from *E. coli* BL21 DE3 expressing the pGEX-6P-1 construct or the pT7-7 construct) was dialyzed in 50 mM Tris-Cl, 150 mM NaCl, pH 7.4 for 16

h at 4 ºC. DJ-1Δ15 purified from *E. coli* expressing the pGEX-6P-1 construct interacts with *E.coli* ATPase subunits to form a high molecular weight complex (see Chapter 3). To remove this complex (and thus enable us to focus solely on DJ-1Δ15 self-assembly), the protein was centrifuged at 100,000xg for 2 h at 4 ºC. The supernatant was recovered and the protein concentration was estimated using the BCA Protein Assay kit. The protein solution was then analyzed by analytical ultracentrifugation (AUC) at the Purdue Biophysical Analysis Laboratory (BAL). DJ-1Δ15 purified from *E. coli* expressing the pT7-7 construct was dialyzed as above and analyzed via AUC without the sedimentation step described above. AUC was carried out at 50,000 rpm on a Beckman-Coulter ultracentrifuge, XLI (Beckman-Coulter, CA). Sedimentation was monitored with both Rayleigh Interference and absorbance optics. Protein (concentration, 0.5-2 mg/mL) was characterized at 20ºC for 12 h in 50 mM Tris-HCl, pH 7.5, 150 mM NaCl and 1 mM 2ME. Sedimentation coefficients and apparent molecular weights, c(s), were determined using SEDFIT v. 12.43 [186, 187].

2.2.7 Size-exclusion chromatography with multi-angle light scattering (SEC-MALS)

SEC-MALS analysis of DJ-1Δ15 was carried out at the BAL. DJ-1Δ15 was dialyzed in 2 L of 50 mM Tris-HCl, pH 7.5, 150 mM NaCl and 1 mM 2ME (same buffer as AUC above). A solution of the protein (1-4 mg/mL) at 0.5 mL/min was applied onto a Superdex-200 column 10/300 GL (GE Healthcare) connected to an ultra violet (UV) absorbance detector, a refractive index refractometer, and a light scattering (LS) detector. Absolute molecular weights of species eluted from

the column were determined using Wyatt's Astra software, and the relative amount of each species was assessed from the areas under the chromatogram peaks

2.2.8 SDS-PAGE and native PAGE

DJ-1Δ15 (purified from *E. coli* BL21 DE3 expressing the pGEX-6P-1 construct or the pT7-7 construct) was dialyzed in 50 mM Tris, 50 mM NaCl, pH 7.5 for 16 h at 4 ºC. The protein concentration was estimated using the BCA Protein Assay kit, and equal amounts of protein (3 µg) were analyzed via electrophoresis on an 8% (w/v) native polyacrylamide gel (no SDS or reducing reagent in either the sample buffer or the running buffer, and the samples were not boiled). Alternatively, the protein samples were analyzed via electrophoresis on a 12% (w/v) SDS PAGE gel. The non-denaturing gel was run at 4 ºC at 80-100V for 2-3 h, whereas the SDS PAGE gel was run at 22 ºC at 80-115V for 1.5 h. The gels were stained using Coomassie Brilliant Blue dye for 20 min at 22 ºC and de-stained using a solution of methanol, acetic acid and water (3:1:6), (v/v). Gel images were obtained and analyzed using a Typhoon imaging system (GE Health Sciences, Piscataway, NJ, USA).

2.2.9 Western blotting

DJ-1 samples were assayed for protein concentration using the BCA Protein Assay Kit, and equal amounts of protein were separated via SDS–PAGE on a 4–20% (w/v) polyacrylamide gel. The proteins were transferred to a 0.2 µm polyvinylidene fluoride (PVDF) membrane, which was then probed with a primary antibody specific for DJ-1 (1: 4000). The membrane was treated with a

secondary anti-mouse alkaline phosphatase-conjugated antibody (1: 6000). Chemifluorescence images were obtained and analyzed using a Typhoon imaging system (GE Health Sciences, Piscataway, NJ, USA).

2.3 Results

2.3.1 Full-length DJ-1 cannot form a hexamer due to steric hindrance involving helix 8.

Helix 8 of full-length DJ-1 is missing on PH1704, a bacterial cysteine protease that is highly homologous to DJ-1 and has been shown to form a hexamer (Fig 2.1). We hypothesized that the absence of a C-terminal helix on PH1704 as opposed to the presence of helix 8 on full-length DJ-1 could account for why PH1704 forms a hexamer whereas DJ-1 forms a homodimer. To address this hypothesis, we overlaid models of the three-dimensional (3D) structures of full-length DJ-1 and PH1704 'half hexamers' using PyMOL. Analysis of the overlaid structures revealed that full-length DJ-1 is unable to form a PH1704-type hexamer because of steric conflicts involving helix 8 (Fig. 2.2A).

2.3.2 The results of a PyMOL analysis suggest that DJ-1Δ15 can adopt a hexameric structure.

The monomeric subunit of DJ-1Δ15 is highly homologous to the *Pyrococcus horikoshii* 1704 gene product (PH1704) [112]. Because DJ-1Δ15 lacks helix 8 (Fig. 2.2B), similar to PH1704 which exists as a hexamer, we hypothesized that DJ-1Δ15 can adopt a hexameric structure. To address this hypothesis, a model of the 3D structure of full-length DJ-1 was loaded into PyMOL, and the 15 C-

terminal amino acid residues were deleted to generate a model of the DJ-1Δ15 3D structure. Analysis of the model revealed that DJ-1Δ15 could form a closed hexamer (Fig 2.3). Formation of this closed hexamer was made possible by (i) the truncation of helix 8, and (ii) a 90° rotation between two DJ-1Δ15 subunits at the interface that is homologous to the subunit interface of the full-length DJ-1 homodimer. The interfaces of the unrotated and rotated subunits of members of the DJ-1/ThiJ/PfpI superfamily have been referred to as patch 1 and patch 1', respectively [113]. In the absence of the subunit rotation, DJ-1Δ15 dimers retained the patch 1 configuration and could only assemble to form an open hexamer (Fig 2.4).

Further analysis of the closed DJ-1-Δ15 hexamer revealed that C106 and H126 on one subunit were positioned at distances of 9.5 Å and 5.5 Å (respectively) from a glutamateresidue at position 84 of an adjacent subunit (E84') (Fig 2.5A). This positioning of C106, H126, and E84' implied that the three residues could potentially form a catalytic triad, similar to that of PH1704 in which residues C100 and H101 are positioned at distances of 7.3 Å and 2.6 Å (respectively) from E74' (of an adjacent subunit (Fig. 2.5B). The two subunits carrying these residues interact at a new interface, referred to as patch 2 [113].

2.3.3. Recombinant DJ-1Δ15, but not full-length WT DJ-1, forms high molecular weight species that are larger than a homodimer (SDS-PAGE/Western blot analysis).

Based on our PyMOL results (see above), we hypothesized that DJ-1Δ15 could form high molecular weight species that are larger than a homodimer, in contrast

to DJ-1. To address this hypothesis, full-length DJ-1 and DJ-1Δ15 were analyzed by (i) SDS PAGE (denaturing and reducing) followed by Western blot analysis using an antibody that recognizes both DJ-1Δ15 and full-length DJ-1; and (ii) native PAGE (non-denaturing and non-reducing) with Coomassie blue staining. As predicted, purified DJ-1Δ15 had a lower molecular weight compared to full-length DJ-1 due to the truncation of the 15 amino acids from the C terminus region (Fig 2.6). A Western blot showed the presence of high MW species in the DJ-1Δ15 sample (Fig 2.7). In contrast, the results of native PAGE analysis showed no significant high-order oligomer signal (corresponding to an oligomer with an apparent molecular weight greater than that of dimeric DJ-1) in lanes loaded with two different purified DJ-1 del15 samples (Fig. 2.8). Thus, the Western blot results suggest that DJ-1Δ15 forms higher molecular weight species, consistent with the results of our PyMOL analysis (see above), but the native PAGE data suggest that oligomeric DJ-1Δ15 is a minor species and/or is unstable under non-denaturing electrophoresis conditions.

2.3.4 Recombinant DJ-1Δ15 forms high molecular weight species that are larger than a homodimer (analytical ultracentrifugation).

The next experiments were designed to investigate whether DJ-1Δ15 consists of an equilibrium population of monomers, dimers, and hexamers (and potentially also trimers). We hypothesized that DJ-1Δ15 forms distinct species with different molecular weights. To address this hypothesis, DJ-1Δ15 was analyzed via AUC. Sedimentation-velocity analysis of a sample of DJ-1Δ15 purified from *E. coli* as an untagged protein (following expression of the pT7-7 construct) revealed the

presence of three species with strikingly different sedimentation speeds, corresponding to the DJ-1Δ15 monomer (1.8S), dimer (3.0S) and a high molecular weight species (5.2 - 5.7S) (Fig 2.9). Similar results were obtained upon sedimentation-velocity analysis of a sample of DJ-1Δ15 that was purified from *E. coli* as a GST-tagged protein (following expression of the pGEX-6P-1 construct) and subsequently cleaved to remove the GST tag (Fig. 2.10). The smaller peak (1.1S) detected in the DJ-1Δ15 preparation *E. coli* expressing the pGEX-6P-1 construct might be a DJ-1Δ15 truncated species. The results further showed that the distribution of DJ-1Δ15 among the different species varied with protein concentration

In additional studies, a DJ-1Δ15 (untagged) sample was analyzed via SEC MALS, a method that involves (i) the chromatographic fractionation of protein species according to molecular weight, and (ii) monitoring protein elution by measuring light scattering signals that increase with increasing molecular weight of the eluted species. The results showed the presence of peaks eluting earlier than the dimeric peak suggesting that DJ-1Δ15 formed species that were larger than a homodimer (data not shown). In summary, these data further support our conclusion from molecular modelling (PyMOL) studies that DJ-1Δ15 can form high molecular weight species.

2.4 Discussion

In this chapter, we investigated whether DJ-1Δ15 can form oligomers that are larger than a homodimer, both computationally and biochemically in a cell-free

system. Our results suggest that DJ-1Δ15 has the ability to form high MW oligomers, including potentially a hexamer. In addition, the results of PyMOL analysis suggest that formation of DJ-1Δ15 hexamer may allow for the formation of a catalytic triad by bringing E84 from one subunit in proximity to C106 and H126 from another. Whether residue E84 is critical for DJ-1Δ15 to function as a protease remains to be elucidated.

2.4.1 Full-length WT DJ-1 does not form a hexamer due to the presence of helix 8 at the C-terminus.

DJ-1 belongs to a superfamily of proteins with the ability to form functional oligomers (chaperones and/or proteases. Purified recombinant DJ-1 exists primarily as a homodimer [184, 185]. The monomeric subunit of DJ-1 is highly homologous to the *Pyrococcus horikoshii* 1704 gene product (PH1704), a bacterial cysteine protease which forms a hexamer. DJ-1 has an additional α helix (helix 8) at the C-terminus compared to PH1704. The results of our PyMOL analysis clearly showed that full-length DJ-1 cannot form a hexamer due to steric hindrance involving this additional α helix.

Full-length DJ-1 has been reported to exist as a zymogen that becomes activated as a result of the cleavage of the C-terminal helix via a redox-sensitive mechanism [46]. The results of computational and biochemical analyses suggested that DJ-1Δ15 has the ability to form oligomers that are larger than the homodimer, including a hexamer (discussed in greater detail below). Chen at al further predicted that the DJ-1Δ15 variant has an ‘unmasked’ active site involved in proteolytic function [46]. Our results suggest that the truncation may convert

the full-length zymogen into the proteolytically active form by enabling conformational changes required for hexamer formation, which may in turn be necessary for the assembly of a catalytic triad encompassing residues from multiple subunits. The presence of helix 8 suggests that there is a selective advantage to having DJ-1 only exist as an active protease under specific conditions (e.g. high oxidative stress), whereas the zymogen design does not appear to confer a selective advantage on PH1704.

2.4.2 Removal of 15 C-terminal amino acid residues facilitates formation of a hexamer.

Our computational analysis via PyMOL showed that DJ-1Δ15 can readily form a hexamer as a result of the removal of the 15 C-terminal amino acid residues. This truncation allows for a 90° rotation between two subunits, resulting in the conversion of the patch 1 interface to the patch 1' interface. In turn, only DJ-1Δ15 dimers with a patch 1' interface can undergo self-assembly to form a closed hexamer (or trimer of dimers). In contrast, only an open hexamer could form upon the self-assembly of dimers that have not undergone a 90° rotation to generate the patch 1' interface. An open hexamer would be predicted to have a relatively low thermodynamic stability because (i) it lacks inter-subunit interactions involved in forming a closed structure, and (ii) it may expose greater hydrophobic surface area (i.e. at the unclosed ends of the open hexameric structure) compared to a closed hexamer.

Taken together, these data suggest that the formation of a DJ-1Δ15 closed hexamer (if it occurred in solution) would be made possible because of the

absence of helix 8 and would involve a 90°rotation between two DJ-1 subunits, converting patch 1 to patch 1’ in each of the three pairs of subunits constituting the hexamer. Moreover, the formation of a DJ-1Δ15 hexamer would potentially allow for the formation of a catalytic triad consisting of Cys 106 and His 126 from one subunit and E84’ from an adjacent subunit at the patch 2 interface.

2.4.3 Hexamer formation by DJ-1Δ15 may be necessary for the assembly of a catalytic triad involved in proteolysis.

The results of our PyMOL analysis also imply that hexamer formation by DJ-1Δ15 may be necessary for the protease activity of this variant because a new interface (referred to as patch 2) formed upon the assembly of a trimer of dimers may lead to the formation of a catalytic triad, in contrast to the catalytic diad proposed by Chen et al. [46]. Our results showed that closed hexamer formation by DJ-1-Δ15 brings residue E84’ from one subunit in proximity to the other residues of the potential catalytic triad, Cys106 and His 126 from another subunit. Similarly, the relative positions of the three residues were the same in patch 2 of the hexamer formed from unrotated DJ-1 del15 dimers (with a patch 1 interface rather than a patch 1' interface (data not shown). Future mutagenesis studies will be aimed at determining whether the assembly of such a catalytic triad is responsible for the observed protease activity of DJ-1-Δ15. Previous studies indicated that the distance between the glutamate and cysteine in a catalytic triad is ~2.6 Å and between glutamate and histidine is ~7 Å [188, 189]. Therefore the distances from E84’-C106 (9.5 Å) is larger than typical distances in a catalytic triad. However, the distances may fall into the typical range as a result

of conformational changes associated with hexamer assembly, and these cannot be detected by PyMOL. Future research will be focused on exploring such conformational changes involved in hexamer assembly via molecular dynamics simulations.

2.4.4 DJ-1Δ15 oligomers larger than a homodimer exist in solution.

AUC results of DJ-1Δ15 suggested that large oligomeric species exist in solution, and the abundance of these species relative to the monomeric or dimeric protein is concentration-dependent. These results suggest that DJ-1Δ15 high order oligomers are in rapid equilibrium with the monomeric and dimeric forms. Furthermore, the presence of bands corresponding to large oligomers on an SDS PAGE gel (detected by Western blotting) suggests that these oligomeric species may be stabilized by covalent linkages. Future studies will be aimed at (i) characterizing the equilibrium distribution of large oligomeric forms of DJ-1Δ15 in greater detail, and (ii) identifying key intersubunit interactions necessary for the assembly of these oligomeric species. Because the levels of DJ-1Δ15 high molecular weight oligomers relative to the monomer or homodimer appear low compared to the predicted levels of PH1704 hexamer [112], we infer that the intersubunit contacts at patch 2 of DJ-1Δ15 may not be as optimal for stabilizing a hexameric structure compared to those of the bacterial enzyme. Future research will be aimed at addressing this hypothesis with a combination of computational and mutagenesis studies. If the hypothesis is true, then this would suggest that residues that could be involved in patch 2 interactions of DJ-1Δ15 may not have been subjected to selective pressure, perhaps because the

formation of a hexamer is less important to the function of DJ-1 (or DJ-1Δ15) compared to that of PH1704.

2.5 Conclusion

In summary, our data suggest that DJ-1Δ15 can potentially form high order oligomeric species. Specifically, we showed via computational analysis that DJ-1Δ15 potentially forms a closed hexamer by forming a new interface (patch 1'). In contrast, full-length DJ-1 cannot adopt a hexameric structure due to steric conflicts involving helix 8. Formation of the DJ-1Δ15 hexamer may be necessary for the protease activity of this variant because the new interfaces formed upon assembly of a trimer of dimers may lead to the formation of a catalytic triad. Studies of DJ-1Δ15 in solution showed that DJ-1Δ15 forms oligomeric species larger than a homodimer in a concentration-dependent manner. Further efforts are underway to determine whether the formation of these high molecular weight species is responsible for the observed protease activity of DJ-1Δ15.

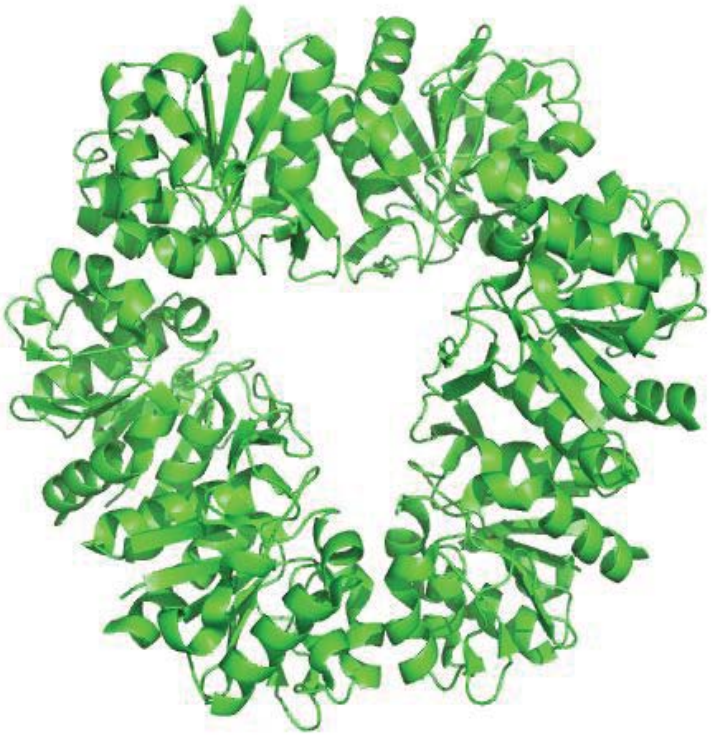

Figure 2.1 Structural model of the PH1704 hexamer.

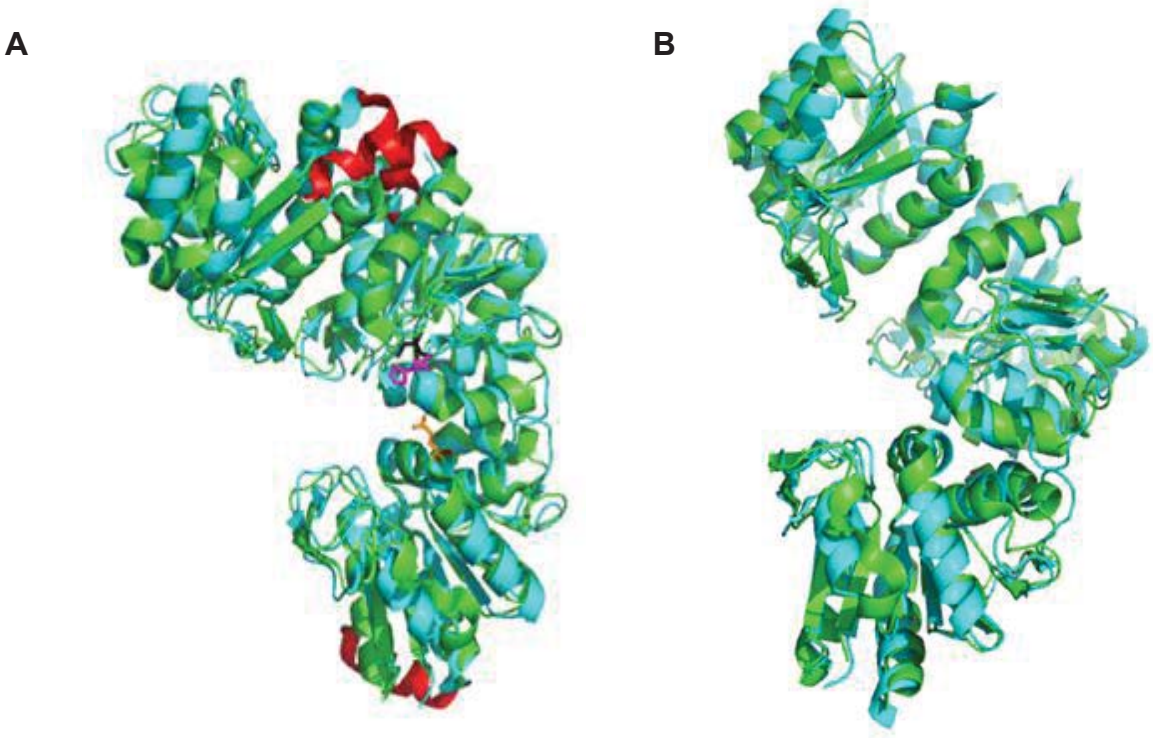

Figure 2.2 Overlaid structures of PH1704 half-hexamer (1G2I, green) and WT DJ-1 (1P5F, cyan) or DJ-1Δ15.

(A) WT DJ-1 does not form a hexamer because helix 8 causes steric hindrance at the patch 1' interface. Helix 8, C106, H126, and E84' of DJ-1 are shown. **(B)** DJ-1Δ15 overlays well with PH1704 due to the absence of helix 8.

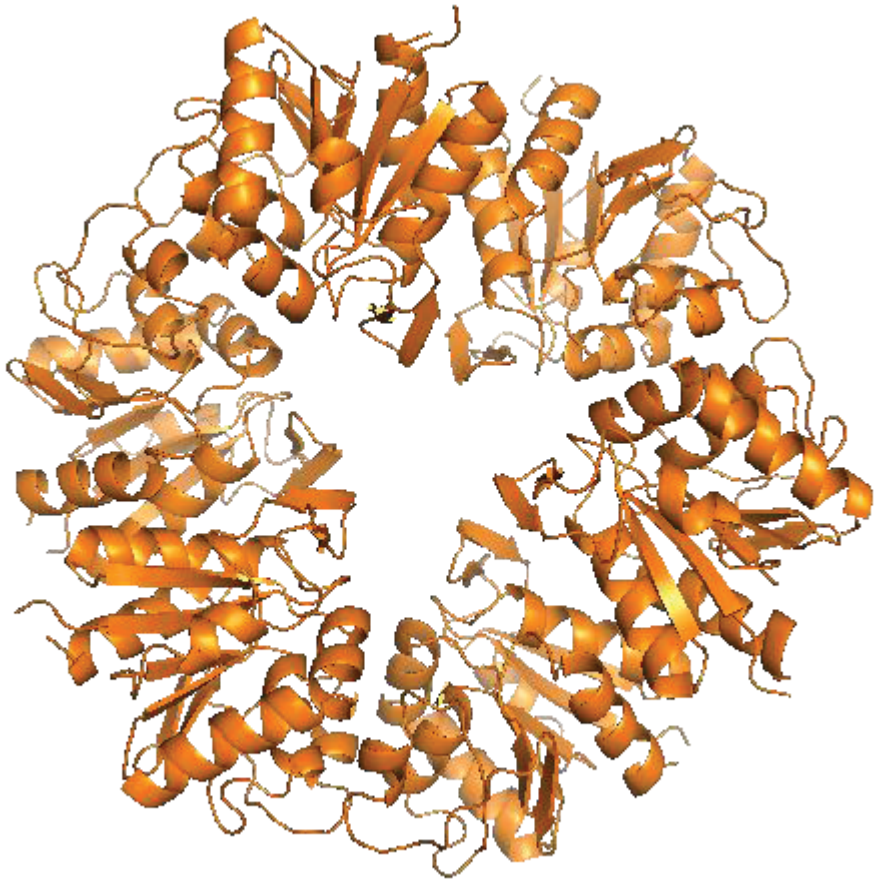

Figure 2.3 Structural model showing a closed hexamer that could be formed by DJ 1Δ15.

DJ-1Δ15 can form a closed hexamer as a result of removal of the 15 C-terminal residues and a 90° rotation between two subunits, allowing for conversion of the patch 1 interface to the patch 1' interface. This conformational change is necessary for patch 2 interactions leading to the assembly of a hexamer (trimer of dimers) with a closed structure. (Structural model generated by Fletcher Jones).

Figure 2.4 Structural model showing an open hexamer that could be formed by DJ1Δ15.

DJ-1Δ15 is expected to form an open hexamer upon self-assembly in the absence of a 90°rotation between two subunits, so that the patch 1 interface is not converted to the patch 1' interface. (Structural model generated by Fletcher Jones).

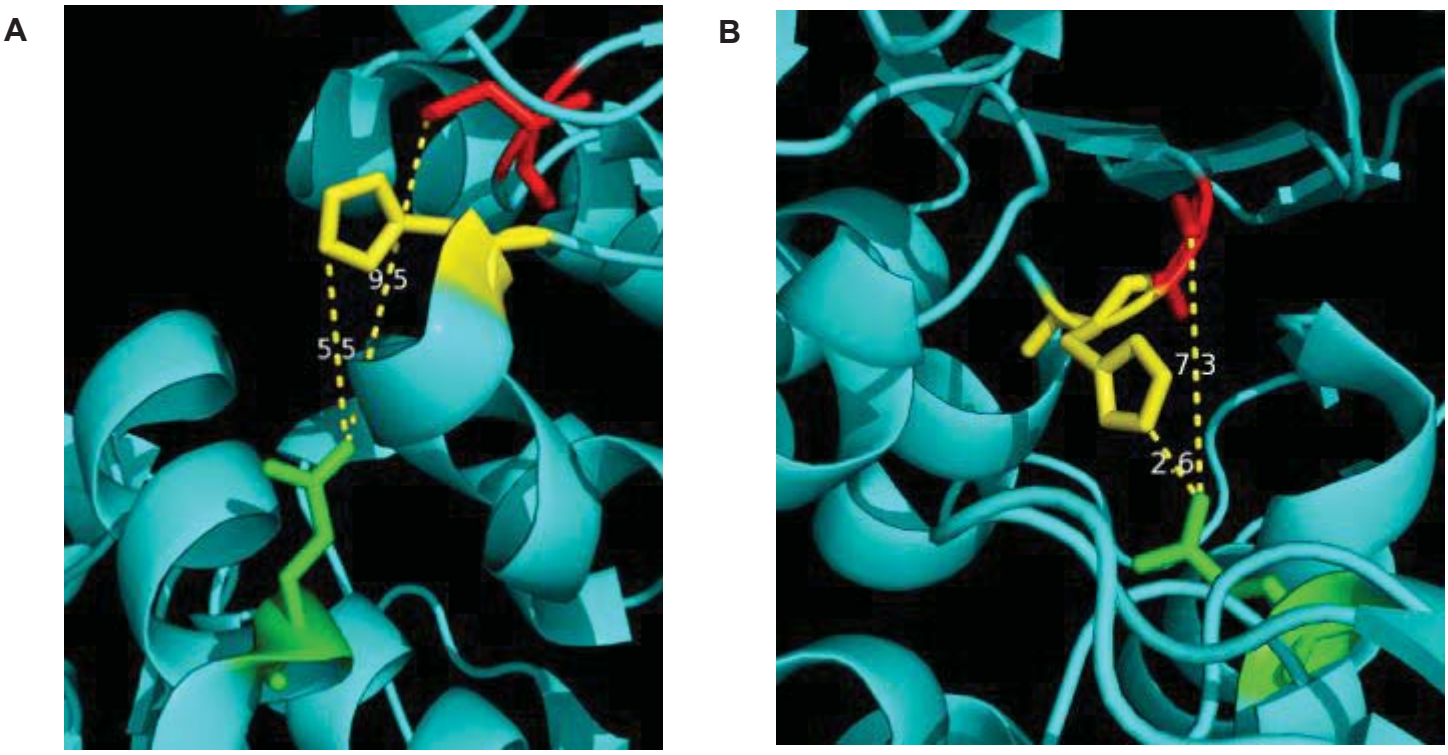

Figure 2.5 Potential DJ-1Δ15 catalytic triad.

(A) Formation of the DJ-1Δ15 hexamer brings a glutamate residue 84 (E84') from one subunit to within 9.5 Å of cysteine 106 (C106) and 5.5 Å of histidine (H126), and this positioning of the three residues may result in the assembly of a catalytic triad. **(B)** PH1704 forms a catalytic triad with E74' from one subunit placed within 7.3 Å of C100 and 2.6 Å of H101.

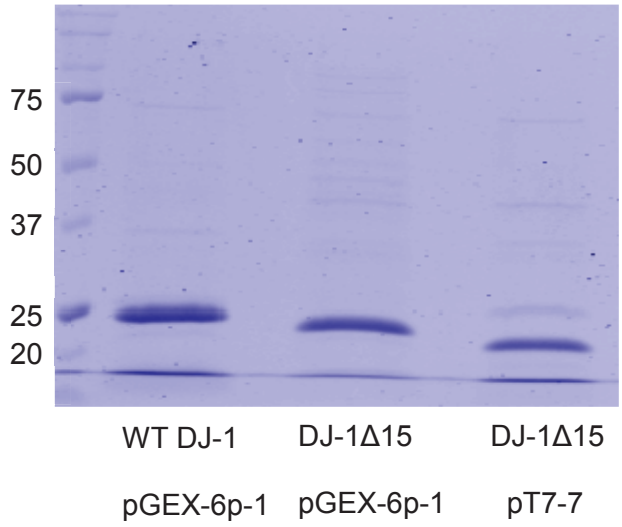

Figure 2.6 SDS-PAGE gel showing that DJ-1Δ15 has a lower molecular weight compared to WT DJ-1.

The following proteins (3 µg) were analyzed: WT DJ-1 purified from *E. coli* expressing a pGEX-6p-1 construct; DJ-1Δ15 purified from *E. coli* expressing a pGEX-6p-1 construct; and DJ-1Δ15 purified from *E. coli* expressing a pT7-7 construct. The gel was stained with Coomassie Brilliant Blue R-250. N=2

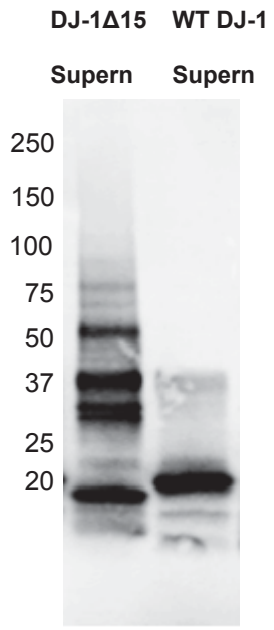

Figure 2.7 Western blot of SDS-PAGE gel showing evidence of DJ-1Δ15 oligomerization.

WT DJ-1 and DJ-1Δ15 were ultracentrifuged at 100,000 rpm (300,000 xg) at 4ºC for 30 min. The supernatant (supern) was carefully removed and analyzed via Western blotting using a DJ-1 specific primary antibody (1:4000). N=2

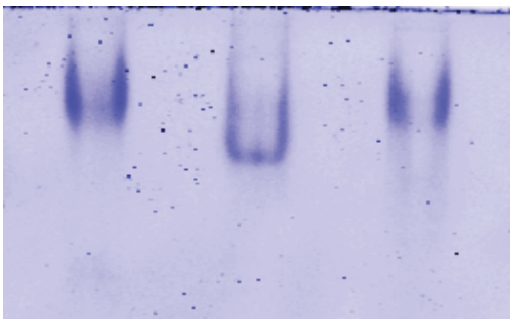

Figure 2.8 Native PAGE gel showing that high order oligomer are only minor in two different preparation of DJ-1Δ15. N=2

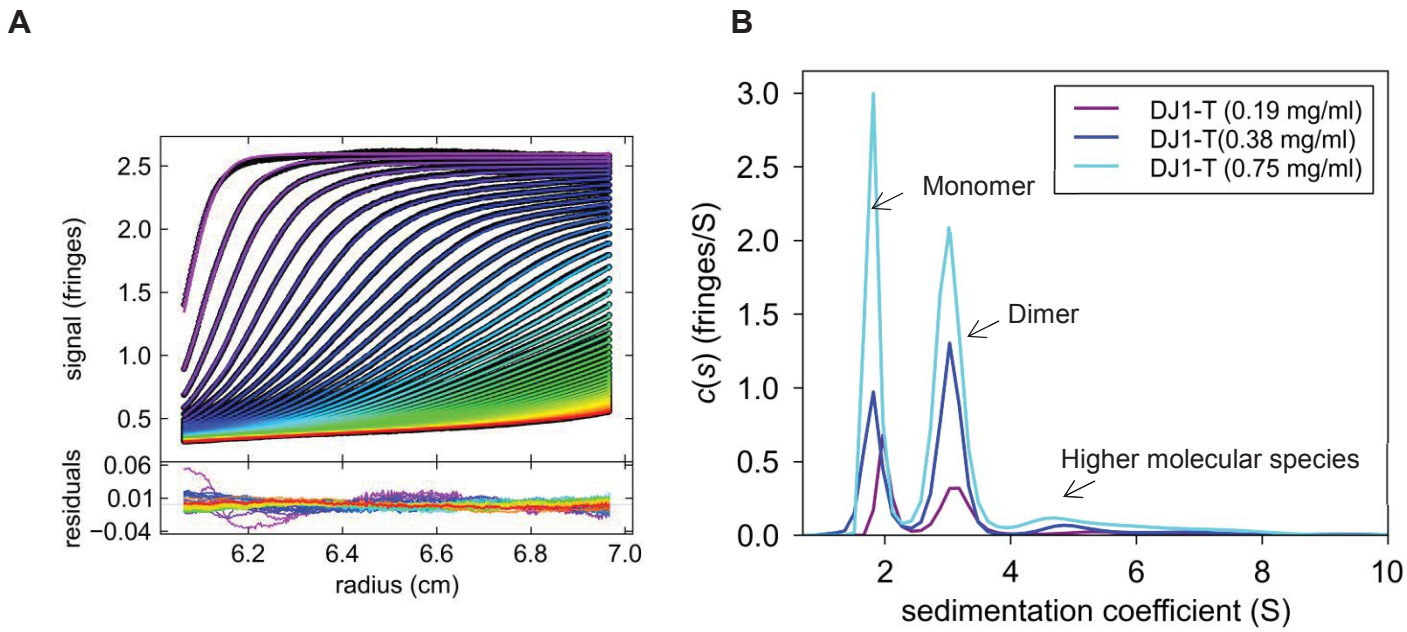

Figure 2.9 Analysis of DJ-1Δ15 purified as an untagged protein via AUC.

(A) Sedimentation-velocity data showing total protein signal (interference fringes) versus radial distance in an ultracentrifugation cell with DJ-1Δ15 at different sedimentation times. **(B)** Plot showing the distribution of species with different sedimentation coefficients (S) at three different concentrations of protein (0.75 mg/ml, 0.38 mg/ml and 0.19mg/ml). N=2

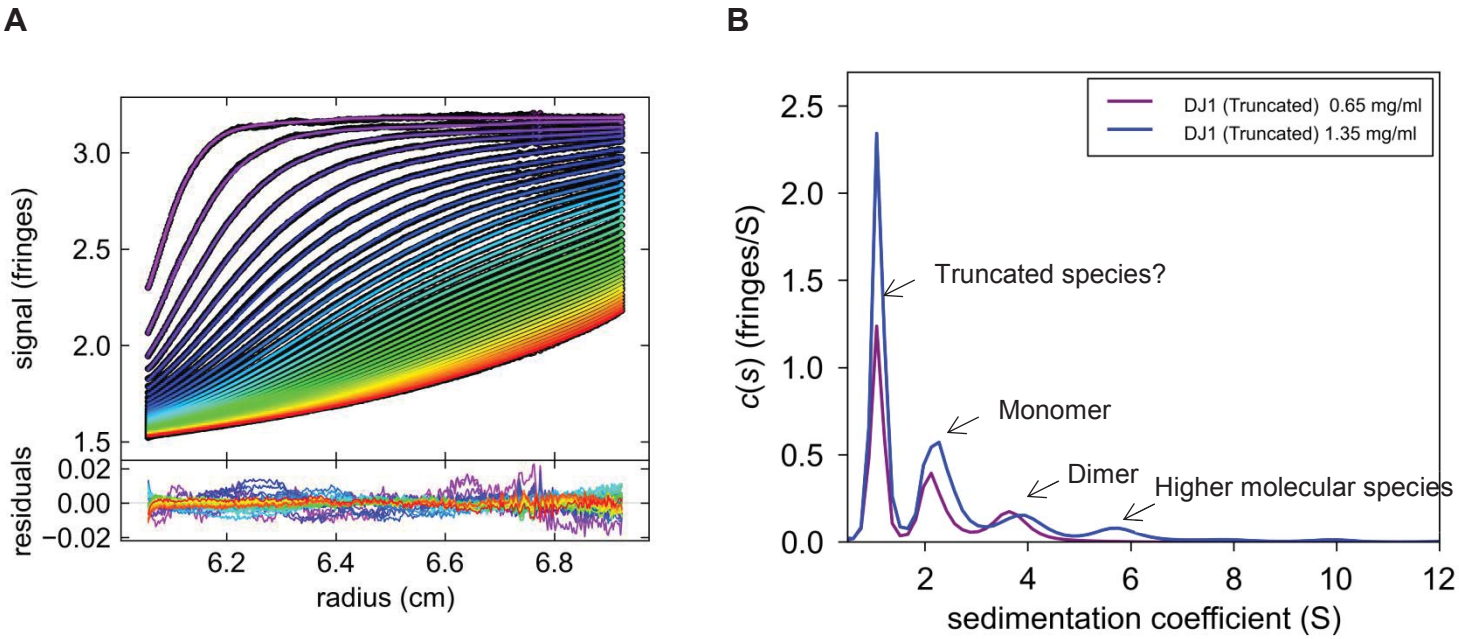

Figure 2.10 AUC analysis of DJ-1Δ15 purified as a GST-tagged protein and subsequently cleaved for tag removal).

(A) Sedimentation-velocity data showing total protein signal (interference fringes) versus radial distance in an ultracentrifugation cell with DJ-1Δ15 at different sedimentation times. **(B)** Plot showing the distribution of species with different sedimentation coefficients (S) at two different concentrations of protein (1.35 mg/ml and 0.65 mg/ml). N=1

CHAPTER 3: DJ-1 INTERACTS WITH *E.COLI* F_1 ATP SYNTHASE

3.1 Introduction

DJ-1 has been implicated in many cellular protective functions including a peroxiredoxin function and the ability to act as molecular chaperone [108, 141, 142, 190], but the exact mechanism for its neuroprotective function is unknown. Molecular chaperones are large a class of proteins that suppress protein misfolding, aggregation and aid in refolding denatured proteins [191, 192]. Included in this large class of proteins are multiple heat shock proteins (Hsps) [191, 192], many of which function in an ATP-dependent manner [191, 192]. Another class of proteins, peroxiredoxin (Prxs), functions as both molecular chaperones and peroxidases [193]. A number of Prxs have been shown to form high molecular weight structures, up to five dimers linked by hydrophobic interactions [194]. The dual functions of Prxs are modulated by oxidative stress, which can induce dramatic changes in quaternary structure [195].

DJ-1 has been described as an atypical Prx that scavenges hydrogen peroxide (H_2O_2) via oxidation of Cys106 [190]. The reaction of cysteinyl thiolates with H_2O_2 yields multiple oxidation forms: sulfenic acid (–SOH), sulfinic acid ($–SO_2H$), sulfonic acid ($–SO_3H$), and disulfide (–S-S–), including glutathione *S*-conjugate

and disulfide *S*-oxides [196-199]. Hyperoxidation of Prxs to the sulfinic acid form results in inactivation. In some cases this inactivation can be reversed by sulfiredoxin, a protein that provides an ATP molecule which is a target for nucleophilic attack by the cysteine sulfinic acid, resulting in the formation of sulfinic acid phosphoryl ester intermediate. In turn, reaction of this intermediate with a sulfiredoxin cysteine residue (or a small-molecule reductant) releases a phosphate and results in the formation of a thiosulfinate intermediate, which can be reduced to regenerate the sulfenic acid form of the Prx [200] .

Analysis of the DJ-1 crystal structure revealed a previously undescribed potential ATP binding site that included two arginine residues, Arg 28 and Arg 48, near the oxidizable Cys106 residue. These residues could potentially serve as binding sites for the beta and gamma phosphates of ATP. A former graduate student in the lab, Kristen Lesniak, showed that a nonhydrolyzable analog of ATP (ATPγS) stabilized DJ-1 in a pulse-proteolysis assay (unpublished data). In addition, a preparation of recombinant human wild-type DJ-1 purified from *E. coli* was found to bind and hydrolyze ATP and GTP, but not CTP, TTP, or ADP.

In this study we carried out a series of biochemical experiments to determine the source of the ATPase activity in our DJ-1 preparations. Our results show that DJ-1 interacts with *E.coli* F_1 ATP synthase and this interaction may be relevant to DJ-1 chaperone activity. Our data also suggest that the reduced form of DJ-1 preferentially interacts with F_1 ATPase. These findings provide new insights into the biochemical mechanism by which DJ-1 preserves mitochondrial function in neurons exposed to PD-related insults – namely, by interacting with F_1 ATPase,

a protein complex that is structurally and functionally well conserved between *E. coli* and eukaryotic mitochondria.

3.2 Materials and Methods

3.2.1 Materials

The bicinchoninic acid (BCA) protein assay kit was obtained from Pierce Biotechnology (Rockford, IL). The ECF substrate was purchased from GE Healthcare (Piscataway, NJ). Coomassie Brilliant Blue R250 and SDS were obtained from Amresco (Solon, OH). All other chemicals were purchased from Sigma-Aldrich (St. Louis, MO).

3.2.2 Antibodies

The following antibodies were used in these studies: mouse anti human DJ-1 (3E8) (Enzo Life Sciences, Farmingdale, NY), secondary anti mouse IgG conjugated with alkaline phosphatase (Promega, Madison, WI, USA, Cat. # S3721), secondary anti rabbit IgG conjugated with alkaline phosphatase (Promega, Madison, WI, USA, Cat # S3731). Anti ATP beta subunit (ATPB) (7E3F2) (Abcam, Cambridge, MA, USA).

3.2.3 DJ-1 protein purification

DJ-1 was purified as explained earlier in Chapter 2.

3.2.4 A continuous fluorimetric assay to measure ATPase activity

ATPase activity was monitored via a continuous fluorimetric assay. In the presence of phosphate, nucleoside phosphorylase (PNP) will convert 7-methyl-guanosine (M^7Guo), a fluorescent substrate, to 7-methyl-guanine (M^7Gua), a

non-fluorescent molecule, thus decreasing the fluorescence [201]. WT DJ-1 was dialyzed against 2 L of 50 mM Tris-HCl, pH 7.5, 50 mM NaCl, and 1 mM $MgCl_2$. Protein concentration was determined using the BCA assay, and 15 µg of DJ-1 was mixed with 7-methyl-guanosine (M^7Guo) (4 mM), 0.1 units of PNP, 1 mM $MgCl_2$, and 1 mM ATP in a 1 mL quartz spectrometer cuvette (Sigma Aldrich, St. Louis MO). The decrease in fluorescence was observed at 410 nm (the excitation wavelength was 300 nm) using a FluoroMax 3 fluorescence spectrophotometer (HORIBA Jobin Yvon, Edison, NJ).

3.2.5 Filtration of DJ-1 samples

WT DJ-1 was dialyzed against 2 L of 50 mM Tris-HCl, pH 7.5, 50 mM NaCl, and 1 mM $MgCl_2$. The protein was later applied to a 100 kDa spin filter (Millipore Billerica, MA). The filter was spun at 2,000 xg for 4 min at 4 ºC. The filtrate was recovered, and protein concentration was determined using the BCA kit before analysis of ATPase activity.

3.2.6 Size Exclusion Chromatography (SEC)

WT DJ-1 (~1 mg/mL final concentration) was dialyzed against 50 mM Tris-HCl, pH 7.5, 50 mM NaCl, and 1 mM $MgCl_2$, and an aliquot (200 µg) was applied to a Superdex 200 10/30 size exclusion chromatography (SEC) column (GE Healthcare). The protein was eluted with the same buffer used for dialysis at a flow rate of 0.5 mL/min, monitoring absorbance at 280 nm. Apparent molecular weights of eluted proteins were determined using a calibration curve established with the following standards: blue dextran (>600 kDa), bovine serum albumin (BSA, 66.2 kDa), ovalbumin (43 kDa), and lysozyme (14.3 kDa).

3.2.7 Ultracentrifugation

WT DJ-1 was dialyzed in 2 L of a buffer consisting of 50 mM Tris-HCl, pH 7.5, 50 mM NaCl, and 1 mM $MgCl_2$ for 16 h at 4ºC. The protein was then ultracentrifuged at 47,000 rpm (100,000 xg) at 4ºC for 2 h using a Beckman ultracentrifuge (Dr. Chris Hrycyna, Purdue University, Chemistry). The supernatant was removed, and the pellet was resuspended in dialysis buffer.

3.2.8 Sucrose gradient centrifugation

A series of sucrose solutions (5%-50%, w/v) was prepared in 50 mM Tris-HCl, pH 7.5, 50 mM NaCl, 1 mM $MgCl_2$. An aliquot of each solution (2 mL) was carefully layered into an ultracentrifuge tube (16x89mm, Beckman), starting with the 50% solution at the bottom. To separate high-MW species in the DJ-1 preparation from the predominant homodimer, the protein sample was loaded on the 5% sucrose solution (top-most layer of the gradient), and ultracentrifugation was carried out at 40,000 rpm (274,000 xg) for 18 h at 4 ºC. Fractions of about 500 µL were collected from the bottom of the tube by puncturing the tube bottom. The samples were analyzed via Western blotting using antibodies specific for DJ-1 and ATPB.

3.2.9 Western blotting

After measuring the concentration of protein solutions using the BCA Protein Assay Kit (Pierce Biotechnology, Rockford, IL, USA), equal amounts of protein were separated via SDS–PAGE on a 4-20% or 12% (w/v) polyacrylamide gels. Due to the low amount of protein in the sucrose gradient fractions, the protein concentration of these fractions was not determined; instead, an equal volume

(12 µL) of each fraction was loaded on the gel. The proteins were transferred to a 0.2 µm polyvinylidene fluoride (PVDF) membrane, which was then probed with a primary antibody specific for DJ-1 (1:4000), oxidized DJ-1 (1:5000), GST (1:5000), or ATPB (1:5000). The membrane was treated with a secondary anti-mouse or anti-rabbit alkaline phosphatase-conjugated antibody (1:6000) or using a secondary fluorescence goat anti-rabbit/Alexa Fluor 488 (Life technologies, Carlsbad CA) and goat anti-mouse Alexa Fluor 594 (Life technologies, Carlsbad CA). Images were obtained and analyzed using a Typhoon imaging system (GE Health Sciences, Piscataway, NJ, USA).

3.2.10 Transmission Electron Microscopy (TEM)

Gradient fractions (10 µL) were deposited on glow–discharged carbon-coated copper grids (FCF400-Cu), and the grids were rinsed with three drops of 50 mM Tris-HCl, pH 7.5, 50 mM NaCl, and 1 mM $MgCl_2$. The grids were then negatively stained with 1% (w/v) uranyl-acetate. Images were generated using an electron microscope (CM200 transmission electron microscope (TEM), (Phillips, Amsterdam, Netherlands) operated at 200 kV, in collaboration with Dr. Lia Stanciu (Department of Materials Engineering, Purdue University).

3.2.11 Mass Spectrometry

Samples obtained from the 50% sucrose gradient fraction were first denatured in a buffer consisting of 8 M urea, 50 mM Tris-HCl, pH 7.5, 50 mM NaCl, and 1 mM $MgCl_2$. To reduce disulfide bonds, DTT was added to a final concentration of 10 mM, and the samples were incubated at 37 ºC for 1 h. Iodoacetamide was added to a final concentration of 20 mM, and the samples were incubated at 22 ºC for 1

h to alkylate the reduced cysteine residues. After dilution with a five-fold excess of buffer, the samples were incubated with trypsin (10 µg per mg of protein) for 12-16 h at 37 ºC. The samples were then desalted using a C-18 capillary column packed with 5 µm C18 Magic bead resin (Michrom; 75 µm i.d. and 12 cm of bed length) and analyzed via mass spectrometry (UPLC: EASY-nLC 1000 Liquid Chromatograph (Thermo Scientific). Mass Spec: Thermo Fisher LTQ-Orbitrap Velos) in collaboration with Lingfei Zeng and Dr. Andy Tao (Department of Biochemistry, Purdue University).

3.2.12 Database search

The LTQ-Orbitrap raw files were searched directly against the human, *E. coli* or *S. japonicum* database using SEQUEST on Proteome Discoverer (Version 1.4, Thermo Fisher). Proteome Discoverer created DTA files from raw data files with minimum ion threshold 15 and absolute intensity threshold 50. Peptide precursor mass tolerance was set to 10 ppm, and MS/MS tolerance was set to 0.6 Da. Search criteria included a static modification of cysteine residues of +57.0214 Da and a variable modification of +15.9949 Da to include potential oxidation of methionine. Searches were performed with full tryptic digestion and allowed a maximum of two missed cleavages on the peptides analyzed from the sequence database. False discovery rates (FDR) were set to 1% for each analysis. Two peptides with high confidence were considered as solid evidence of the protein ID.

3.3 Results

3.3.1 A preparation of recombinant WT DJ-1 loses ATPase activity upon filtration.

To preserve our DJ-1 preparation, we filtered the protein through a filter with a molecular weight cutoff of 100 kDa to remove any microbial contaminants. We tested the ATPase activity of our DJ-1 preparation before and after filtration using a continuous fluorescence assay (PNP). Surprisingly, our results showed that the ATPase activity of the DJ-1 preparation was absent in the filtrate (Fig 3.1). These data suggested that the ATPase activity was associated with either a high molecular weight form of DJ-1 or another high molecular weight protein in the DJ-1 preparation.

To further confirm the filtration results, we used a size exclusion chromatography (SEC) approach. The homodimer purified using a superdex-200 column was analyzed for ATPase activity using the PNP assay with or without ATP. The results showed that homodimer ATPase activity, and doubling the amount of the DJ-1 homodimer used in the assay did not change the results (Fig 3.2).

Taken together, these results suggest that (i) the ATPase activity was associated with either a high molecular weight form of DJ-1 or another high molecular weight protein in the DJ-1 preparation, and (ii) DJ-1 homodimer, isolated via SEC did not show ATPase activity.

3.3.2 A preparation of recombinant WT DJ-1 contains DJ-1-immunoreactive high molecular weight (high-MW) species.

Our next goal was to determine the molecular basis for the ATPase activity in our DJ-1 preparations. We hypothesized that DJ-1 forms a high molecular weight complex under oxidizing conditions, similar to Prx [195]. In addition, we hypothesized that the high MW form of DJ-1 has ATPase activity, based on our observation that the ATPase activity in our DJ-1 preparations could be removed by filtration. To address this hypothesis, we first examined whether a portion of the DJ-1 in our recombinant protein preparations existed as a high-MW complex. We separated high-MW species using two well-established separation methods, ultracentrifugation and sucrose gradient ultracentrifugation.

As an initial approach to separate WT DJ-1 high-MW species, the dialyzed protein was ultra-centrifuged. The dimeric DJ-1 fraction (supernatant) was removed by careful pipetting, while the high-MW species fraction (pellet) at the bottom of the tube was resuspended in buffer. The supernatant and pellet fractions and an aliquot of WT DJ-1 with mixed species (not ultracentrifuged 'uncentr') were fractionated on an SDS PAGE gel and analyzed via Western blotting with an antibody specific for DJ-1. Our results showed evidence of higher amounts of DJ-1-positive high molecular weight bands in the pellet fraction compared to the supernatant (S/N) fraction. In addition, there was a decreased intensity of monomeric DJ-1 in the pellet fraction (Fig 3.3).

As an alternative method, we analyzed our DJ-1 samples via sucrose gradient centrifugation. Dialyzed WT DJ-1 was overlaid on the top-most sucrose fraction

(5%). After centrifugation, three fractions from each of several zones of the gradient (corresponding to sucrose percentages of 20%, 30%, and 50%, v/v) were collected, and an aliquot of each fraction (500 µL) was analyzed via Western blotting. Our results showed higher levels of high-MW species in the 50% sucrose fraction compared to the other fractions (Fig 3.4). Taken together, our results suggest that our DJ-1 preparation contains DJ-1-immunoreactive high-MW.

3.3.3 The high MW fraction from our WT DJ-1 preparation contains ATPase activity.

Our next goal was to examine whether the ATPase activity observed in our preparations of human WT DJ-1 was associated with the high-MW species described in the previous section. Based on our earlier observation that DJ-1 samples lost the ability to hydrolyze ATP upon filtration, we hypothesized that the ATPase activity would track with fractions enriched with high-MW species. To address this hypothesis, high-MW species were separated using the two ultracentrifugation methods described above.

The fractions obtained via ultracentrifugation (non-sucrose gradient) were analyzed for the release of inorganic phosphate in the absence or presence of ATP using a continuous fluorescence assay (PNP). The results showed that the pellet fraction had a higher ATPase activity, whereas the S/N fraction showed no ATPase activity (Fig 3.5).

Data from the sucrose gradient ultracentrifugation analysis revealed that fractions at the bottom of the gradient (with ~40-45% sucrose) had a relatively high level of

ATPase activity, whereas fractions with lower percentages of sucrose showed markedly less ATPase activity (Fig 3.6).

Taken together, these results suggest that a high-MW, DJ-1-immunoreactive species in our preparations of recombinant human WT DJ-1 purified from *E.coli* has ATPase activity.

3.3.4 Sucrose fractions with ATPase activity contain ring-like structures.

Previous studies have reported that DJ-1 acts a molecular chaperone [141, 142], and a number of molecular chaperones have been shown to form high molecular species [194]. The next set of experiments was designed to determine the structural properties of high-MW weight protein species in sucrose fractions with ATPase activity. As one possibility, we hypothesized that DJ-1 might undergo self-assembly to form a high-MW chaperone, perhaps under oxidizing conditions as described for various peroxiredoxins [195], and such a DJ-1 high-MW chaperone might have ATPase activity. Alternatively, we considered the possibility that DJ-1 might interact with another high MW protein with ATPase activity. To address these hypotheses, we analyzed the fractions obtained by sucrose gradient ultracentrifugation via electron microscopy (EM). Our results showed that fractions with the highest percentage of sucrose (40-45%), which also showed high ATPase activity (see above), consisted of ring-like structures with a diameter of approximately 20-50 nm (Fig 3.7). In contrast, these structures were absent from fractions with lower percentages of sucrose and negligible ATPase activity. Similarly, we did not observe ring-like structures in the

supernatant obtained via ultracentrifugation of a DJ-1 preparation in the absence of sucrose (this supernatant fraction consisted mainly of DJ-1 homodimer and did not show any ATPase activity). Moreover, a sample of purified GST lacked the ring-like structures (data not shown).

From these findings, we infer that high-MW species present in fractions with ATPase activity consist of ring-like structures, whereas these structures are absent from fractions containing homodimeric DJ-1, which also lack ATPase activity. Our data show that the ATPase activity present in the high-MW fraction of our DJ-1 preparations tracks with ring-like structures observable by EM, raising the possibility that the ATPase activity could be associated with these structures.

3.3.5 Analysis of the high MW fraction of our DJ-1 preparation by mass spectrometry revealed the presence of *E. coli* F_1 ATP synthase subunits.

As mentioned above, we considered two hypotheses to account for the presence of DJ-1 protein and ATPase activity in a high MW fraction obtained from our DJ-1 preparation by sucrose gradient sedimentation: first, that DJ-1 might oligomerize to form a high MW chaperone with ATPase activity; and second, that DJ-1 might interact with another high-MW protein with ATPase activity. Two key findings led us to favor the second hypothesis: (i) we were unable to generate a high-MW form of DJ-1 with ATPase activity upon incubation under oxidizing or reducing conditions; and (ii) a preparation of the C106A mutant of DJ-1 also had ATPase activity, contrary to our prediction that the oxidation of this residue might play a

role in the conversion of DJ-1 to a high-MW form by analogy with the self-assembly mechanism of redox-sensitive peroxiredoxins [195].

To determine the protein composition of the high-MW (high sucrose) fraction from our DJ-1 preparation, a sample of the high MW fraction was subjected to tryptic digestion and analyzed via mass spectrometry (MS) in collaboration with Dr. Andy Tao (Purdue University). A sample of recombinant (purified) GST was also analyzed via MS as a control. The peptide masses obtained from the MS analysis were searched against three databases: human, *E.coli* and *Schistosoma japonicum* (the species from which is derived the GST tag). The MS data revealed the presence of DJ-1 in the human database search, with a score of 93.41. The *E.coli* database search revealed the presence of *E. coli* F_1 ATP synthase subunits: alpha α, beta β, delta δ, and gamma γ. Highest scores were obtained for the β and α subunits (Table 3.1), which are known to assemble into ring-like structures. Other *E. coli* proteins revealed by the MS analysis included F_0 subunit b, in addition to a number of other ATP-binding proteins (Table 3.1). The *Schistosoma japonicium* database search revealed the presence of GST with a score of 210.52. Since we did not observe any ATPase activity with GST (Fig 3.8), we predicted that we would not detect ATPase subunits in the GST mass spec data. This was confirmed. These results suggest that the proteins in the high-MW fraction of our DJ-1 preparation include DJ-1, *E.coli* F_0 and F_1 ATPase subunits, other ATP-binding proteins, and GST. Therefore, we concluded that (i) DJ-1 might be interacting with other *E.coli* proteins in our recombinant protein preparation to form a complex that has ATPase activity and

potentially exists as ring-like structures and (ii) purified GST protein lacked the ATPase activity.

3.3.6 Analysis of the high MW fraction of our DJ-1 preparation by Western blotting revealed the presence of the beta subunit of *E. coli* F_1 ATP synthase (ATPB).

The MS data presented above suggested that *E. coli* ATP synthase was present in the high MW fraction of our DJ-1 preparation. To obtain additional evidence in support of this idea, we examined the fractions obtained by sucrose-gradient sedimentation of our DJ-1 preparation via Western blotting. The primary antibodies used in this analysis were specific for human DJ-1 or the *E. coli* F_1 ATP synthase beta subunit (ATPB). The results showed that ATPB (50 kDa) was present primarily in the 15% sucrose gradient fractions, but also in the 50% sucrose fractions and to a lesser extent in the 20% and 30% sucrose fractions (Fig 3.9). These results confirm that ATPB is indeed present in the high MW fraction of our DJ-1 preparation, mostly in an unassembled state detected in the 15% sucrose fraction but also in a higher-MW state (presumably as part of assembled F_1 ATP synthase) detected in the 50% sucrose fraction [202].

3.3.7 The ATPase activity in the high-MW fraction of our DJ-1 preparation is inhibited by sodium azide and piceatannol.

Sodium azide and piceatannol are two known classical F_1 ATPase inhibitors [203]. To address whether the ATPase activity in our DJ-1 preparation could be associated with assembled F_1 ATPase, we tested whether the ATPase activity was sensitive to either sodium azide or piceatannol. A preparation of

recombinant DJ-1 was analyzed for ATPase activity with or without sodium azide (1 mM and 5 mM) in the PNP assay, or in the absence or presence of piceatannol in the MG assay. The results showed that sodium azide and piceatannol both abolished the ATPase activity (Fig.3.10 and Fig 3.11). These results suggest that the ATPase activity in our DJ-1 preparation could originate from assembled F_1 ATPase.

3.3.8 Evidence of a potential interaction between DJ-1 and *E coli* F_1 ATP synthase.

The next sets of experiments were designed to test the hypothesis that DJ-1 interacts with F_1 ATP synthase. To address this hypothesis, the supernatant fraction of our DJ-1 preparation (obtained after ultracentrifugation in the absence of sucrose to remove the high-MW species) was incubated with or without purified bacterial F_1 ATPase (obtained from Dr. Ahmad Zulfiqar, Kirksville College of Osteopathic Medicine, MO). The incubation mix was fractionated by sucrose gradient sedimentation. The sucrose gradient fractions were analyzed via Western blotting using primary antibodies specific for DJ-1 and the *E. coli* F_1 ATP synthase beta subunit. The results showed that DJ-1 sediments to fractions with a higher percentage of sucrose after incubation with F_1 ATPase, as evidenced by the presence of DJ-1 immunoreactive bands in lanes corresponding to the 30-50 % sucrose fractions (Fig 3.12). In contrast, DJ-1 was not detected in the same sucrose fractions obtained upon sedimentation of a sample of DJ-1 incubated without F_1 ATP synthase (Fig 3.13). As expected, most of the *E. coli* F_1 ATP synthase sedimented to fractions with a high percentage of sucrose as

inferred from the sedimentation of the *E. coli* F_1 ATP synthase beta subunit. Therefore, we conclude that homodimeric DJ-1 present in the supernatant fraction might interact with *E. coli* F_1 ATP synthase to form a high-MW complex.

3.3.9 DJ-1 in the high MW fraction has a low level of C106 oxidation.

Based on the results above, we investigated whether the oxidation of DJ-1 modulates the protein's interaction with *E coli* F_1 ATP synthase. To address this hypothesis, DJ-1 (supernatant fraction) was incubated with *E coli* F_1 ATP synthase at room temperature, and the mixture was analyzed via sucrose gradient sedimentation. Sucrose fractions were analyzed via Western blotting using antibodies specific for the oxidized form of DJ-1 or total DJ-1. Our results showed that DJ-1 (detected with a total DJ-1 antibody) incubated with *E coli* F_1 ATP synthase sediments to higher sucrose fraction (Fig 3.14), while oxidized DJ-1 (detected with an antibody specific for oxidized DJ-1) does not sediment to higher fractions (Fig 3.15). These findings suggest that the oxidation state of DJ-1 modulates its interaction with F_1 ATPase, and that reduced DJ-1 more readily interacts with *E coli* F_1 ATPase.

3.4 Discussion

DJ-1 has been shown to be involved in many neuroprotective functions, but its biochemical function still remains to be elucidated. In this chapter we described evidence of a possible biochemical function of DJ-1 involving the protein's

interaction with *E.coli* F_1 ATPase, a protein complex that is structurally and functionally well conserved with F_1 ATPase with eukaryotic mitochondria.

3.4.1 A High MW fraction of our DJ-1 preparation is DJ-1-immunoreactive, has ATPase activity and contains ring-like structures

Our results revealed that ATPase activity in our DJ-1 preparation was abolished by filtration. Sucrose gradient sedimentation and Western blot analysis showed the presence of high-MW species immunoreactive with DJ-1 antibody in our preparations of recombinant, human WT DJ-1. In addition, we found that the high-MW fraction had ATPase activity and contained ring-like structures that were visible by EM. Previous studies revealed that DJ-1 functions as a molecular chaperone [141, 142]. In addition the formation of high molecular weight structures by Prxs is modulated by oxidative stress, which can induce dramatic changes in quaternary structure [194] [195]. Accordingly, we inferred as one possibility that DJ-1 might form a high-MW species that functions as an ATP-dependent molecular chaperone. However, two observations contradicted this hypothesis: homodimeric DJ-1 fractions without the high-MW species (after separation via sucrose gradient ultra-centrifugation, SEC, and filtration) did not show any ATPase activity or form ring-like structures, even after incubation, and the C106A mutation had no effect on ATPase activity (data not shown). For this reason, we turned our attention to analyzing the interaction of DJ-1 with *E. coli* proteins that might be responsible for the ATPase activity.

3.4.2 DJ-1 positive Interacts with *E.coli* F_1 ATP synthase to form high-MW species.

MS analysis of the high-MW fraction isolated by sucrose gradient centrifugation revealed the presence of *E. coli* F_1 ATP synthase subunits, which are known to assemble into ring-like structures [204]. A previous proteomics study revealed that DJ-1 interacts with the α- and β-subunits of F_1 ATP synthase in a rat mesencephalic cell line [205]. The fact that the high MW fraction hydrolyzes ATP and GTP, but not CTP, TTP, or ADP, is consistent with the idea that the ATPase activity in our DJ-1 preparation originates from assembled F_1 ATP synthase [206]. Moreover, the high-MW fraction exhibited ATPase activity that was inhibited by sodium azide and piceatannol, two inhibitors of F_1 ATP synthase. In addition, we found that homodimeric DJ-1 sedimented to fractions with a higher percentage of sucrose after incubation in the presence versus the absence of *E.coli* F_1 ATP synthase. Collectively, these results imply that DJ-1 interacts with E. coli F_1 ATP synthase. Importantly, this proposed interaction is specific to DJ-1 because a sample of GST purified using the same bacterial expression system did not show any ATPase activity. Our findings suggest that DJ-1 may interact with F_1 ATP synthase because this interaction may be a key component of the DJ-1 chaperone function. MS results suggested that recombinant human DJ-1 might interact with other bacterial proteins, including *E. coli* F_0 ATP synthase.

Although our studies were carried out with *E.coli* F_1 ATP synthase, we would predict that DJ-1 might interact in a similar way with F_1 ATP synthase from eukaryotic mitochondria given that the bacterial and eukaryotic enzymes have a

high degree of structural and functional similarity [207]. DJ-1 has been described as an atypical Prx that scavenges hydrogen peroxide (H_2O_2) via oxidation of Cys106 [190]. The interaction between DJ-1 and ATP synthase (if validated) would represent a new development in our understanding of how the protein modulates mitochondrial function.

3.4.3 Unoxidized DJ-1 is the form of the protein that apparently interacts with *E.coli* F_1 ATP synthase.

A previous study showed that under conditions of oxidative stress, cysteine 106 (Cys 106) of DJ-1 becomes oxidized to the sulfinic and sulfonic acids (Cys-SO_2H and Cys-SO_3H, respectively) [208]. We found that oxidized DJ-1 does not readily interact with F_1 ATP synthase, suggesting that the interaction of DJ-1 with *E.coli* F_1 ATPase is modulated by C106 oxidation. This observation suggests (as one possibility) that DJ-1 forms a disulfide bond with one of the F_1 ATP synthase subunits, a mechanism that has precedence in disulfide bond formation between DJ-1 and Ask1 kinase [121]

3.5 Conclusion

The data outlined in this chapter suggest that recombinant human DJ-1 (and in particular the reduced form of the protein) interacts with *E. coli* F_1 ATP synthase, thereby enhancing ATP synthase function (e.g. perhaps via a mechanism involving DJ-1 chaperone activity). We expect that a similar interaction is likely to exist between DJ-1 and eukaryotic F_1 (or F_0F_1) ATP synthase. Such an

interaction could play an important role in alleviating mitochondrial dysfunction and the resulting oxidative stress in PD.

A

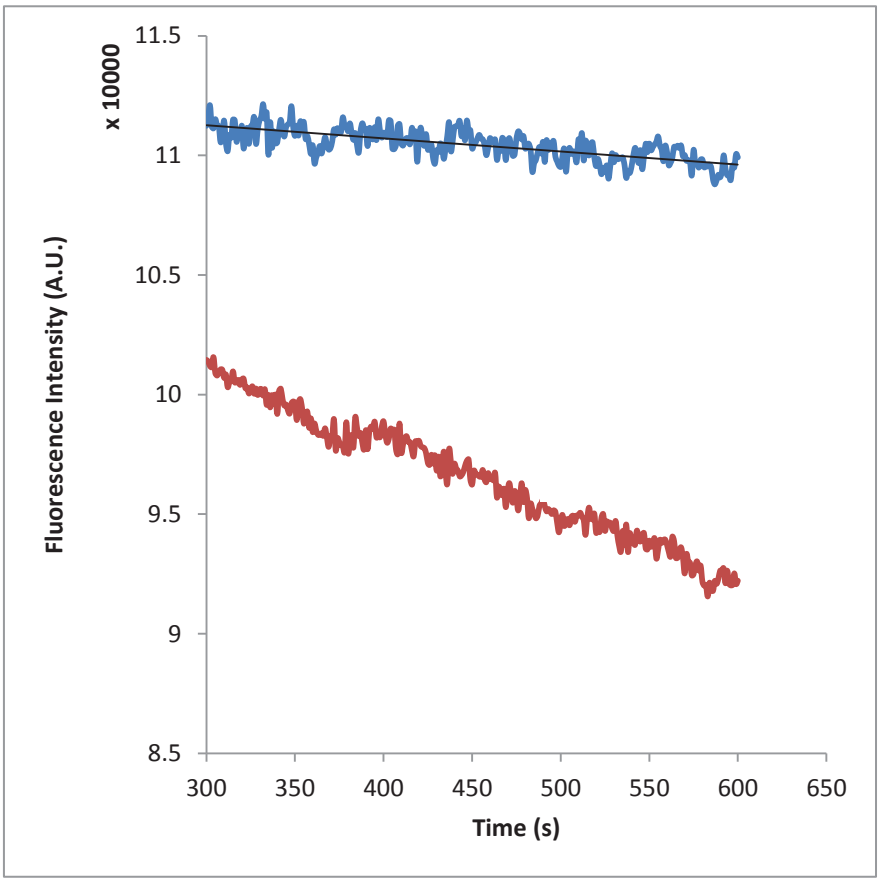

B

Sample	Slope	R^2
WT DJ-1 Filtered + ATP	-5.4	0.52
WT DJ-1 Unfiltered + ATP	-29.3	0.97

Figure 3.1-A ATPase activity associated with purified DJ-1 is eliminated upon filtration.

A. WT DJ-1 was dialyzed against 50 mM Tris-HCl, 50 mM NaCl, 1 mM $MgCl_2$, pH 7.5 . A portion of the protein was filtered through a 100 kDa filter. Equal amounts (15 µg) of the filtered and unfiltered proteins were used in the PNP assay. ATP hydrolysis was monitored by the enzymatic conversion of 7-methylguanosine to 7-methylguanine, which has a lower quantum yield, via a continuous fluorimetric assay in the absence or presence of 1 mM ATP. Excitation, 300 nm; emission, 410 nm. **B.** Table showing the slope and R^2 values for the best-fit curves through the data. N=1

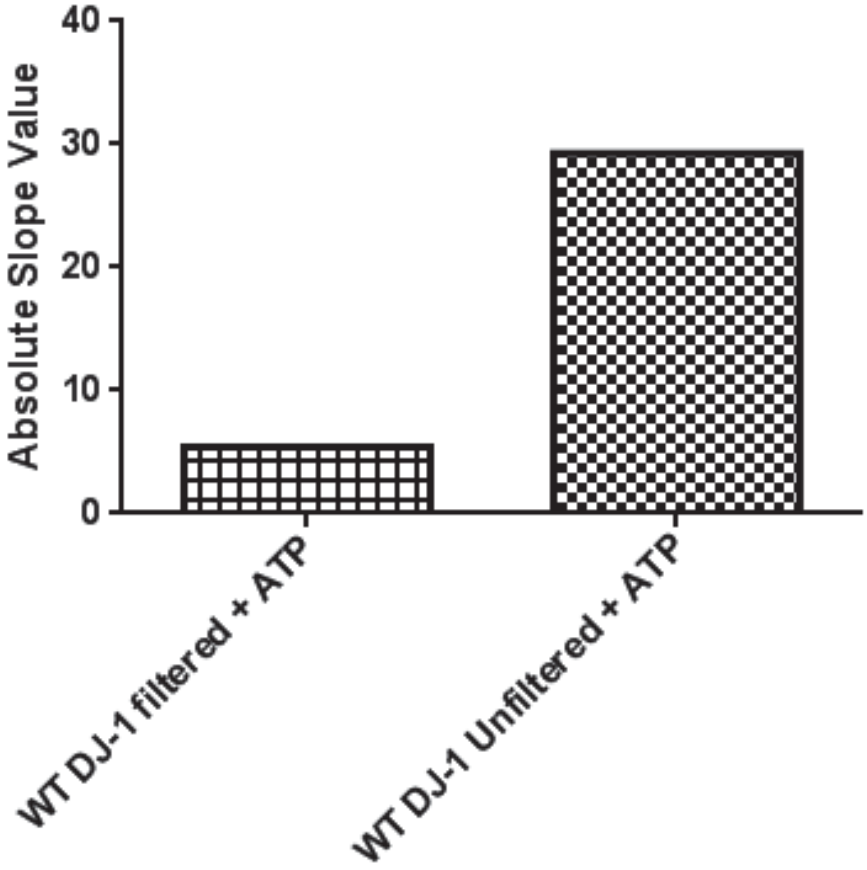

Figure 3.1-C. ATPase activity associated with purified DJ-1 is absent in the filtrate.

Absolute slope values from panel B were plotted for each sample.

A

Sample	Slope	R^2
Uncentrifuged + ATP	-45.6	0.99
Dimer from S200 column + ATP	-12.3	0.92
Dimer (2x) form S200 column + ATP	-11.1	0.89
Uncentrifuged - ATP	-2.9	0.39

B

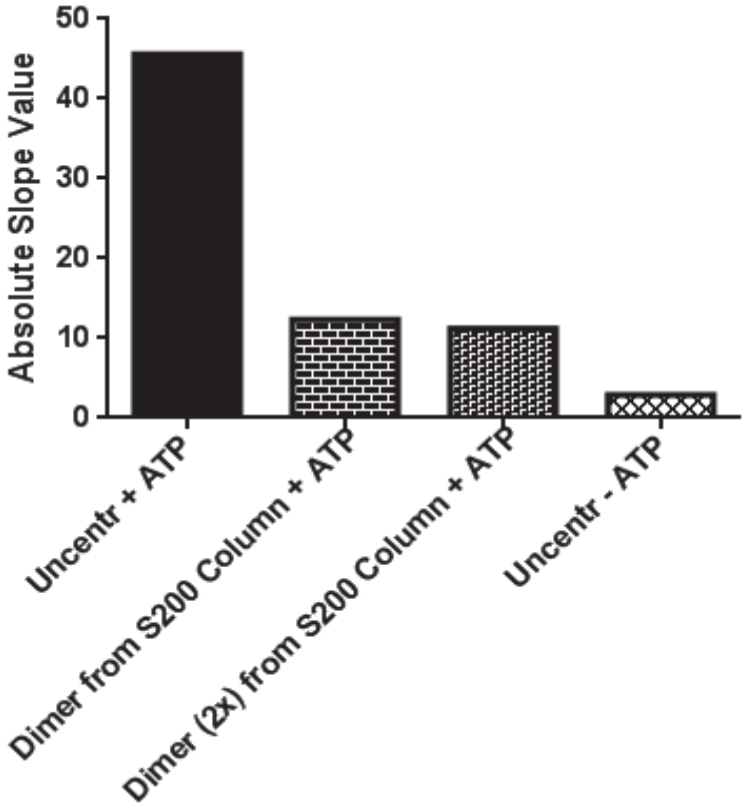

Figure 3.2 ATPase activity associated with purified DJ-1 is absent in the homodimer fraction.

A. WT DJ-1 was dialyzed against 50 mM Tris-HCl, 50 mM NaCl, 1 mM $MgCl_2$, pH 7.5. The protein was loaded onto a Superdex column, S200 and elution peaks were collected by monitoring the ultraviolet absorbance detector. Equal amounts of protein (15 µg) from the S200 column were used in the PNP assay. ATP hydrolysis was monitored by the enzymatic conversion of 7-methylguanosine to 7-methylguanine, which has a lower quantum yield, via a continuous fluorimetric assay in the absence or presence of 1 mM ATP. Excitation, 300 nm; emission, 410 nm. **B.** Absolute slope values from panel A were plotted for each analyzed sample. N=1

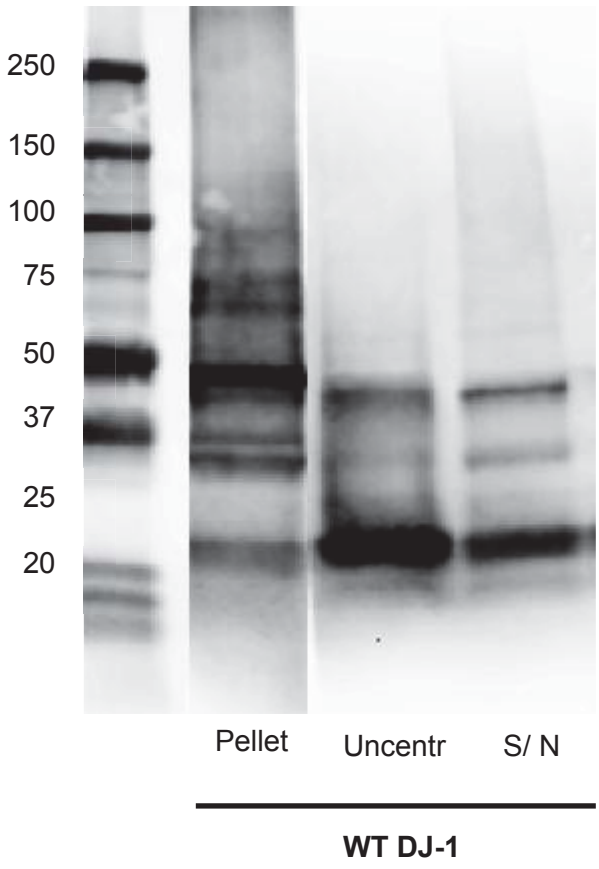

Figure 3.3 WT DJ-1 forms high molecular weight species.

WT DJ-1 was ultracentrifuged at 47,000 rpm (100,000 xg) at 4ºC for 2 h. The supernatant (S/N) was removed, and the pellet was resuspended in buffer. Equal amounts of protein (1 µg) (including the uncentrifuged protein, 'Uncentr') were then analyzed via Western blotting using a DJ-1 specific primary antibody (1:4000). N=2

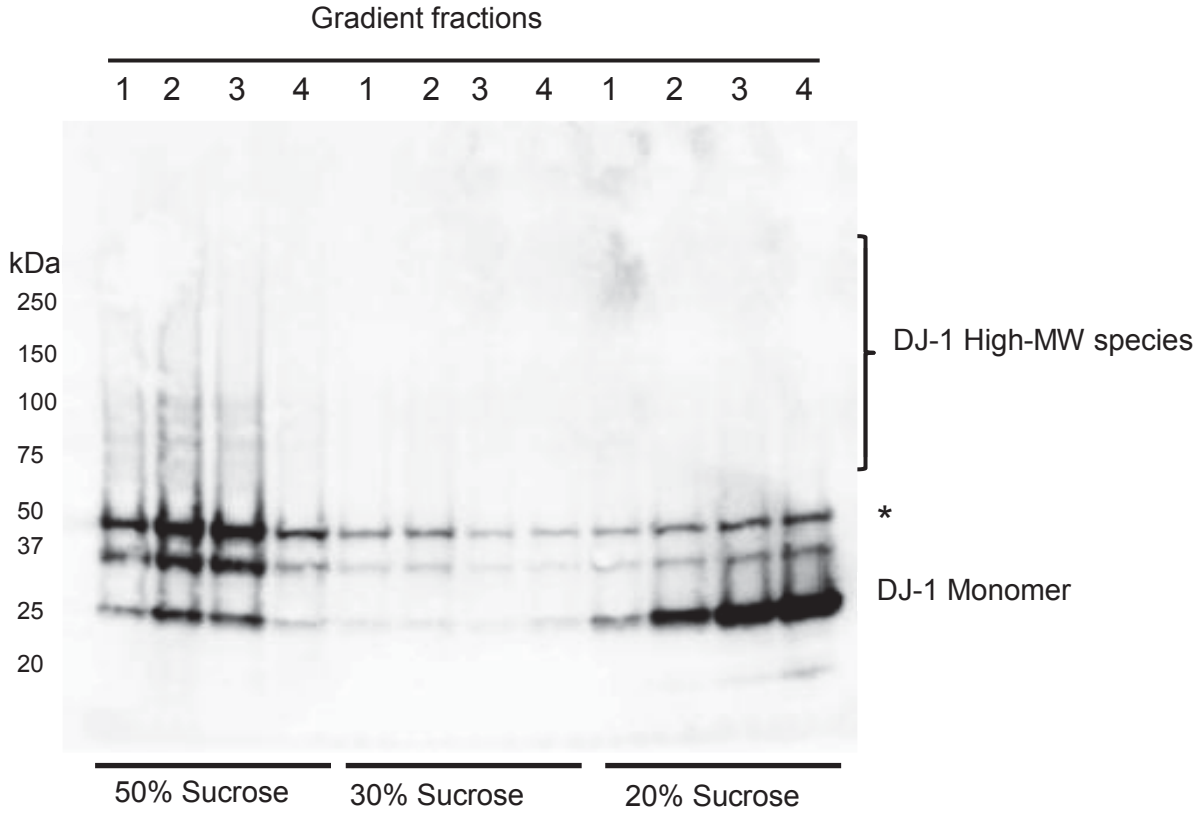

Figure 3.4 WT DJ-1 forms high molecular weight species.

DJ-1 high-MW species were separated via ultracentrifugation through a sucrose gradient (20-50% w/v) at 40,000 rpm (274,000 x g) for 18 h at 4 ºC. Gradient fractions were collected and analyzed by SDS-PAGE on a 4-20% gradient gel. The proteins were transferred to a PVDF membrane and probed with an antibody specific for DJ-1. Asterisk indicates a band that could correspond to homodimeric DJ-1 or GST DJ-1. N=3

A

Sample	Slope	R^2
Uncentrifuged - ATP	-7.4	0.85
Buffer - ATP	-3.8	0.64
Uncentrifuged + ATP	-34	0.99
Pellet + ATP	-31	0.99
S/N + ATP	-7.5	0.86
Pellet - ATP	-4.4	0.72
S/N - ATP	-2.6	0.55
Buffer + ATP	-4	0.71

B

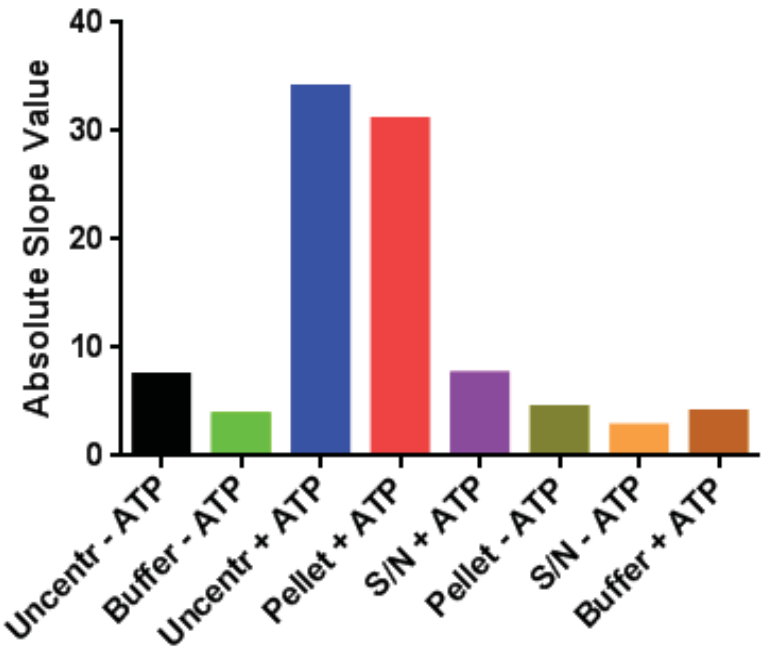

Figure 3.5 DJ-1 associated high molecular weight fractions have ATPase activity.

A. WT DJ-1 was dialyzed against 50 mM Tris-HCl, 50 mM NaCl, 1 mM $MgCl_2$, pH 7.5. The protein was ultracentrifuged at 47,000 rpm (100,000 xg) at 4ºC for 2 h. The supernatant (S/N) was removed, and the pellet was resuspended in buffer. Equal amounts of protein (15 µg) (including the uncentrifuged protein, 'Uncentr') were used in the PNP assay. ATP hydrolysis was monitored by the enzymatic conversion of 7-methylguanosine to 7-methylguanine, which has a lower quantum yield, via a continuous fluorimetric assay in the absence or presence of 1 mM ATP. Excitation, 300 nm; emission, 410 nm. **B.** Absolute slope values from panel A were plotted for each analyzed sample. N=2

A

Sample	Slope	R^2
DJ-1 No Sucrose + ATP	-51.6	0.99
DJ-1 No Sucrose - ATP	-7.4	0.83
DJ-1 50% Sucrose + ATP	-53.1	0.99
DJ-1 50% Sucrose - ATP	-13	0.9
DJ-1 30% Sucrose + ATP	-25.2	0.98
DJ-1 20% Sucrose + ATP	-17.6	0.95
DJ-1 15% Sucrose + ATP	-15.6	0.94
DJ-1 5% Sucrose + ATP	-16.5	0.94
50% Sucrose + ATP	-17.9	0.92

B

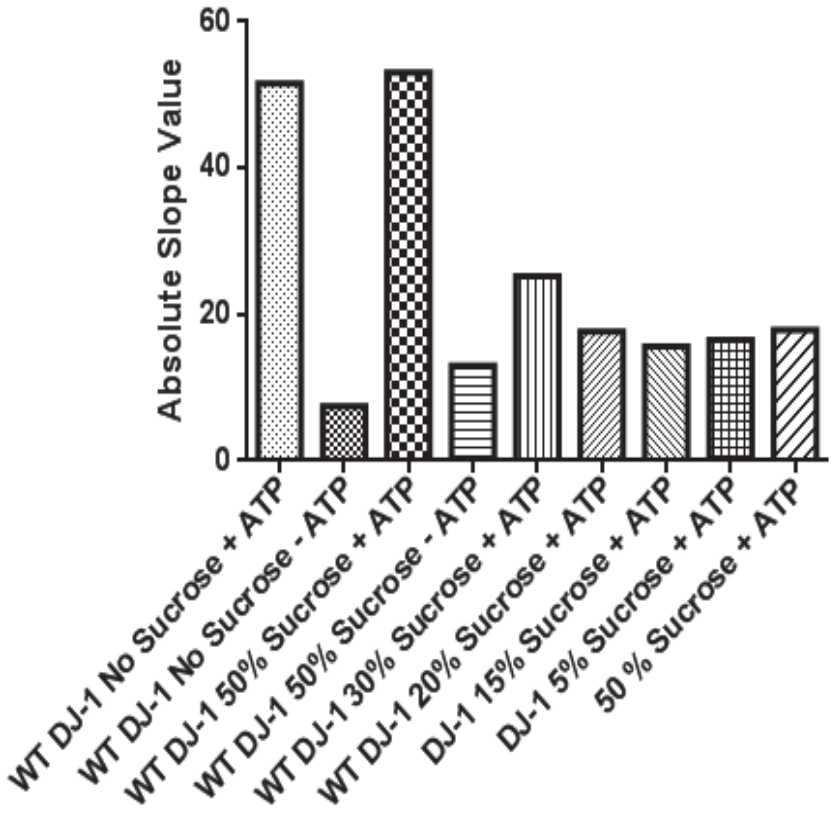

Figure 3.6 DJ-1 fractions with a high sucrose percentage had a high ATPase activity.

A. WT DJ-1 was dialyzed against 50 mM Tris-HCl, 50 mM NaCl, 1 mM $MgCl_2$, pH 7.5. The protein sample was loaded on a 5% sucrose (top most sucrose percentage layer), and ultracentrifugation was carried out at 40,000 rpm (274,000 xg) for 18 h at 4 ºC. Fractions of about 500 µL each were collected from the bottom of the tube. Equal amounts of protein (15 µg) were used in the PNP assay. ATP hydrolysis was monitored by the enzymatic conversion of 7-methylguanosine to 7-methylguanine, which has a lower quantum yield, via a continuous fluorimetric assay in the absence or presence of 1 mM ATP. Excitation, 300 nm; emission, 410 nm. **B.** Absolute slope values from panel A were plotted for each analyzed sample. N=2

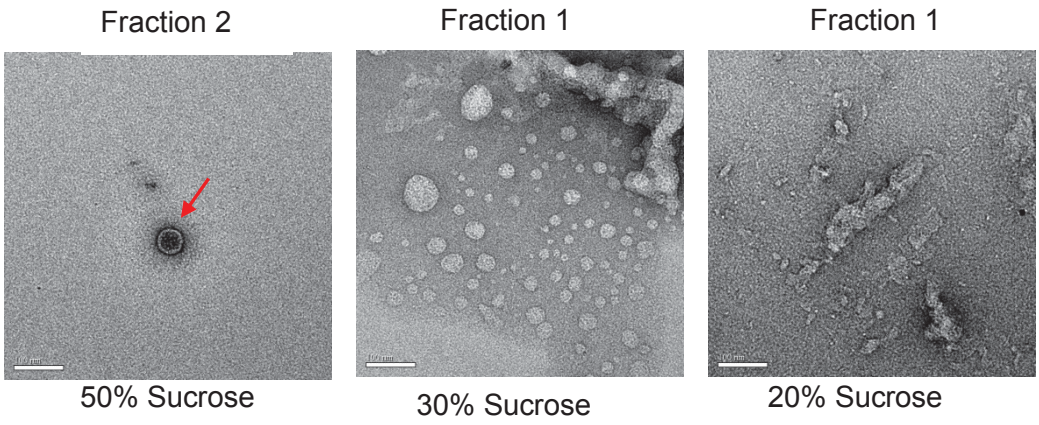

Figure 3.7 WT DJ-1 oligomer consists of ring-like structures.

Fractions collected from a sucrose gradient (Figure 3.6) (10 µL) were deposited on carbon-coated copper grids and negatively stained using 2 % uranyl-acetate. The images were taken using an electron microscope. Collaboration with Dr. Stanciu's lab. Ring-like structures (arrow) were only present in the 50% sucrose fraction. N=2

A

Sample	Slope	R^2
DJ-1 + ATP	-40.3	0.99
GST + ATP	-19.8	0.96
DJ-1 - ATP	-17.4	0.95
Buffer + ATP	-20.1	0.95
GST - ATP	-14.7	0.94

B

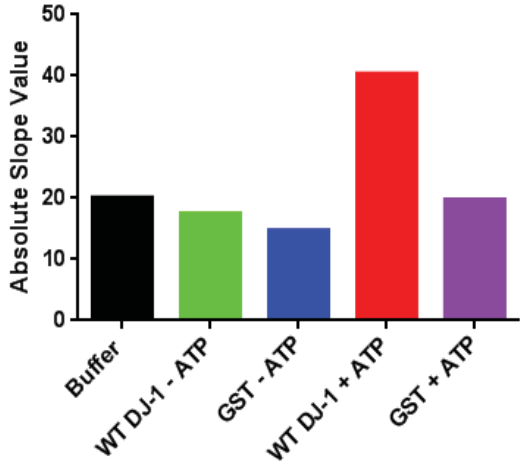

Figure 3.8 GST lacks ATPase activity.

A. GST was dialyzed against 50 mM Tris-HCl, 50 mM NaCl, 1 mM $MgCl_2$, pH 7.5. Equal amounts of protein (15 µg) were used in the PNP assay. ATP hydrolysis was monitored by the enzymatic conversion of 7-methylguanosine to 7-methylguanine, which has a lower quantum yield, via a continuous fluorimetric assay in the absence or presence of 1 mM ATP. Excitation, 300 nm; emission, 410 nm. **B.** Absolute slope values from panel A were plotted against each analyzed sample. N=1

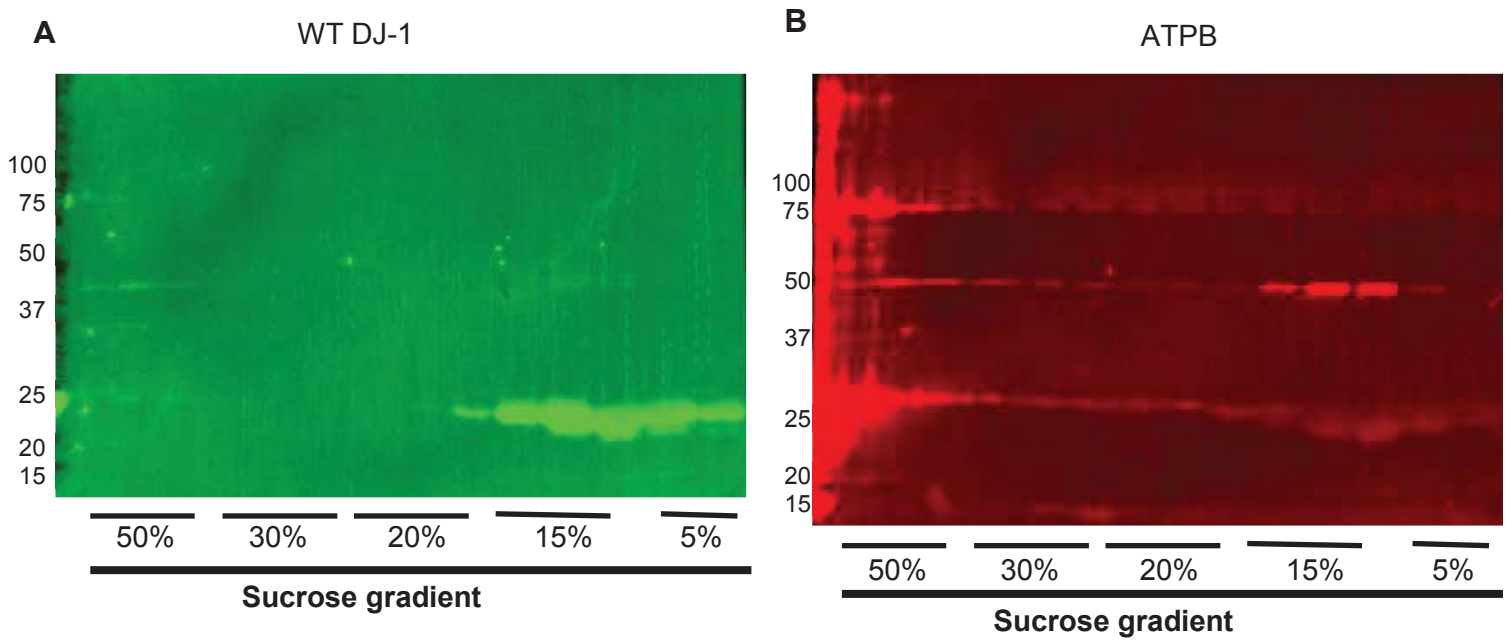

Figure 3.9 WT DJ-1 sucrose fractions are immunoreactive for the *E.coli* ATPB subunit.

WT DJ-1 was dialyzed and separated via ultracentrifugation through a sucrose gradient (5-50% w/v) at 40,000 rpm (274,000 x g) for 18 h at 4 ºC. Gradient fractions were collected and analyzed by SDS-PAGE on a 4-20% gradient gel. The proteins were transferred to a PVDF membrane and probed with an antibody specific for DJ-1 (A) and E.coli ATPase beta subunit (ATPB) (B). N=2

A

Sample	Slope	R^2
Buffer	-7.26	0.85
WT DJ-1 - ATP	-7.56	0.82
WT DJ-1 + ATP	-68.87	0.97
WT DJ-1 + ATP + 1 mM Sodium azide	-18.81	0.98
WT DJ-1 + ATP + 5 mM Sodium azide	-17	0.97

B

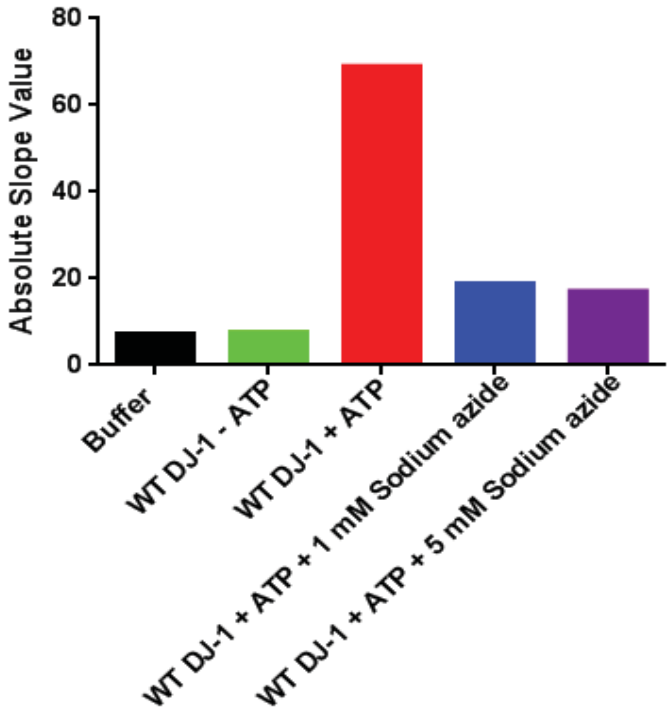

Figure 3.10 ATPase activity associated with purified DJ-1 is inhibited by sodium azide.

A. WT DJ-1 was dialyzed against 50 mM Tris-HCl, 50 mM NaCl, 1 mM $MgCl_2$, pH 7.5. Equal amounts of protein (15 µg) were used in the PNP assay. ATP hydrolysis was monitored by the enzymatic conversion of 7-methylguanosine to 7-methylguanine, which has a lower quantum yield, via a continuous fluorimetric assay in the absence or presence of 1 mM ATP with 1 mM and 5 mM sodium azide. Excitation, 300 nm; emission, 410 nm, **B.** Absolute slope values from panel A were plotted against each analyzed sample. N=1

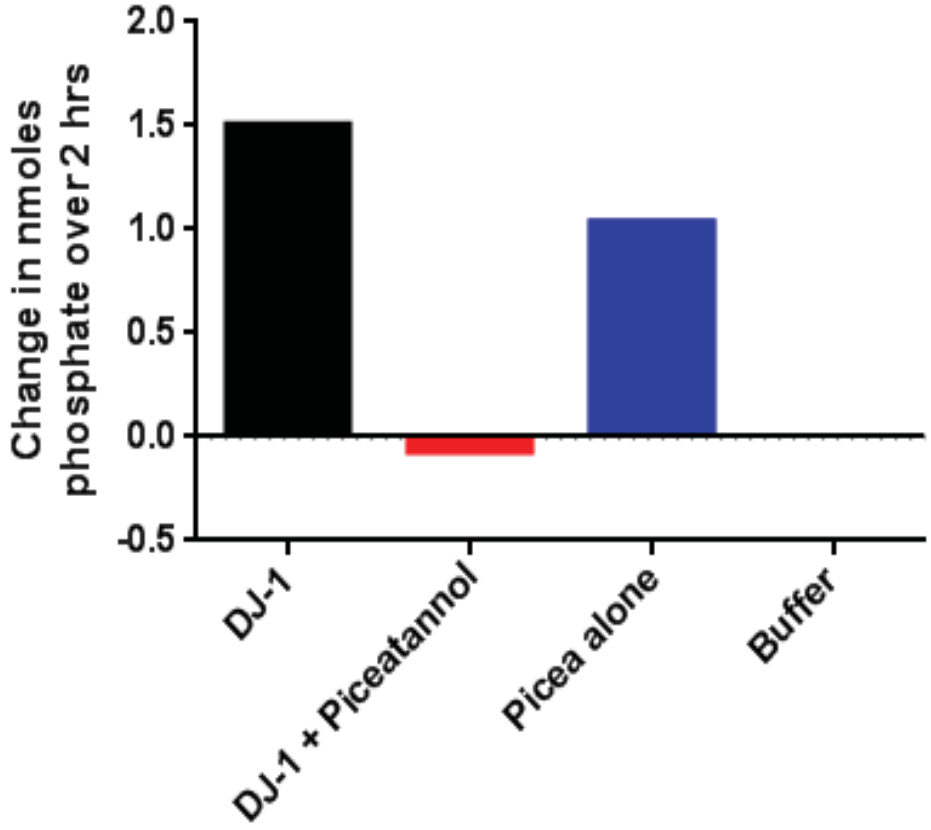

Figure 3.11 ATPase activity associated with purified DJ-1 is inhibited by piceatannol. WT DJ-1 protein (1 µg) was incubated in the presence of 1 mM ATP, with or without 20 µM piceatannol, for 2 h at 37 ºC. Hydrolysis of ATP was monitored using a malachite green assay designed to monitor the formation of a green molybdophosphoric acid complex, which reports on the free organic phosphate concentration. The values were obtained by reading the absorbance at 620 nm. N=1

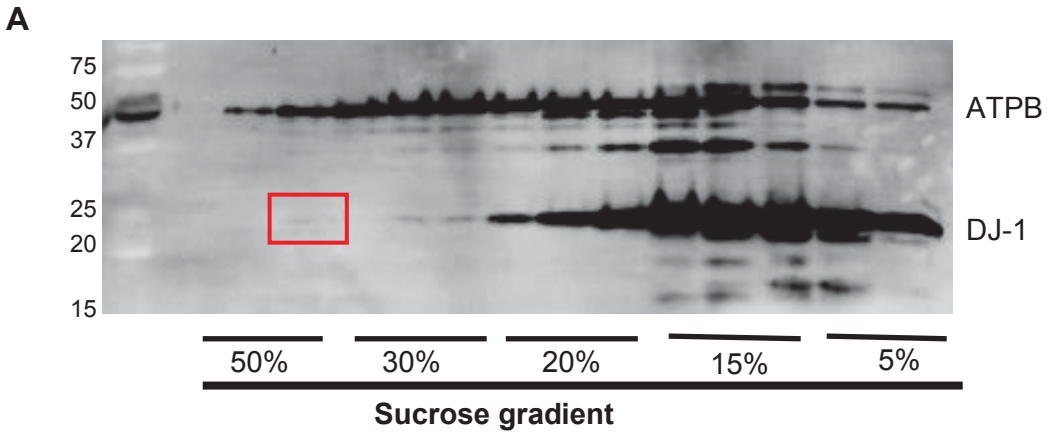

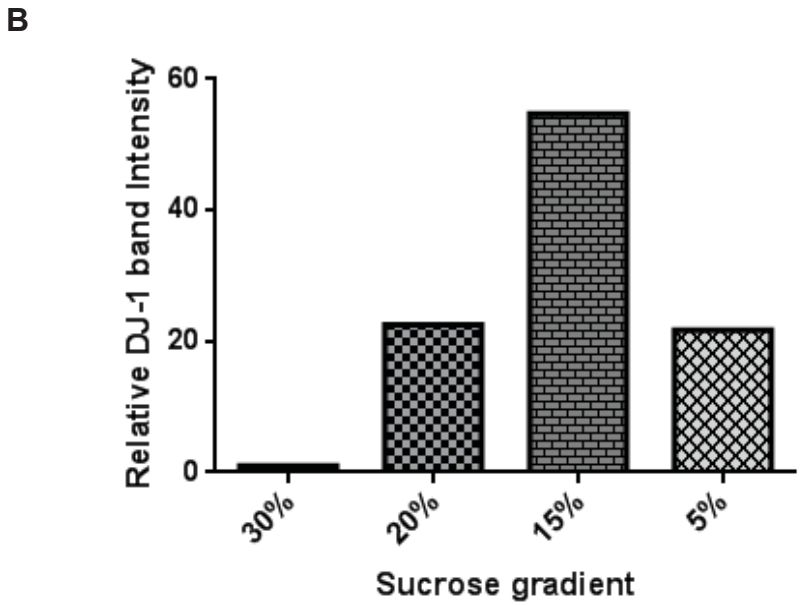

Figure 3.12 WT DJ-1 sediments to the 30-50% sucrose fractions after incubation with F_1 ATPase.

A. WT DJ-1 (supernatant) was incubated with *E.coli* F_1 ATPase at room temperature for 1 h. The complex formed was separated via ultracentrifugation using a sucrose gradient (5%-50% w/v) at 40,000 rpm (274,000 x g) for 16 h at 4 ºC. Gradient fractions were collected and analyzed by SDS-PAGE on a 4-20% gradient gel. The proteins were transferred to a PVDF membrane and probed with an antibody specific for DJ-1 and E.coli ATPase beta subunit (ATPB). **B**. Quantification of the relative DJ-1 band intensities in different percentages of sucrose using Image J**.** N=1

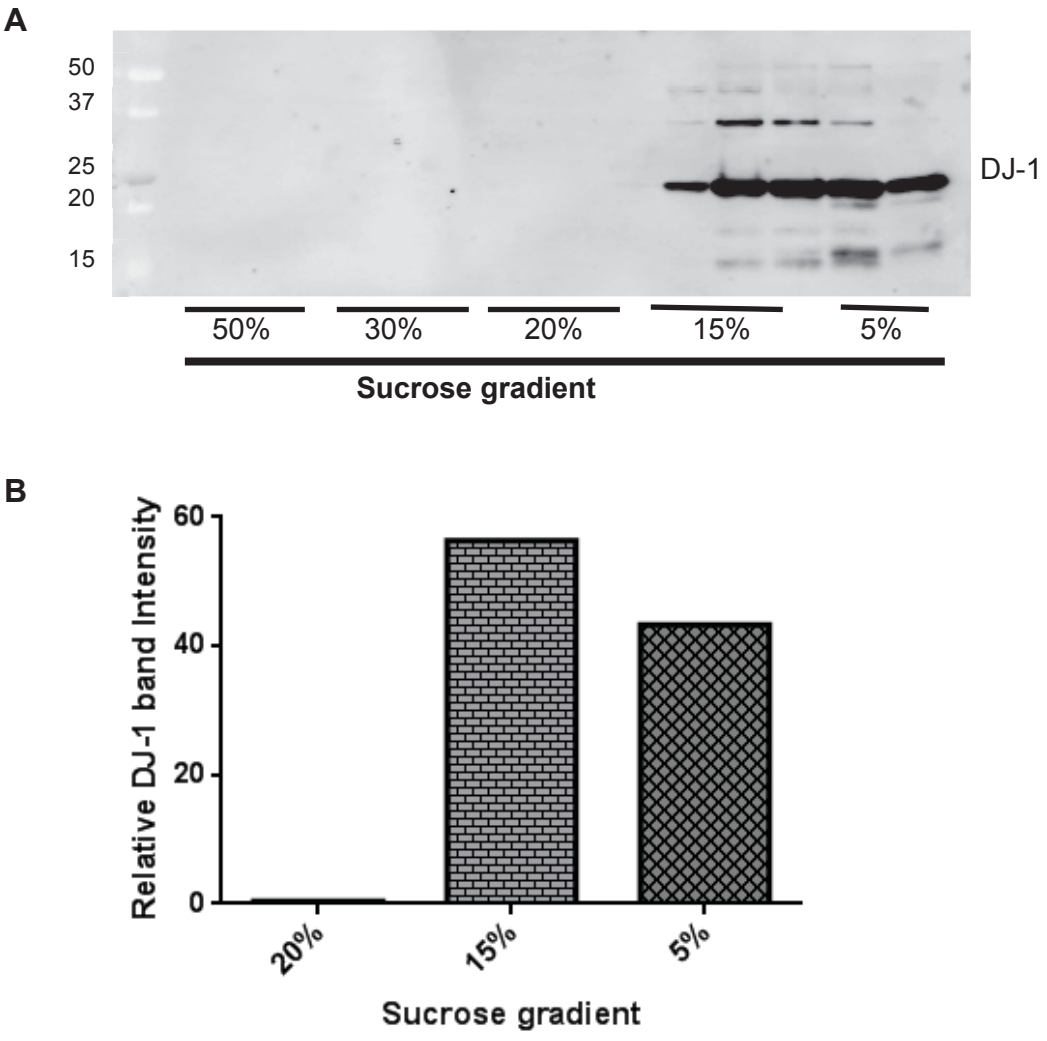

Figure 3.13 WT DJ-1 sediments to the 15% sucrose fractions without incubation with F_1 ATPase.

A. WT DJ-1 (supernatant) was incubated without *E.coli* F_1 ATPase at room temperature for 1 h. The sample was separated via ultracentrifugation using a sucrose gradient (5%-50% w/v) at 40,000 rpm (274,000 x g) for 16 h at 4 ºC. Gradient fractions were collected and analyzed by SDS-PAGE on a 4-20% gradient gel. The proteins were transferred to a PVDF membrane and probed with an antibody specific for DJ-1**. B.** Quantification of the relative DJ-1 band intensities in different percentages of sucrose using Image J. N=2

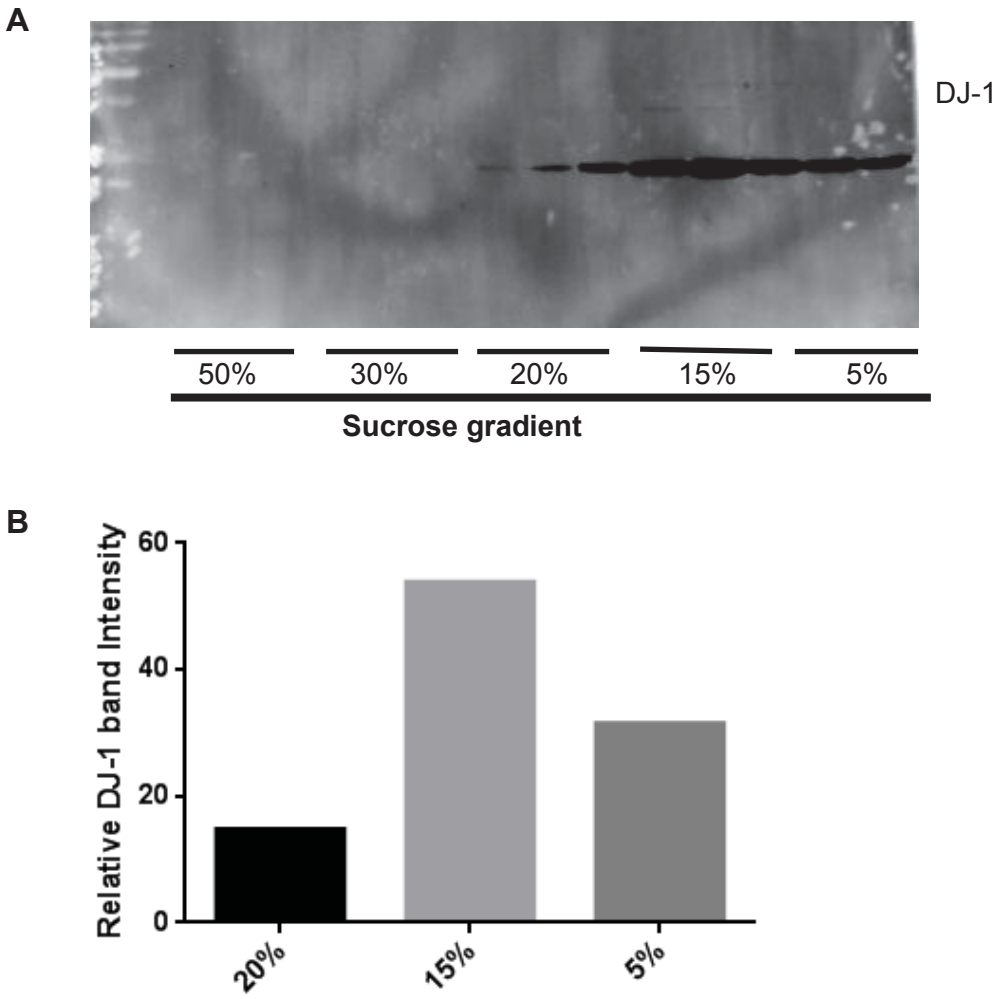

Figure 3.14 Unoxidized DJ-1 sediments with F_1 ATP synthase to higher sucrose fractions.

A. WT DJ-1 (supernatant) was incubated without *E.coli* F_1 ATP synthase at room temperature for 1 h. The sample was separated via ultracentrifugation using a sucrose gradient (5%-50% w/v) at 40,000 rpm (274,000 x g) for 16 h at 4 ºC. Gradient fractions were collected and analyzed by SDS-PAGE on a 4-20% gradient gel. The proteins were transferred to a PVDF membrane and probed with an antibody specific for DJ-1 (unoxidized). **B**. Quantification of the relative DJ-1 band intensities in different percentages of sucrose using Image J. N=1

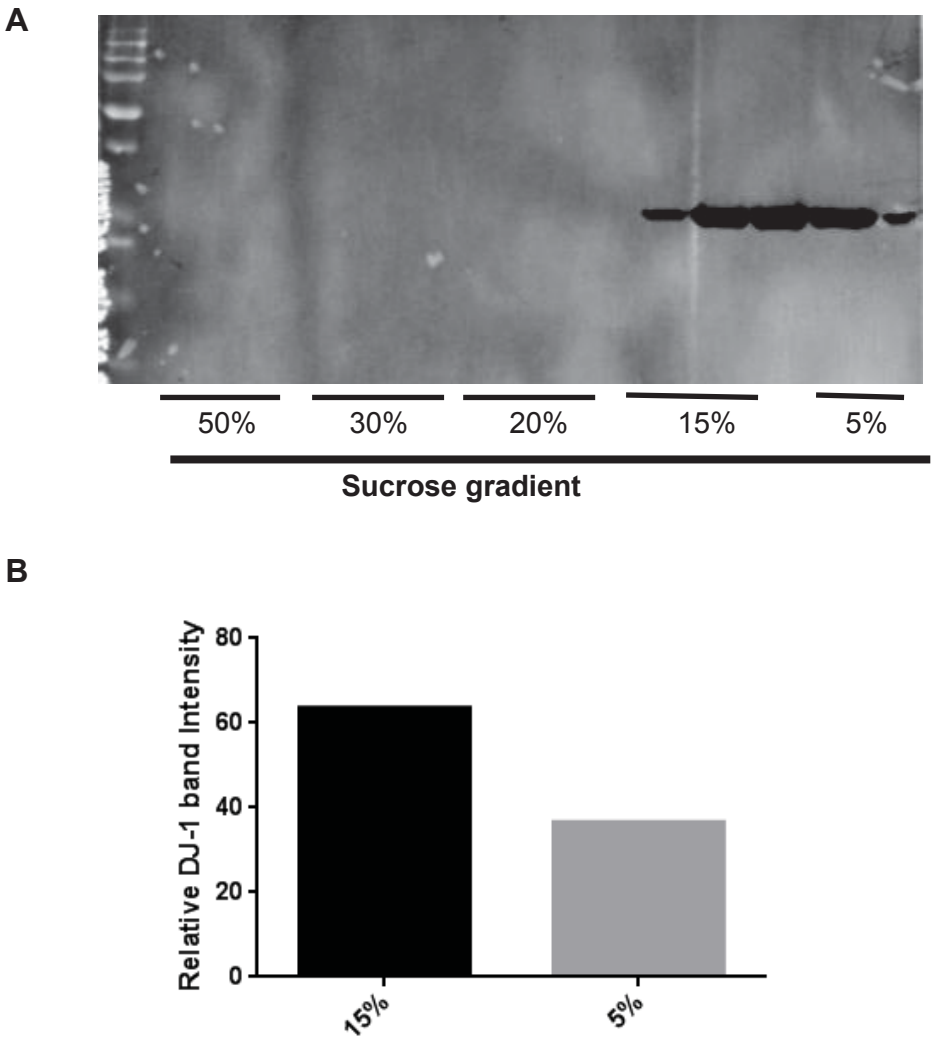

Figure 3.15 Oxidized DJ-1 does not sediment with F_1 ATPase to higher sucrose fractions.

A. WT DJ-1 supernatant was incubated without *E. coli* F_1 ATPase at room temperature for 1 h. The sample was separated via ultracentrifugation using a sucrose gradient (5%-50% w/v) at 40,000 rpm (274,000 x g) for 18 h at 4 ºC. Gradient fractions were collected and analyzed by SDS-PAGE on a 4-20% gradient gel. The proteins were transferred to a PVDF membrane and probed with an antibody specific for oxidized DJ-1. **B.** Quantification of the relative DJ-1 band intensities in different percentages of sucrose using Image J. N=1

Table 3.1 Proteomic analysis of DJ-1 high–MW species.

Recombinant human WT DJ-1 sucrose fractions enriched with high-MW species were trypsinized to generate peptides for mass spectrometry analysis. The table lists protein identified in the *E.coli* database

Description	Score	Coverage	# Proteins	# Peptides
Magnesium-transporting ATPase, P-type 1	360.80	47.55	1	46
ATP synthase subunit alpha	327.88	74.07	1	34
ATP synthase subunit beta	284.89	93.91	1	36
ATP-dependent zinc metalloprotease FtsH	271.81	59.01	1	34
ATP-dependent protease ATPase subunit HslU	223.17	58.92	1	27
ATP-dependent Clp protease ATP-binding subunit ClpX	187.67	74.76	1	26
ATP-binding component of serine protease	120.06	30.34	1	21
Uncharacterized ABC transporter ATP-binding protein yjjK	114.09	56.94	1	24
Lead, cadmium, zinc and mercury-transporting ATPase	105.42	36.20	1	19
ATP-dependent RNA helicase RhlB	104.31	54.63	1	20
ATP synthase subunit b	102.74	55.77	1	16
Oligopeptide transport ATP-binding protein oppD	90.14	51.63	1	13
ATP synthase gamma chain OS	79.60	60.98	1	15
ATP-binding component of transport system for maltose	70.79	50.94	1	16
ATP-independent RNA helicase dbpA	65.04	31.95	1	9
Oligopeptide transport ATP-binding protein oppF	61.99	41.32	1	13
ATP synthase subunit delta	52.95	52.54	1	7
Putative ATP-binding component of a transport system	46.84	65.80	1	9
Putative ATP-binding component of a transport system	45.41	45.23	1	8
ATP-dependent RNA helicase hrpA	40.58	9.92	1	10
ATP-binding component of high-	37.80	46.69	1	8
ATP-binding component of a membrane	34.28	42.79	1	6
Holliday junction ATP-dependent DNA helicase RuvB	33.30	34.23	1	7

Glutamine transport ATP-binding protein glnQ	30.50	33.75	1	6
Uncharacterized ABC transporter ATP-binding protein ydcT	27.07	23.44	1	5
Lipoprotein-releasing system ATP-binding protein lolD	24.52	26.18	1	4
Spermidine/putrescine import ATP-binding protein potA	23.89	26.46	1	6
ATP-binding/permease protein cydC	18.59	12.91	1	5
ATP-binding component of 3rd arginine transport system	18.46	33.06	1	4
Uncharacterized ABC transporter ATP-binding protein	15.34	9.74	1	2
Dipeptide transport ATP-binding protein dppF	14.15	11.68	1	3
ATP-dependent transporter sufC	13.45	22.18	1	4
Uncharacterized ABC transporter ATP-binding protein yejF	13.44	5.10	1	2
Methionine import ATP-binding protein metN	12.52	13.70	1	2
Uncharacterized GTP-binding protein yjiA	11.54	11.64	1	3
ATP-binding/permease protein cydD	10.52	6.80	1	2

CHAPTER 4: INTERPLAY OF DJ-1 AND ATP13A2 IN AUTOPHAGY

4.1. Introduction

The localization of ATP13A2 to lysosomal membranes may play a key role in modulating autophagy. A loss of ATP13A2 function has been shown to compromise lysosomal acidification, decrease proteolytic processing of lysosomal enzymes, and reduce the degradation of lysosomal substrates [175]. Because dysfunctional mitochondria are degraded via autophagy [144], impairment of autophagy resulting from ATP13A2 depletion is thought to trigger a buildup of defective mitochondria that produce increased ROS [144, 176]. Expression of ATP13A2 protects mammalian cells from oxidative stress and dysfunctional mitochondria [177]. In addition, loss of ATP13A2 function in human fibroblasts triggers decreased ATP production, mitochondrial genome integrity, and increased oxygen consumption and mitochondrial fragmentation [178].

Loss or mutation of mitochondrial DJ-1 induces an increase in ROS levels, a decrease in respiration rates and mitochondrial membrane potential (MMP), and a disruption of the critical balance between mitochondrial fusion and fission dynamics [144, 190, 209]. Oxidative stress in M17 human neuroblastoma cells results in

DJ-1 re-localization to mitochondria, a phenomenon associated with protection against cytotoxicity [118]. DJ-1 has also been shown to protect neurons from rotenone-induced oxidative stress and cell death [155, 156].

Aggregated aSyn is eliminated from cells via lysosomal autophagy [164, 175]. In addition, aSyn accumulation induces a buildup of ROS which have been shown to disrupt lysosomal membrane integrity, ultimately causing cell death [210, 211]. Furthermore, methamphetamine (METH), an addictive drug that elicits a PD-like neurodegenerative phenotype in the brains of abusers, induces oxidative stress and a build-up of autophagic vacuoles (autophagosomes) in neuronal cell lines [212, 213]. DJ-1 is known to inhibit aSyn aggregation and toxicity, suppress oxidative stress, and stimulate lysosomal autophagy [144, 156, 214].

The above sections highlight advances in our understanding of DJ-1 and ATP13A2 neuroprotective activities. However, whether DJ-1 and ATP13A2 interact on a functional level to modulate mitochondrial and lysosomal function is not known. We hypothesized that knockdown of DJ-1 or ATP13A2 would disrupt lysosomal autophagy by causing a buildup of ROS that permeabilize lysosomal membranes. Defects in lysosomal autophagy were characterized by monitoring effects of DJ-1 and ATP13A2 knockdown on autophagosome accumulation in cells cultured in the absence and presence of METH.

4.2. Materials and Methods.

4.2.1 Materials

The bicinchoninic acid (BCA) protein assay kit was obtained from Pierce Biotechnology

(Rockford, IL). The ECF substrate was purchased from GE Healthcare (Piscataway, NJ). Coomassie Brilliant blue R250 and SDS were obtained from Amresco (Solon, OH). Trizma base, 2-mercapto ethanol (2ME), ammonium persulfate (APS), glycine, urea, iadoacetamide, sucrose, paraformaldehyde (PFA), protease inhibitor cocktail, trypsin and ammonium chloride (NH_4Cl) were purchased from Sigma-Aldrich (St. Louis, MO). DTT was purchased from Gold Biotechnology, fetal bovine serum (FBS), penicillin-streptomycin, Lipofectamine 2000, Opti-MEM, Trypsin-EDTA were obtained from Invitrogen (Carlsbad, CA).

4.2.2 Antibodies

The following antibodies were used in these studies: mouse anti human DJ-1 (clone 3E8) (Enzo Life Sciences, Farmingdale, NY), secondary anti mouse IgG conjugated with alkaline phosphatase (Promega, Madison, WI, USA), secondary anti rabbit IgG conjugated with alkaline phosphatase (Promega, Madison, WI, USA). Anti ATP13A2 (Novus Biologicals, Littleton, CO, catalogue # NB110-41486).

4.2.3 Preparation of lentiviral and adenoviral constructs

A lentiviral construct encoding a short hairpin RNAs (shRNAs) was used to down-regulate rat DJ-1. An shRNA-encoding cassette spanning amino acid residues 20–26 of rat DJ-1 [215] was ligated into the entry vector

pENTR/U6(Invitrogen) and subsequently transferred to the lentiviral vector pLenti6/BLOCK-iT DEST (Invitrogen) by recombination [126]. Plasmids encoding human shRNA DJ-1 (clone 4918) and human shRNA ATP13A2 (clone BC 030267) were obtained from Dr. Benjamin Dehay (University of Bordeaux). A lentiviral construct encoding rat shRNA ATP13A2 (Open Bio system, Clone ID TRCN0000101716) was used to knockdown ATP13A2 protein in N27 cells. A non-mammalian shRNA was used as a control plasmid DNA (Sigma Aldrich, Cat. SHC002). A cDNA encoding ATP13A2 (clone BC 030267) obtained from Dr. Susan Lindquist was ligated into pENTR/U6 and subsequently transferred to the adenoviral vector pAd/CMV/V5-DEST (Invitrogen) by recombination [216].

4.2.4 Generation of N27 and SH-SY5Y stable cell lines with ATP13A2 or DJ-1 knockdown

N27 rat dopaminergic neuronal cells were plated in the wells of a 6 well plate (70,000 cells per well) in RPMI 1640 media with 15% (v/v) FBS and 1% (v/v) penicillin-streptomycin (Pen-Strep). The cells were transduced with lentivirus encoding rat shRNA ATP13A2 (MOI 5) or rat shRNA DJ-1 (MOI 50) An additional set of cells was transduced with non-mammalian targeting shRNA virus to generate a negative-control stable cell line. After 24-48 h, the media containing the virus was replaced with media containing puromycin, a mammalian selection marker (final concentration of 2 µg/mL), to select for cells that were transduced by the lentivirus. Media with puromycin was replaced with fresh media every 2 days for the first week to remove the dead cells, and thereafter media was replaced with fresh media every 3 days. Individual colonies

started forming on the plate after about 4-6 weeks. Each colony was carefully selected using a glass colony ring, to which a layer of grease was applied on the edge facing the plate surface to facilitate attachment of the ring to the plate. The colonies were propagated in media containing puromcyin (2 μg/mL), and an aliquot of the cells was frozen and stored in a liquid nitrogen tank.

SH-SY5Y human neuroblastoma cells were plated in the wells of a 6 well plate (100,000 cells per well) in RPMI 1640 media with 15% (v/v) FBS and 1% (v/v) Pen-Strep. The cells were transfected with a plasmid encoding human shRNA DJ-1 and human shRNA ATP13A2 in the presence of Lipofectamine 2000 for 24 h at 37 ºC. Media containing the transfection reagent was replaced with RPMI media without Pen-Strep for 24 h, to allow the cells to recover. The media was then replaced with media with Pen-Strep and puromycin (2 μg/mL). The media was replaced with fresh media every 2-3 days for about 4-6 weeks, and colonies were selected and propagated as described above for the generation of N27 stably transduced cell lines. Additional sets of cells were transfected with a scrambled human shRNA DJ-1 construct or a scrambled human shRNA ATP13A2 construct to generate negative-control stable cell lines.

4.2.5 Acridine Orange (AO) labeling

To visualize acidic vesicles (e.g. autophagosomes) and lysosomes, cells were incubated for 10 min at 37 ºC in an atmosphere containing 5 % (v/v) CO_2 in RPMI 1640 media supplement with AO (1 μg/mL), a lysosomotropic metachromatic fluorochrome that emits an intense orange fluorescence after accumulating in lysosomes and other acidic vesicles or organelles [161]. The media was replaced

with phenol-red free media, and the cells were imaged on a confocal microscope at 60x magnification (Nikon TE2000-U inverted fluorescence microscope, Nikon Instruments, Melville, NY). A decrease in AO fluorescence intensity was interpreted to mean an increase in lysosomal membrane permeability (LMP) or the permeability of acidic vesicles, suggesting that membrane disruption had occurred.

4.2.6 Western blotting

Cells were treated with NH_4Cl (25 mM) for 4 h (in the case of an 8 h METH incubation, NH_4Cl was included during the final 4 h). Cells were dislodged from the plate by pipetting, collected by centrifugation, washed with phosphate-buffered saline (PBS)(136 mM NaCl, 0.268 mM KCl, 10 mM Na_2HPO4, 1.76 mM KH_2PO4, pH 7.4), and lysed in RIPA buffer (25 mM Tris–HCl, pH 7.4, 150 mM NaCl, 1 mM EDTA, 1% (v/v) Triton X-100, 0.1% (w/v) SDS, 1% (w/v) sodium deoxycholate, protease inhibitor cocktail(Sigma), and 1 mM phenylmethanesulfonylfluoride (PMSF)). After centrifugation at 13,000 g, the detergent-soluble (supernatant) fraction was recovered. The protein concentration in the soluble fraction was measured using the BCA Protein Assay Kit (Pierce Biotechnology, Rockford, IL, USA), and equal amounts of protein were separated via SDS–PAGE on a 4–20% (w/v) polyacrylamide gel. The proteins were transferred to a 0.2 μm or 0.45 μm PVDF membrane, which was probed with a monoclonal antibody specific for mammalian aSyn (Syn-1, 1:1000), DJ-1 (1:250,000), ATP13A2 (1:2000). The secondary antibody was an anti-rabbit IgG or an anti-mouse IgG conjugated to alkaline phosphatase (AP).

Chemifluorescence images were obtained and analyzed using a Typhoon imaging system (GE Health Sciences, Piscataway, NJ, USA). To confirm that equal amounts of protein were loaded in all lanes, the blots were reprobed with a primary antibody specific for β-actin (1:50000).

4.2.7. O_2 Consumption

O_2 consumption was monitored as described [217]. Stably transduced N27 cells were plated in a 10 cm dish. The cells were harvested via centrifugation at 700 x g (10 min, 4 ºC) and resuspended in O_2 consumption buffer (20 mM HEPES, pH 7.2). Cellular respiration was measured using a Clark-type oxygen electrode attached to a voltmeter (Digital Model 10 Controller, Rank Brothers, Ltd, Cambridge, UK). The electrode was allowed to stabilize at 37 °C for 30 min to ensure air saturation. To normalize the background current, the voltmeter was set to zero using a polarizing voltage of 0.40 V. An aliquot of 1 x 10^6 cells (400 µL) was loaded into the respiration chamber, where the sensitivity control was set to 1 V. This reflected 100% of the O_2 concentration (0.21 mM) in the air-saturated reaction medium present before the start of respiration [217]. The sample was constantly stirred at 840 rpm using a magnetic stir bar located inside the chamber. Using the Pico Technology software program (PicoTechnology, Ltd., Cambridgeshire, UK), the O_2 level remaining in the chamber at any time during respiration was automatically logged (with 10 sec intervals) as a voltage (Vo2). The Vo2 reflected the voltage generated by the reaction of O_2 with the electrode (Vo2 steadily decreased as O_2 was consumed) [217]. Percentage O_2 response versus time was plotted.

4.2.8 Fluorescence microscopy using tandem GFP-RFP-LC3 construct.

GFP-RFP-LC3 stable cell lines were generated by Dr. Amy Griggs. In brief, SH-SY5Y human neuroblastoma cells were plated in the wells of a 6 well plate (100,000 cells per well) in RPMI 1640 media with 15% (v/v) FBS and 1% (v/v) Pen-Strep. The cells were transfected with a plasmid encoding GFP-RFP-LC3 in the presence of Lipofectamine 2000 for 6 h at 37 ºC. Media containing the transfection reagent was replaced with RPMI media without Pen-Strep for 24 h, to allow the cells to recover. The media was then replaced with media with Pen-Strep and G418 (600 µg/mL). The media was replaced with fresh media every 2-3 days for about 4-6 weeks, and colonies were selected and propagated as described in section 4.2.4 above.

The cells were transduced with adenoviruses encoding WT ATP13A2 or the control protein LacZ (MOI of each virus = 50). After 48 h, the cells were incubated with METH (200 µM) for 24 h. The cells were fixed with 4% w/v paraformaldehyde (PFA) and imaged using a confocal microscope (excitation wavelengths, 488 and 594 nm; emission wavelengths, 525 and 617 nm respectively). The tandem LC3 construct was used to monitor autophagic flux based on a difference in the pH stability of GFP versus RFP [218]. The acidic pH in autolysosomes (cellular structures resulting from the fusion of autophagosomes with lysosomes) quenches the GFP fluorescence signal, whereas the RFP fluorescence signal is preserved under acidic conditions [218].

4.2.9 RNA isolation and qRT-PCR

Cells were harvested by centrifugation at 1300 x g for 10 min at 4 ºC. mRNA was extracted using the E.Z.N.A total RNA kit I (Omega Bio-Tek). Total RNA (200 ng) was reverse-transcribed by the iScript Select cDNA Synthesis Kit (170–8896) (Bio-Rad). Quantitative PCR (qRT-PCR) was performed using the iQ SYBR Green PCR Kit (Bio-Rad) using forward and reverse primers specific for ATP13A2, DJ-1, or the control GAPDH. ATP13A2, DJ-1 and GAPDH levels were normalized and fold change was calculated using the following formula:

$$2^{-\Delta\Delta C_t} = 2^{-\left\{(C_{t,TG}-C_{t,CG})_{KD}-(C_{t,TG}-C_{t,CG})_{control}\right\}}$$

Where $C_{t,TG}$ represents the crossing threshold for the target gene, $C_{t,CG}$ represents the crossing threshold for the target gene, 'KD' refers to mRNA obtained from ATP13A2 or DJ-1 knockdown cells, and 'control' refers to mRNA obtained from cells transduced with a control (non-targeting) vector.

4.3. Results

4.3.1 Decreased levels of DJ-1 and ATP13A2 mRNA and protein in N27 stable knockdown cells.

To generate N27 rat dopaminergic neuronal cells with a stable knockdown of DJ-1 or ATP13A2, the cells were transduced with lentivirus encoding shRNA DJ-1 or shRNA ATP13A2. Additional cells were transduced with lentivirus encoding non-mammalian targeting shRNA to generate a control stable cell line. Analysis of the N27 shRNA DJ-1 cell lysates by qRT-PCR and Western blotting revealed an 80% decrease in DJ-1 mRNA levels (Fig 4.1A) and a corresponding 60%

knockdown in DJ-1 protein levels (Fig 4.1B, C) compared to the control knockdown stables. Analysis of lysates from two clonal lines of N27 shRNA ATP13A2 ('colony 10' and 'colony 12') by qRT-PCR and Western blotting revealed a 90% decrease in the level of ATP13A2 mRNA (colony 10 line) (Fig 4.2A) and a complete loss of ATP13A2 protein in both clonal lines (predicted molecular weight, 129 kDa) (Fig 4.2B). Furthermore, we generated both DJ-1 and ATP13A2 knockdown stables in SH-SY5Y human dopaminergic neuroblastoma cells (data not shown).

4.3.2 N27 ATP13A2 knockdown cells show an increase in LC3 II levels.

Previous studies have reported that cells depleted of ATP13A2 via RNAi-mediated knockdown exhibit decreased proteolytic processing of lysosomal enzymes, reduced degradation of lysosomal substrates, increased mitochondrial mass, and increased ROS production [175, 176]. Based on these studies, we tested the effect of our generated N27 ATP13A2 knockdown cells on lysosomal degradation. We hypothesized that knockdown of ATP13A2 should increase the accumulation of autophagosomes. To address this hypothesis, N27 ATP13A2 knockdown cells (colony 10 and colony 12) and control (non-targeting) stable cells were treated with or without METH in the absence or presence of NH_4Cl, an inhibitor of autophagosome degradation by lysosomes. METH induces oxidative stress and a build-up of autophagic vacuoles (autophagosomes) in neuronal cell lines [212, 213]. Autophagosomes levels were monitored by measuring levels of an autophagic marker, LC3 II, via Western blotting. The results showed an

increased level of LC3 II in lysates from colony 10 cells (Fig 4.3) and colony 12 cells (Fig 4.4) compared to control cells, in the absence or presence of METH (the effect was more pronounced in cells co-treated with METH). For both ATP13A2 knockdown clonal cell lines treated with METH, the magnitude of the increase in LC3 II levels was dependent on the time of METH treatment (4 h versus 8 h). Similar effects of ATP13A2 knockdown and METH treatment on LC3 levels were obtained with ATP13A2 knockdown cells cultured in the presence of NH_4Cl, except that the LC3 levels in these cell lysates were markedly greater. These results suggest that ATP13A2 knockdown in N27 cells induces an increase in autophagosome formation and/or disrupts the lysosomal degradation pathway, thereby triggering autophagosome accumulation. In addition, METH sensitizes the cells to the effects of ATP13A2 knockdown, causing further increases in LC3-II autophagosome levels.

4.3.3 ATP13A2 overexpression enhances autophagosome clearance.

We hypothesized that overexpression of ATP13A2 would enhance the clearance of autophagosomes. To address this hypothesis we overexpressed ATP13A2 or the control protein LacZ from adenoviral constructs in cells stably expressing a ‘tandem’, GFP-RFP-LC3 construct that enables one to monitor autophagic flux based on the fact that GFP and RFP can both be visualized in autophagosomes, whereas GFP (but not RFP) is destabilized (and thus not visible by microscopy) in more acidic compartments such as autolysosomes. The results show that overexpression of ATP13A2 (but not the control protein LacZ) decreases the

number of autophagosomes and autolysosomes in METH-treated cells (Fig. 4.5). These data suggest that ATP13A2 may enhance autophagosome clearance (thus inhibiting autophagosome accumulation) in METH-treated cells, potentially by enhancing autophagosome-lysosome fusion and/or lysosomal function [175].

4.3.4 ATP13A2 knockdown reduces the METH-induced up-regulation of acidic cellular compartments.

A loss of ATP13A2 function has been shown to compromise lysosomal acidification [175]. Accordingly, we hypothesized that the knockdown of ATP13A2 would disrupt lysosomal pH in our cell culture models. To address this hypothesis, N27 ATP13A2 knockdown cells were treated with or without METH, and levels of lysosomes and acidic organelles (e.g. autophagosomes) were monitored using AO, a lysosomotropic metachromatic fluorochrome that emits an intense red fluorescence after accumulating in acidic cellular compartments. Our results showed that METH induced an increase in AO-positive cellular structures in control N27 cells expressing a non-targeting shRNA, whereas this effect was suppressed in ATP13A2 knockdown cells (Fig 4.6). These results suggest that ATP13A2-deficient N27 cells show a decrease in METH-induced accumulation of AO-positive structures, perhaps because of a defect in the acidification of cellular compartments on the autophagic or endocytic pathway.

4.3.5 ATP13A2 knockdown increases levels of mitochondrial protein carbonyls.

The next experiment was designed to determine the effect of ATP13A2 knockdown on mitochondrial oxidative stress. We hypothesized that ATP13A2

would increase levels of mitochondrial protein carbonyls, a marker of mitochondrial oxidative stress. To address this hypothesis, MES23.5 dopaminergic neuronal cells were transduced with lentivirus encoding shRNA ATP13A2. Mitochondrial fractions were isolated and analyzed for protein carbonyls The results showed that cells depleted of ATP13A2 have elevated levels of mitochondrial protein carbonyls compared to control (untransduced) cells (Fig 4.7). These results suggest that shRNA ATP13A2 sensitizes mitochondrial proteins to oxidation, potentially by triggering increases in mitochondrial ROS.

4.3.6 N27 DJ-1 knockdown cells show an increase in LC3-II levels.

Cells lacking DJ-1 exhibit a decrease in mitochondrial degradation, an increase in mitochondrial mass, and an increase in ROS levels [144]. Other studies have shown that DJ-1 suppresses the formation of protein carbonyls in rat primary midbrain cultures [126]. ROS accumulation may cause lysosomal membrane permeability (LMP), thus disrupting lysosomal degradation pathways. Accordingly, we hypothesized that DJ-1 knockdown would cause an accumulation of autophagic vesicles in neuronal cells. To address this hypothesis, N27 DJ-1 knockdown cells and cells stably transduced with a control (non-targeting shRNA) vector (section 4.3.1) were treated with or without METH, in the absence or presence of NH_4Cl. Autophagosome levels were monitored by determining the cellular content of the autophagic marker, LC3-II. Our results showed that knockdown of DJ-1 in N27 cells increased levels of LC3-II compared to control cells, in the absence or presence of METH (the effect was more

pronounced in cells co-treated with METH) (Fig. 4.8). Similar effects of DJ-1 knockdown and METH treatment on LC3 levels were obtained with DJ-1 knockdown cells cultured in the presence of NH_4Cl, except that the LC3 levels in these cell lysates were markedly greater. These results suggest that DJ-1 knockdown in N27 cells induces an increase in autophagosome formation and/or disrupts the lysosomal degradation pathway, thereby triggering autophagosome accumulation. In addition, METH sensitizes the cells causing a further increase in autophagosome levels.

4.3.7 N27 cells depleted of ATP13A2 or DJ-1 show a decrease in O_2 consumption.

Impairment of autophagy resulting from ATP13A2 depletion is thought to trigger a buildup of defective mitochondria that produce increased ROS [144, 176]. On the other hand, DJ-1 dysfunction induces an increase in ROS levels, a decrease in respiration rates and mitochondrial membrane potential (MMP), and a disruption of the critical balance between mitochondrial fusion and fission dynamics [144]. Based on these studies, we hypothesized that knockdown of either ATP13A2 or DJ-1 in N27 cells would disrupt mitochondrial function, hence decreasing the rate of O_2 consumption. To address this hypothesis, N27 cells depleted of ATP13A2 or DJ-1 were characterized in terms of their rates of cellular respiration using a Clark-type oxygen electrode attached to a voltmeter. The results revealed that cells depleted of ATP13A2 or DJ-1 showed a decreased rate of O_2 consumption compared to control cells transduced with a non-targeting shRNA vector (Fig. 4.9). Taken together, these results suggest that a loss of ATP13A2 or DJ-1

function results in a disruption of mitochondrial respiration as evident in the observed decrease in O_2 consumption.

4.3.8 DJ-1 depletion via shRNA knockdown results in down-regulation of ATP13A2 expression in N27 cells, and vice-versa.

Depletion of ATP13A2 or DJ-1 in N27 cells leads to the same biological outcome namely, an increase in LC3-II accumulation (Fig 4.3, Fig 4.4 and Fig 4.8). Accordingly, we hypothesized that the two proteins might interact on a functional level to modulate mitochondrial or/and lysosomal function. As one approach to address this hypothesis, we investigated whether the expression levels of ATP13A2 and DJ-1 are co-regulated by examining the effects of depleting each protein via shRNA-mediated knockdown on the expression level of the other. Levels of ATP13A2 mRNA and protein were examined in N27 DJ-1 knockdown cells via qRT-PCR and Western blotting, respectively, whereas DJ-1 mRNA levels were examined in N27 ATP13A2 knockdown cells via qRT-PCR. N27 DJ-1 knockdown cells showed a 90% decrease in ATP13A2 mRNA (Fig. 4.10A) and a 90% decrease in ATP13A2 protein (Fig 4.10B) relative to control cells transduced with a non-targeting shRNA vector. Levels of DJ-1 mRNA in N27 ATP13A2 knockdown cells were decreased by 35-40% relative to control cells (Fig. 4.11). These results are the first to suggest that DJ-1 and ATP13A2 are co-regulated in N27 cells.

4.3.9 DJ-1 is down-regulated in primary midbrain cultures depleted of ATP13A2, whereas ATP13A2 is up-regulated in midbrain cultures depleted of DJ-1.

Additional experiments were carried out to determine whether ATP13A2 and DJ-1 are co-regulated in rat primary midbrain cultures. On the basis of results obtained with N27 knockdown cells (4.3.8), we hypothesized that midbrain cultures depleted of DJ-1 would exhibit a decrease in ATP13A2 expression levels, and vice versa. To address this hypothesis, primary mid brain cultures transduced with lentivirus encoding a DJ-1 shRNA or an ATP13A2 shRNA were analyzed by qRT-PCR to determine levels of ATP13A2 and DJ-1 mRNAs. The results showed an approximately 72% decrease in DJ-1 mRNA levels in cultures depleted of ATP13A2 (70% knockdown of ATP13A2 mRNA) compared to control cultures (Fig 4.12). Surprisingly, we observed a 70% increase in ATP13A2 mRNA levels in cultures depleted of DJ-1 (72% knockdown of DJ-1 mRNA) compared to control cultures (Fig 4.13). Collectively, these data provide evidence that DJ-1 and ATP13A2 are co-regulated in rat primary midbrain cultures.

4.4. Discussion

4.4.1 Knockdown of ATP13A2 causes LC3-II accumulation.

A loss of ATP13A2 function causes impaired lysosomal acidification [175]. Autophagosomes fuse with lysosomes to degrade or recycle their components. An optimal lysosomal pH among other factors is important for this fusion event.

Disruption of this process leads to an accumulation of autophagosomes. Our data showed an increase in LC3-II levels in N27 ATP13A2 knockdown cells, and this effect was enhanced in the presence of METH. These results suggest, as one possibility, that ATP13A2 knockdown elicits an increase in lysosomal pH, resulting in inhibition of autophagosome-lysosome fusion and thus autophagosome accumulation, as evident by increased LC3-II levels. Additional results revealed a time-dependent increase in LC3-II levels in N27 ATP13A2 knockdown cells and control cells cultured in the presence versus the absence of METH. METH has been shown to induce oxidative stress by increasing the levels of ROS in striatal, mesencephalic and cortical astrocytes [219]. Furthermore, METH induces neurotoxicity in dopamine neurons by disrupting dopamine sequestration in synaptic vesicles leading to oxyradical stress, autophagy and neurite degeneration [220]. In addition, impairment of autophagy resulting from ATP13A2 depletion is thought to trigger a buildup of defective mitochondria that produce increased ROS [144, 176]. ROS causes lysosomal membrane permeability (LMP), disrupting lysosomal function [221]. Therefore, we infer that METH-induced accumulation of autophagosomes may reflect up-regulation of autophagy and/or a disruption of autophagosome-lysosome fusion, and both effects could be enhanced by ATP13A2 depletion. ATP13A2 dysfunction could lead to induction of autophagy based on NH_4Cl results (NH_4Cl combined with ATP13A2 KD gives much higher LC3-II levels than NH_4Cl in control cells). This could be an indirect effect of oxidative stress leading to proteasome inhibition and as a result induction of autophagy [222, 223].

4.4.2 ATP13A2 overexpression enhances lysosomal clearance in SH-SY5Y cells.

ATP13A2 overexpression has been shown to rescue zinc toxicity and promote mitochondrial fusion in human olfactory neurosphere cultures [183]. Additional evidence suggests that ATP13A2 enhances autophagic flux and inhibit autophagosome accumulation, potentially by enhancing lysosomal function and/or autophagosome-lysosome fusion [175]. Here, we showed using SH-SY5Y cells expressing a tandem GFP-RFP-LC3 construct that METH induced an increase in the relative number of puncta that emitted red and green fluorescence (corresponding to autophagosomes) or only red fluorescence (corresponding to autolysosomes), and this effect was diminished in cells overexpressing ATP13A2. These results suggest that overexpression of ATP13A2 enhances autophagosome clearance, perhaps via a mechanism involving enhanced lysosome acidification resulting in increased autophagosome-lysosome fusion and/or lysosomal degradation. It is also possible that ATP13A2 over-expression results in a decrease in METH-induced autophagosome formation via an indirect mechanism involving alleviation of oxidative stress.

4.4.3 Knockdown of ATP13A2 disrupts autophagy and lysosomal pH.

The results of AO staining experiments showed a METH-dependent increase in the relative number of red puncta corresponding to acidic vesicles or organelles in control N27 cells, whereas this increase was abolished in N27 ATP13A2

knockdown cells. Examples of cellular structures that could take up the AO stain include autophagosomes [224], macropinosomes [225], or lysosomes. Our results suggest that there is a decrease in the acidification of these structures in cells depleted of ATP13A2. A disruption of lysosomal pH would be predicted to cause an accumulation of autophagosomes, and thus the AO staining data are consistent with data showing that LC3-II-positive vesicles accumulate in ATP13A2 knockdown cells (see above).

4.4.4 ATP13A2 knockdown increases levels of protein carbonyls in ME23.5 cells.

Impairment of autophagy resulting from ATP13A2 depletion is thought to trigger a buildup of defective mitochondria that produce increased ROS [144, 176]. Here we showed that knockdown of ATP13A2 in MES23.5 cells increased the level of mitochondrial protein carbonyls, an indicator of oxidative stress. Based on the data presented here (see above) and by other groups [175] that ATP13A2 is involved in lysosomal autophagy, we infer that the increase in the levels of mitochondrial protein carbonyls in ATP13A2 knockdown cells reflects a buildup of dysfunctional mitochondria. Normally, dysfunctional mitochondria would be degraded via mitophagy, a process involving mitochondrial uptake by a phagophore that develops into an autophagosome which in turn fuses with a lysosome. Impairment of lysosome acidification is expected to lead to an accumulation of autophagosomes and a buildup of dysfunctional mitochondria that trigger ROS accumulation. ROS-mediated LMP completes a vicious cycle of

lysosomal impairment, disruption of mitophagy, accumulation of dysfunctional mitochondria, and oxidative stress.

4.4.5 Knockdown of DJ-1 disrupts lysosomal function thus increasing autophagosome accumulation.

Loss or mutation of mitochondrial DJ-1 induces an increase in ROS levels, a decrease in respiration rates and mitochondrial membrane potential (MMP), and a disruption of the critical balance between mitochondrial fusion and fission dynamics [144]. Knockdown of DJ-1 in both N27 cells and SH-SY5Y cells increased levels of autophagosomes as evident from Western blotting data showing an increase in cellular LC3-II content. An increase in LC3-II content might be due to disrupted lysosomal function, leading to inefficient autophagosome elimination via the lysosomal degradation pathway. The increase in LC3-II levels was enhanced in N27 cells depleted of DJ-1 upon treatment of the cells with METH. We attribute this outcome to a disruption of autophagosome-lysosome fusion caused by ROS-induced LMP, a phenomenon that could result from oxidative stress associated with DJ-1 knockdown and METH exposure [161]. We can also infer that DJ-1 contributes to the up-regulation of autophagy triggered by METH, perhaps as a cellular defense mechanism involving Erk-dependent signaling [144]. In addition, we infer that METH-induced accumulation of autophagosomes may reflect METH-induced up-regulation of autophagy and/or a disruption of autophagosome-lysosome fusion.

4.4.6 N27 cells depleted of ATP13A2 or DJ-1 exhibit decreased rates of cellular respiration.

N27 cells stably transduced with an shRNA construct targeting ATP13A2 or DJ-1 showed a decrease in O_2 consumption compared to control cells. In contrast, human mutant ATP13A2 fibroblasts showed an increase in O_2 consumption compared to control fibroblasts [178]. A key difference between N27 cells and fibroblasts is that only the N27 cells produce dopamine. Cytosolic dopamine undergoes auto-oxidation to form dopamine *o*-quinone, a process that leads to a buildup of ROS [18]. In turn, dopamine *o*-quinone forms adducts with Parkin (a protein involved in mitochondrial quality control) [226] and subunits of mitochondrial complex I [40, 227]. Therefore, we infer (as one possibility) that the decrease in O_2 consumption in N27 cells depleted of ATP13A2 could be due to a buildup of mitochondria that have become dysfunctional (at least in part) via a mechanism involving damage to mitochondrial proteins by dopamine *o*-quinone. In contrast, the increase in O_2 consumption in ATP13A2 mutant fibroblasts presumably reflects a compensatory response to a reduction in ATP levels in these cells [178].

4.4.7 ATP13A2 and DJ-1 show evidence of co-regulated expression.

Our findings from studies of N27 cells depleted of ATP13A2 and DJ-1 suggest that the two proteins may share a common (or partially overlapping) neuroprotective pathway. Consistent with this idea, data obtained by qRT-PCR revealed that the level of ATP13A2 mRNA was decreased in N27 DJ-1

knockdown cells, and vice versa. Similarly, there was a decrease in DJ-1 mRNA levels in primary midbrain cultures depleted of ATP13A2 by shRNA-mediated knockdown. These results, the first to show that ATP13A2 and DJ-1 are co-regulated, suggest that expression of the genes encoding the two proteins might be modulated by a common transcription factor that binds to shared promoter motifs. Contrarily, we found that ATP13A2 mRNA increased in primary midbrain cultures depleted of DJ-1 by shRNA-mediated knockdown. These results suggest that the gene expression patterns of ATP13A2 and DJ-1 in N27 cells versus primary midbrain cultures are overlapping but non-identical, perhaps reflecting differences in N27 gene expression patterns associated with immortalization and/or the fact that primary midbrain cultures consist of a mixture of glial and neuronal cell types. The fact that ATP13A2 expression is increased in primary midbrain cultures implies that ATP13A2 up-regulation may have evolved as a protective mechanism to alleviate toxic effects of DJ-1 down-regulation (e.g. oxidative stress, disrupted autophagy) in neuronal and/or glial cells. Further studies are needed to address whether DJ-1 over-expression can rescue cellular dysfunction associated with ATP13A2 knockdown, and vice versa.

4.5 Conclusion

The data outlined in this chapter suggest that ATP13A2 and DJ-1 both regulate lysosomal autophagy. Knockdown of either protein increased LC3-II levels, suggesting an accumulation of autophagosomes. Furthermore, we showed that METH induced further increases in LC3-II levels in cells depleted of ATP13A2 or

DJ-1. This effect can be attributed to increases in ROS that could in turn trigger LMP, thereby disrupting lysosomal-autophagosome fusion. Finally, gene expression data suggest that (i) ATP13A2 and DJ-1 are co-regulated in N27 cells, and (ii) neurotoxic effects of DJ-1 depletion may be rescued by ATP13A2 up-regulation in primary midbrain cultures. These findings are important because they shed light on the role of lysosomal autophagy in ATP13A2- and DJ-1-mediated protection against neurotoxicity elicited by METH. In addition they provide insight into the biochemical mechanism by which DJ-1 preserves mitochondrial function in neurons exposed to PD-related insults, and they highlight the interplay between DJ-1 and ATP13A2 in regulating lysosomal degradation.

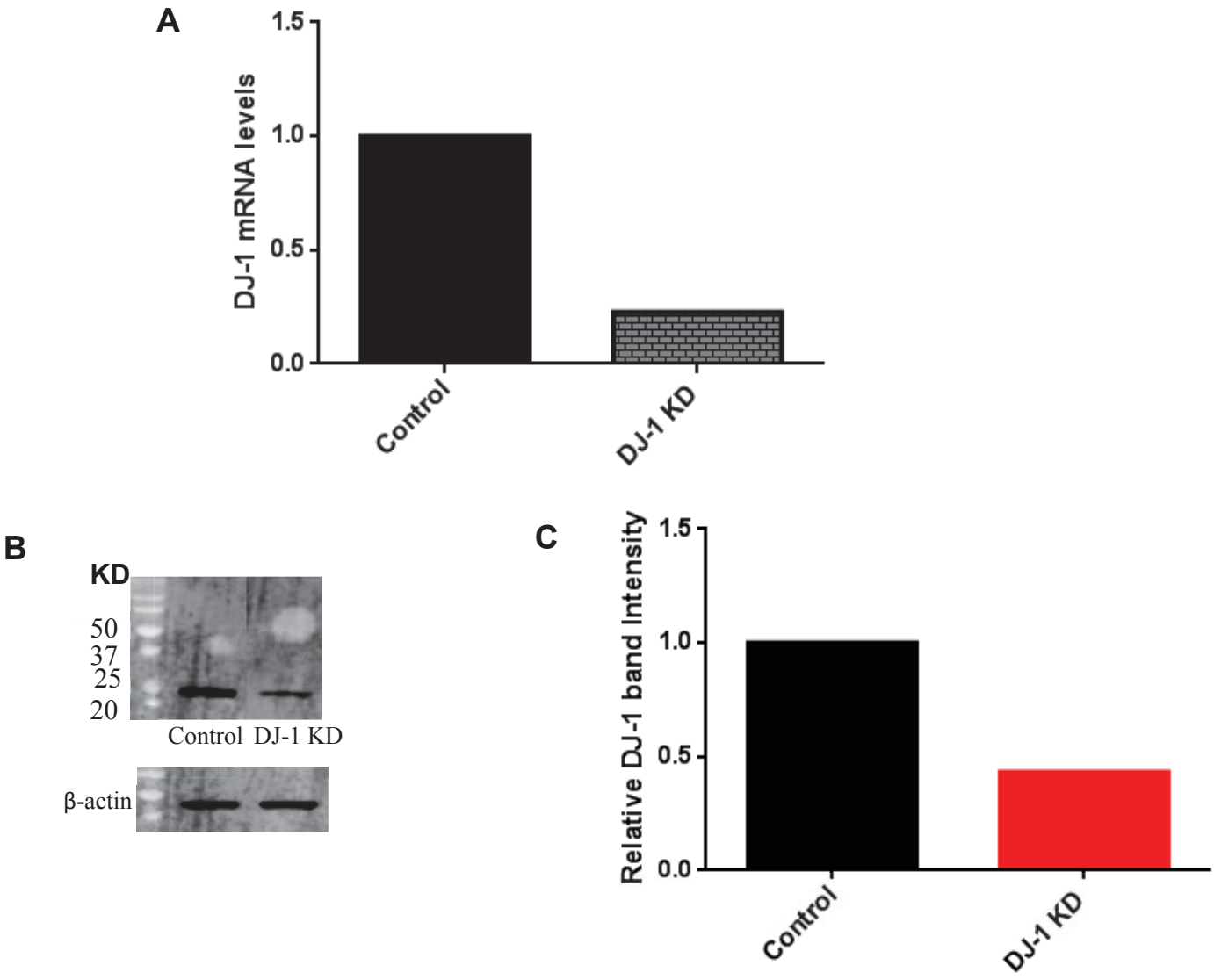

Figure 4.1 Levels of DJ-1 mRNA and protein in N27 stable knockdown cells.

A. qRT-PCR data showing reduced DJ-1 mRNA levels in N27 DJ-1 knockdown cells versus control cells. **B.** N27 cells were stably transduced with a lentivirus encoding an shRNA specific for DJ-1 or a control shRNA that does not target any mammalian genes. Lysates from control and DJ-1 knockdown cells (one clonal line of each) were analyzed via Western blotting (30 µg of protein per lane) using primary antibodies specific for DJ-1 and beta-actin. **C.** Bar graph showing DJ-1 band intensities normalized to the β-actin signal. N=2

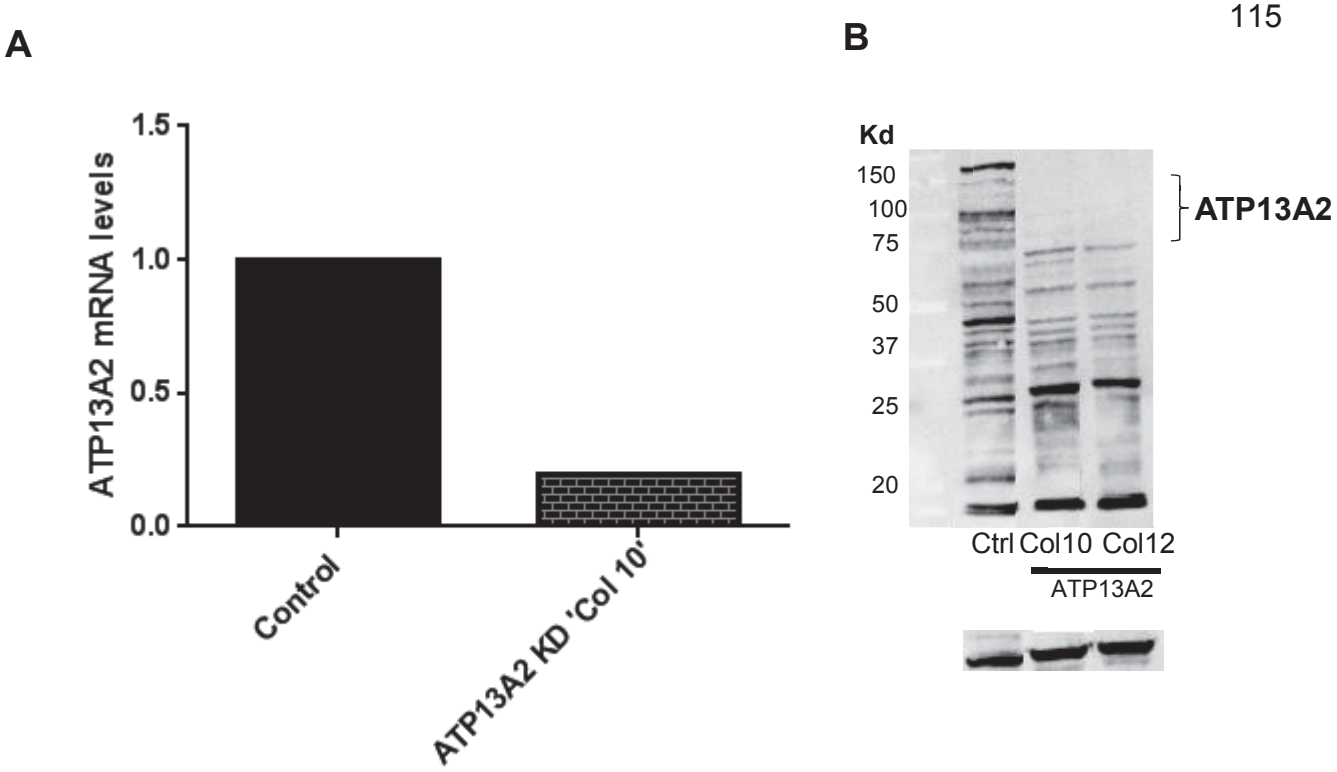

Figure 4.2 Levels of ATP13A2 mRNA and protein in N27 stable knockdown cells.

A. qRT-PCR data showing reduced ATP13A2 mRNA levels in N27 ATP13A2 knockdown cells (colony 10) versus control cells. **B.** N27 cells were stably transduced with a lentivirus encoding an shRNA specific for ATP13A2 or a control shRNA that does not target any mammalian genes. ("Ctrl"). Lysates from control cells (one clonal line) and ATP13A2 knockdown cells (two clonal lines: colony 10 [col 10] and colony 12 [col 12]) were analyzed via Western blotting (30 µg of protein per lane) using primary antibodies specific for ATP13A2 and beta-actin. N=2.

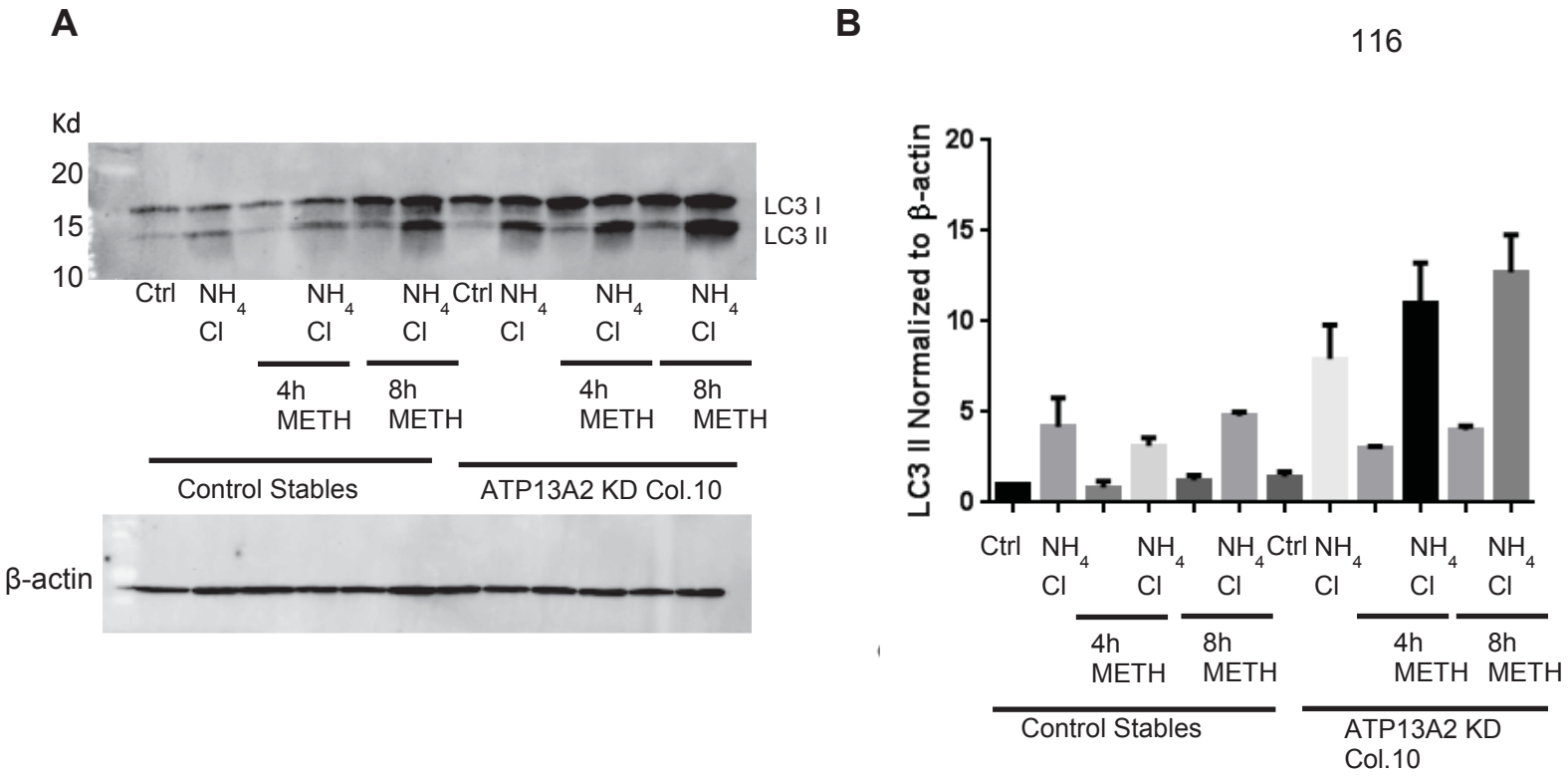

Figure 4.3 ATP13A2 knockdown in N27 cells (colony 10) induces up-regulation of the autophagy marker, LC3-II.

(A) N27 ATP13A2 knockdown cells (colony 10, 'Col 10') and control cells transduced with a non-targeting shRNA vector were cultured in the absence or presence of METH for 4 h or 8 h. Cell lysates were analyzed via Western blotting (30 µg of protein per lane) using primary antibodies specific for LC3 and beta-actin. **(B)** Bar graph showing LC3-II band intensities normalized to the β-actin signal (relative to a value of 1 for 'control untreated'). N=2

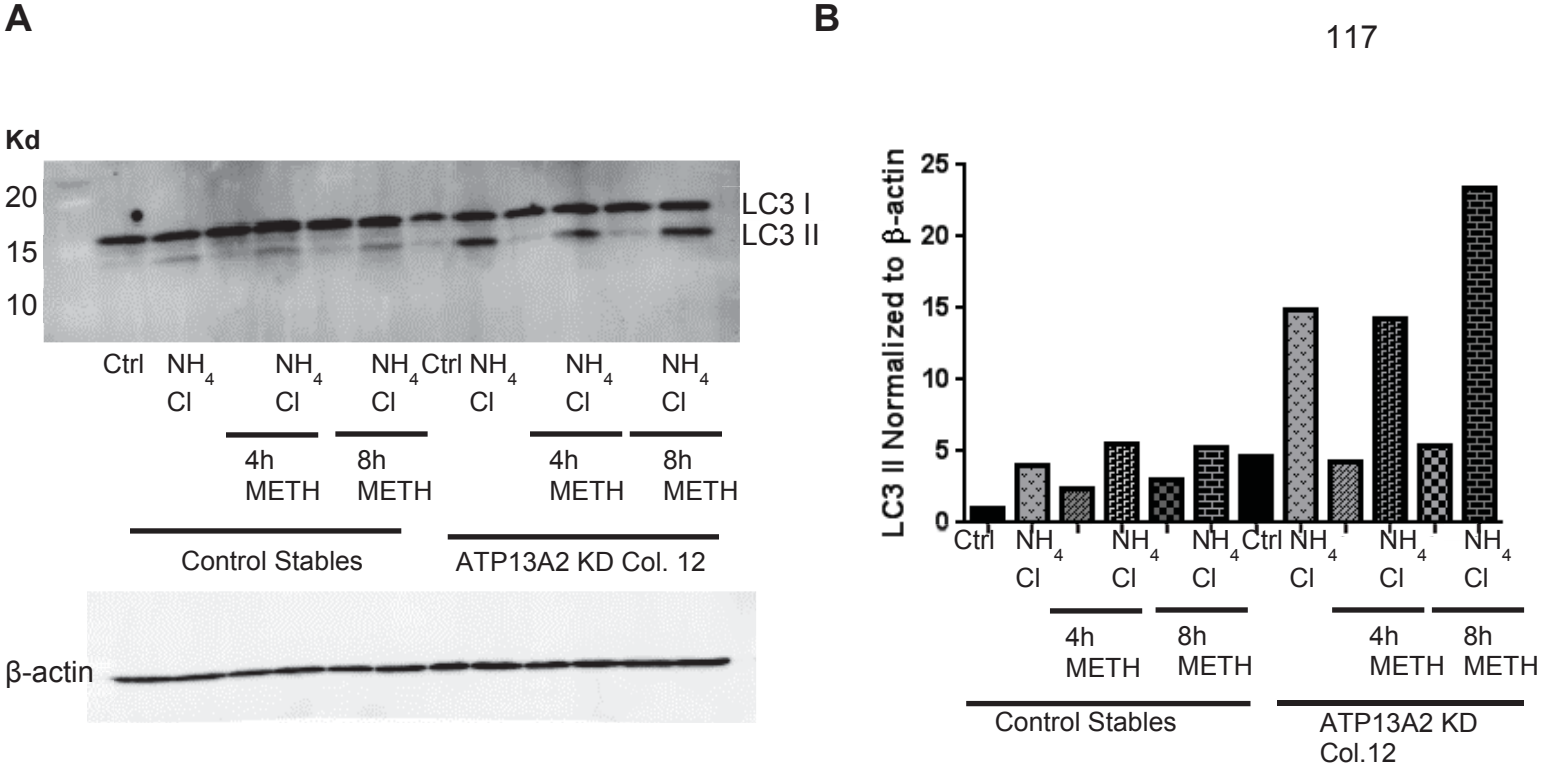

Figure 4.4 ATP13A2 knockdown in N27 cells (colony 12) induces up-regulation of the autophagy marker, LC3-II.

(A) N27 ATP13A2 knockdown cells (colony 12, 'Col 12') and control cells transduced with a non-targeting shRNA vector were cultured in the absence or presence of METH for 4 h or 8 h. Cell lysates were analyzed via Western blotting (30 µg of protein per lane) using primary antibodies specific for LC3 and beta-actin. **(B)** Bar graph showing LC3-II band intensities normalized to the β-actin signal (relative to a value of 1 for 'control untreated'). N=1

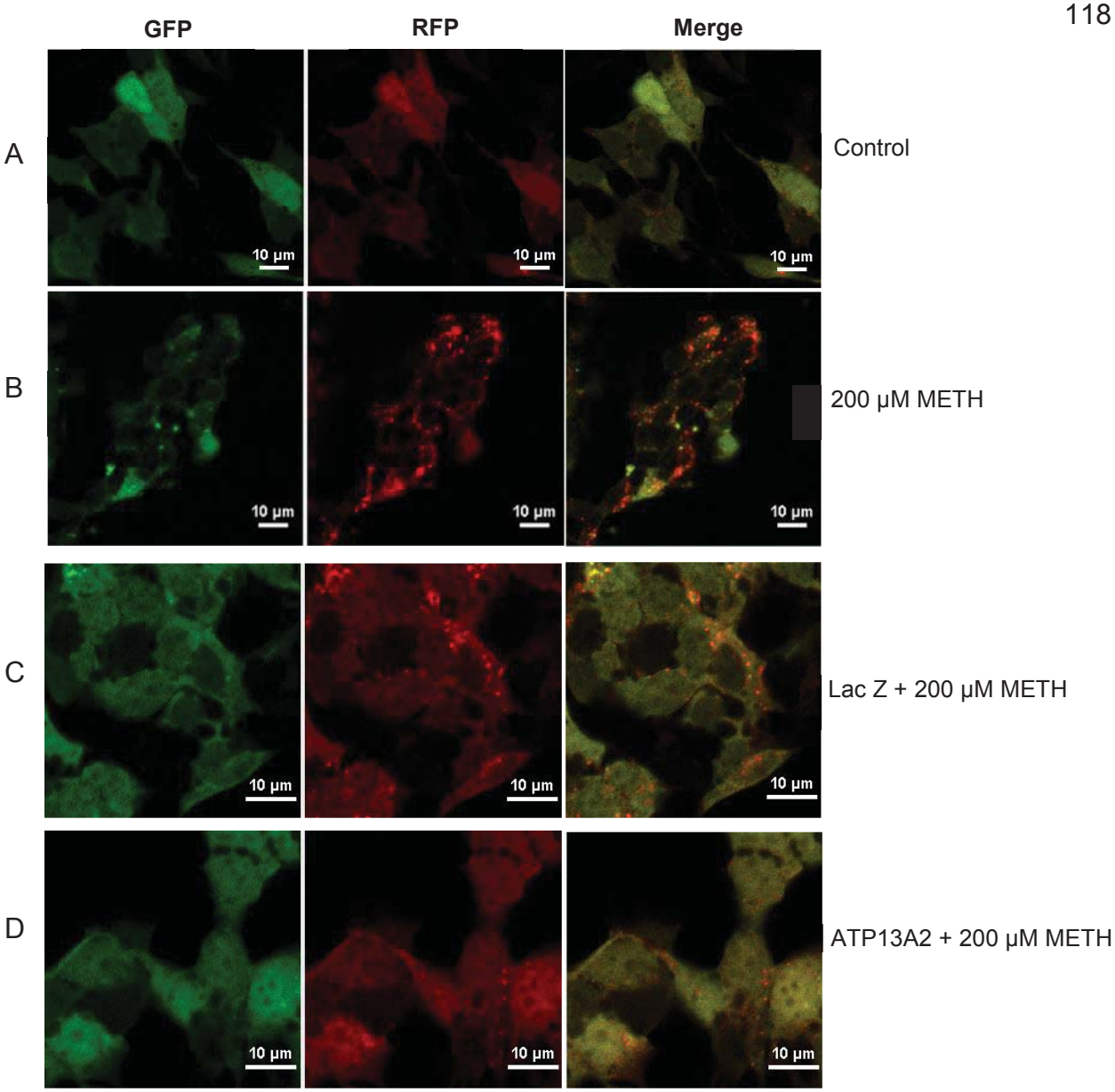

Figure 4.5 METH-induced autophagosome accumulation is suppressed in SH-SY5Y cells expressing ATP13A2.

SH-SY5Y cells stably expressing a 'tandem' GFP-RFP-LC3 construct were untreated (**A**); treated with METH (200 μM) for 24 h (**B**); or transduced with adenovirus encoding LacZ **(C)** or ATP13A2 **(D)** (MOI of each virus = 50) for 48 h before being treated with METH for 24 h. The cells were imaged by fluorescence microscopy. Puncta that emit GFP and RFP fluorescence are thought to correspond to autophagosomes, whereas puncta that emit RFP (but not GFP) fluorescence likely correspond to autolysosomes. N=1

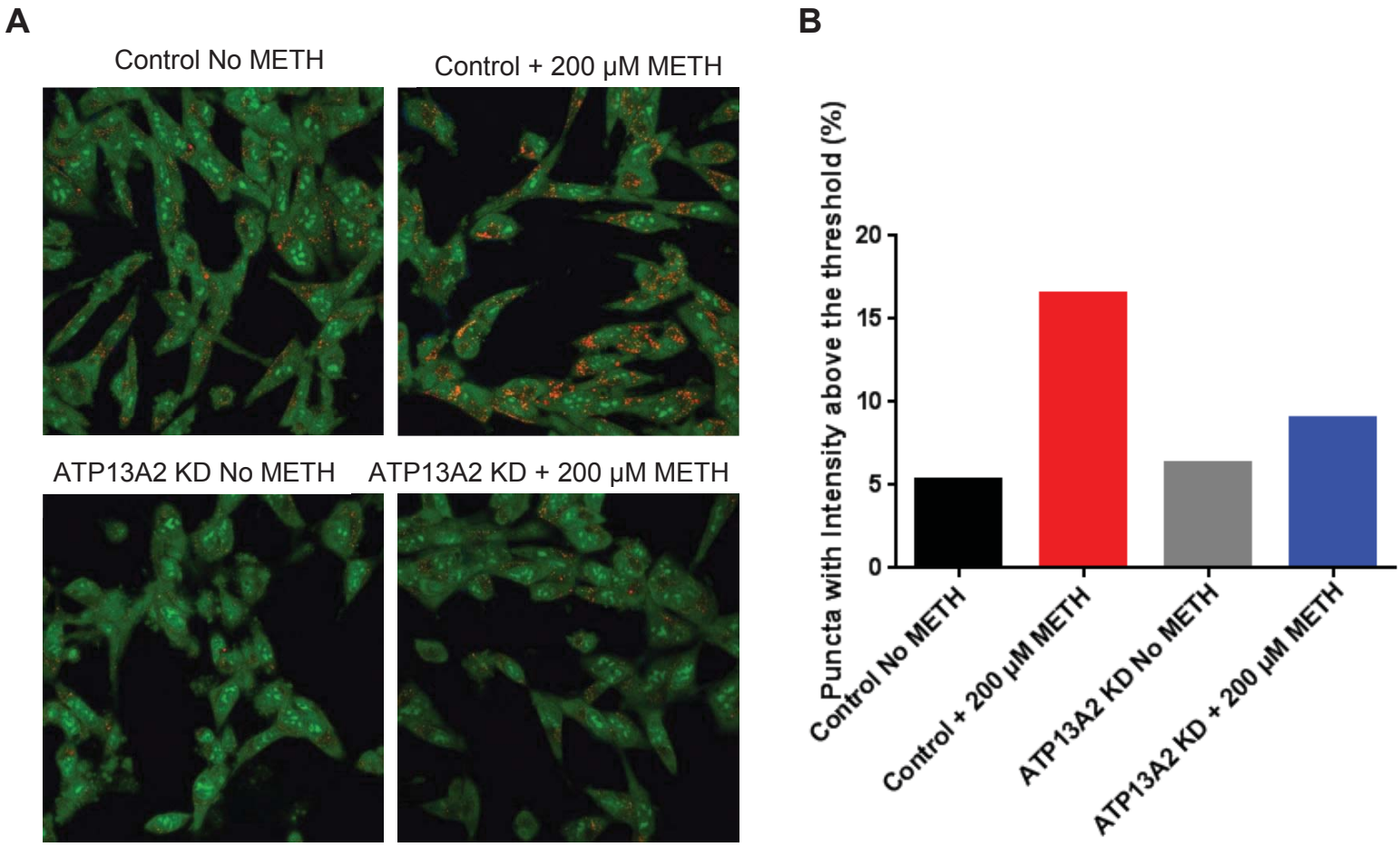

Figure 4.6 ATP13A2 is involved in the METH-induced accumulation of acidic vesicles or organelles.

A. Images showing different levels of red puncta corresponding to acidic vesicles or organelles in N27 ATP13A2 knockdown cells and in control cells transduced with a non-targeting shRNA vector. The cells were treated with or without METH (200 µM, 8 h) and subsequently incubated with acridine orange (AO) (1 µg/mL, 10 min), a fluorescent dye that emits red fluorescence when taken up by acidic vesicles or organelles Live cells were imaged in phenol red-free media by fluorescence microscopy. **B.** Bar graph showing relative numbers of acidic vesicles or organelles in N27 ATP13A2 knockdown cells or control cells treated as described in panel A. For each set of cells, regions of interest were drawn around invidual red puncta and scored for mean fluorescence intensity. The data are presented as the percentage of puncta with a mean intensity greater than a threshold value, defined as the average mean intensity plus two standards deviations for untreated control cells. N=1

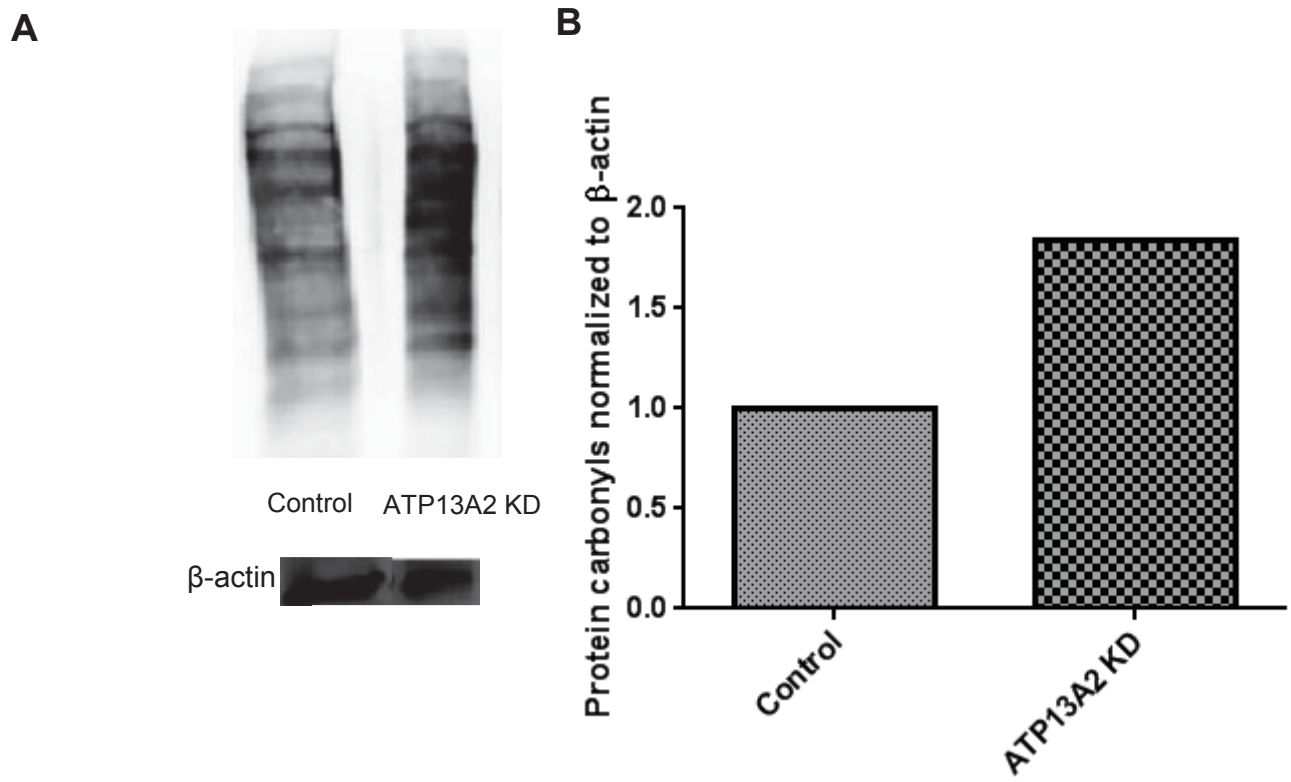

Figure 4.7 Knockdown of ATP13A2 triggers an increase in the oxidation of mitochondrial proteins.

(A) MES23.5 cells were transduced with shPark9 lentivirus (MOI 50). Mitochondrial fractions were isolated after 72 h and analyzed for protein carbonyl levels using the OxyBlot kit (Millipore). The image shows the resulting Western blot (9 µg of protein per lane) probed with an antibody specific for 2,4 dinitrophenylhydrazone (DNP). **(B)** Bar graph showing protein carbonyl band intensities normalized to the β-actin signal (relative to a value of 1 for control cells). N=1

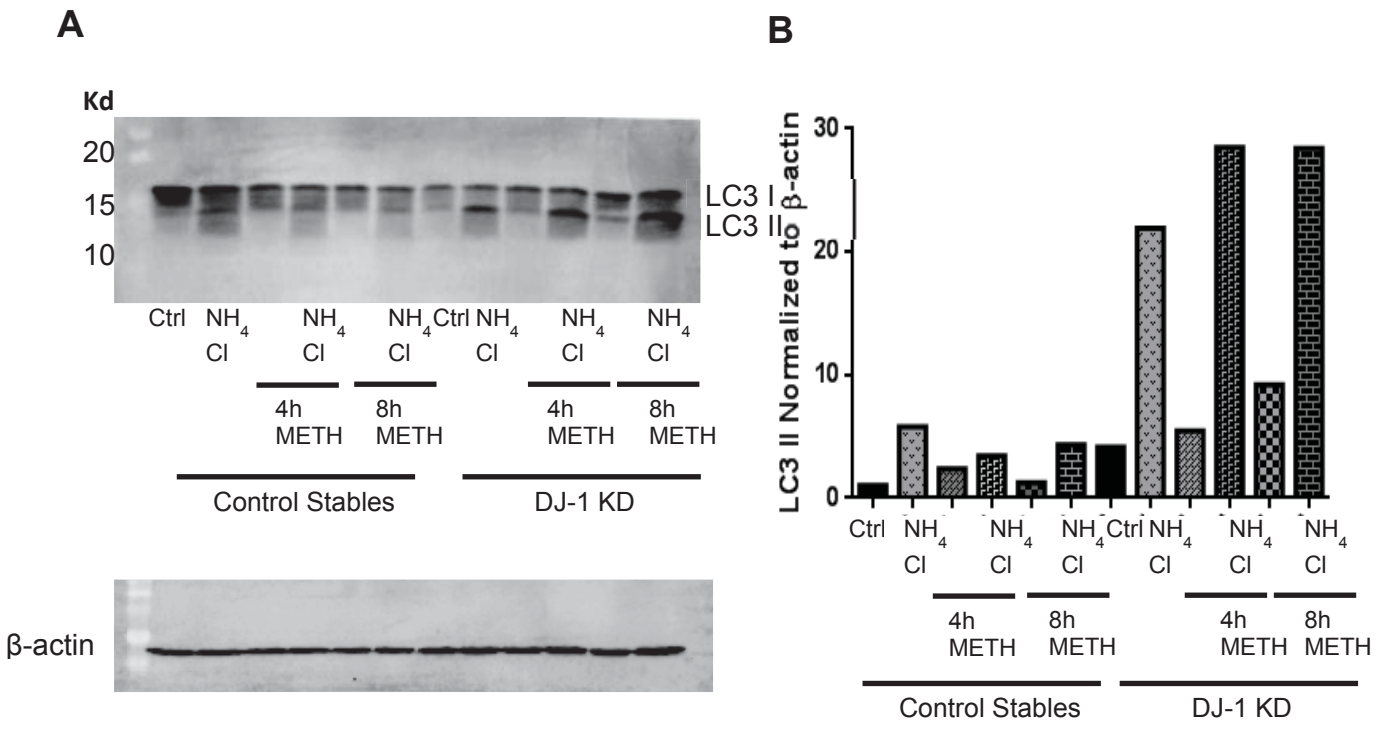

Figure 4.8 DJ-1 knockdown in N27 cells induces up-regulation of the autophagy marker, LC3-II.

(A) N27 DJ-1 knockdown cells and control cells transduced with a non-targeting shRNA vector were cultured in the absence or presence of METH for 4 h or 8 h. Cell lysates were analyzed via Western blotting (30 µg of protein per lane) using primary antibodies specific for LC3 and beta-actin. **(B)** Bar graph showing LC3-II band intensities normalized to the β-actin signal (relative to a value of 1 for 'control untreated'). N=2

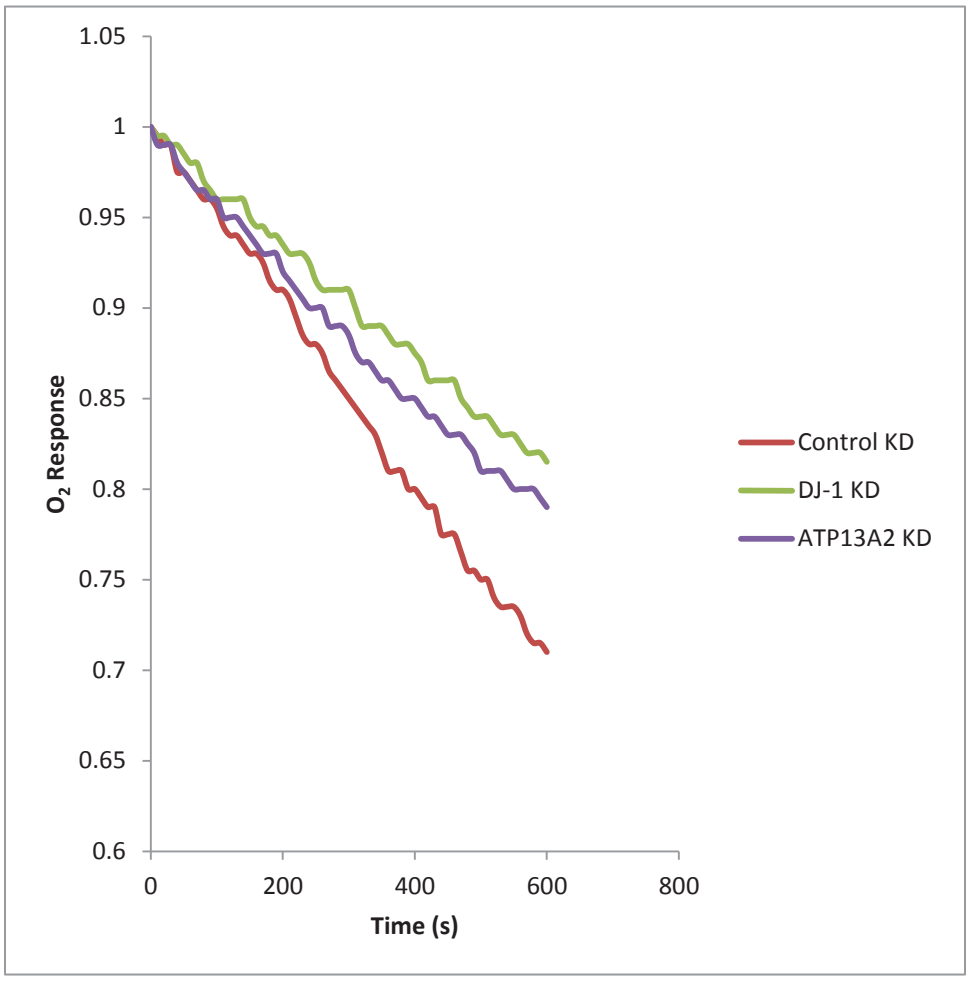

Figure 4.9 N27 cells depleted of DJ-1 or ATP13A2 have reduced rates of O_2 consumption.

N27 cells stably transduced with a lentiviral construct encoding an shRNA specific for ATP13A2 or DJ-1, and control cells transduced with a non-targeting shRNA vector, were analyzed for O_2 consumption rates using a Clark-type oxygen electrode attached to a voltmeter. N=2

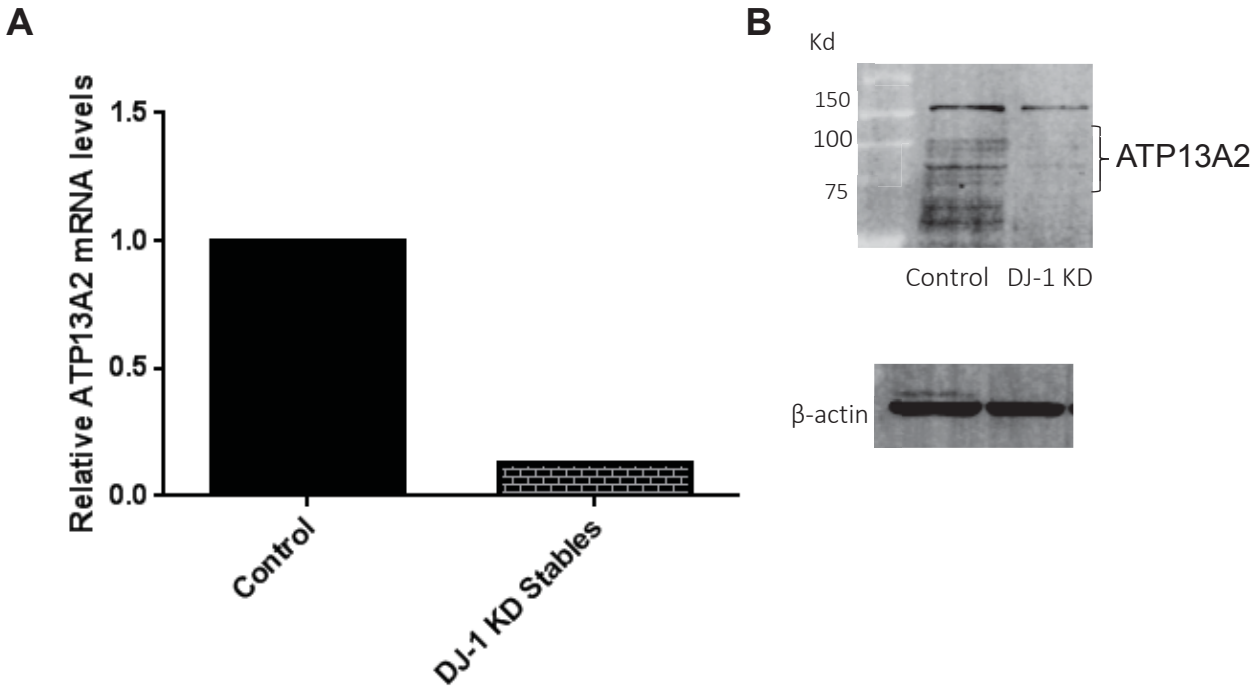

Figure 4.10 ATP13A2 mRNA and protein levels are decreased in N27 cells depleted of DJ-1.

(A) Bar graph showing ATP13A2 mRNA levels determined via qRT-PCR in N27 DJ-1 knockdown cells and in control cells (relative to a value of 1 for control cells). **(B)** Lysates from N27 DJ-1 knockdown cells and control cells transduced with a non-targeting shRNA vector were analyzed via Western blotting (30 µg of protein per lane) using primary antibodies specific for ATP13A2 and beta-actin. N=1

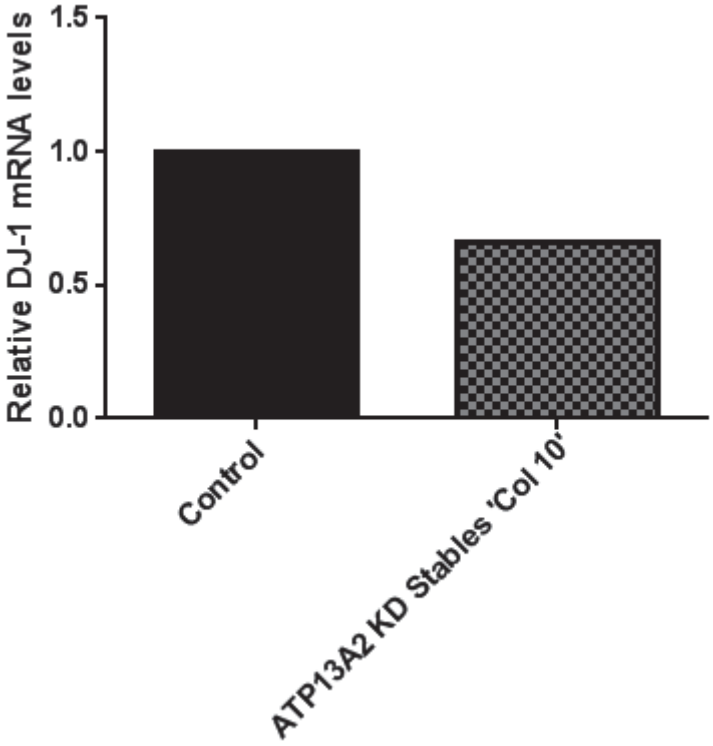

Figure 4.11 DJ-1 mRNA levels are decreased in N27 cells depleted of ATP13A2.

The bar graph shows DJ-1 mRNA levels determined via qRT-PCR in N27 ATP13A2 knockdown cells and in control cells (relative to a value of 1 for control cells). N=1

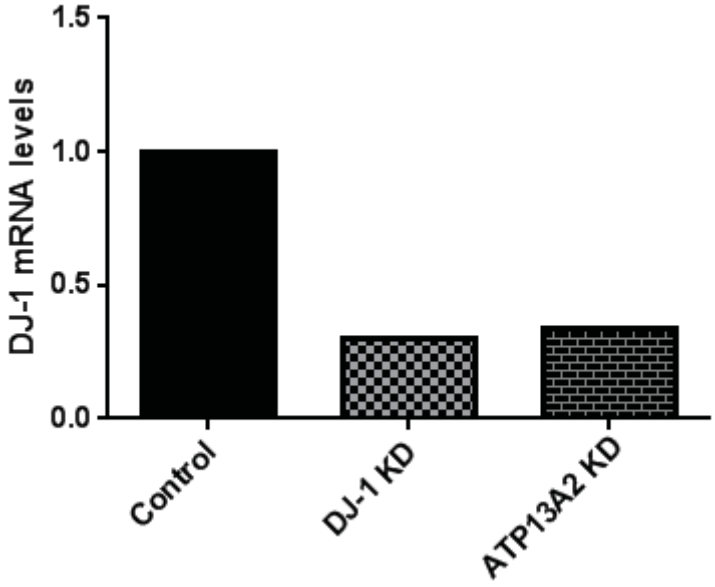

Figure 4.12 DJ-1 mRNA levels are decreased in rat primary midbrain cultures depleted of ATP13A2.

The bar graph shows DJ-1 mRNA levels determined via qRT-PCR in primary midbrain cultures transduced with lentivirus encoding a control (non-targeting) shRNA or an shRNA specific for DJ-1 or ATP13A2 (relative to a value of 1 for control cells). N=1

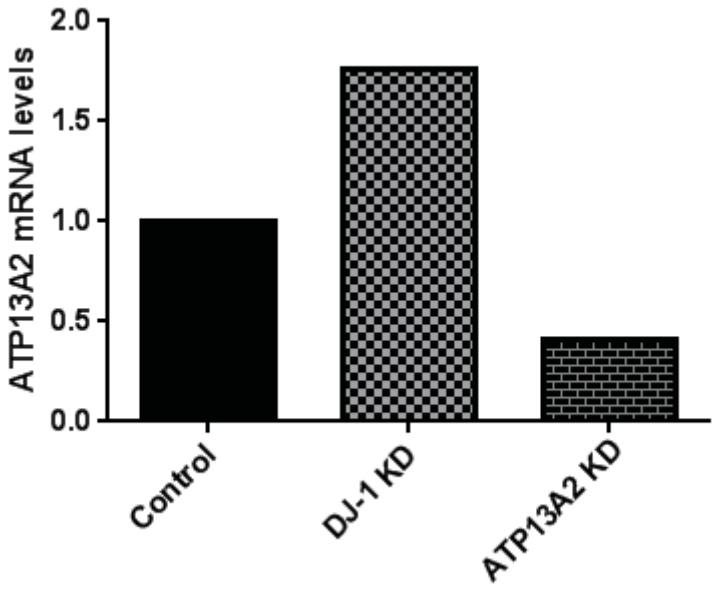

Figure 4.13 ATP13A2 mRNA levels are increased in rat primary midbrain cultures depleted of DJ-1.

The bar graph shows ATP13A2 mRNA levels determined via qRT-PCR in primary midbrain cultures transduced with lentivirus encoding a control (non-targeting) shRNA or an shRNA specific for DJ-1 or ATP13A2 (relative to a value of 1 for control cells). N=1

CHAPTER 5: DISCUSSION

5.1. Summary of our research

The monomeric subunit of DJ-1 is highly homologous to the *Pyrococcus horikoshii* 1704 gene product (PH1704), a bacterial cysteine protease which forms a hexamer. DJ-1 has an additional α helix (helix H8) at the C-terminus compared to PH1704. A recent study has shown that a truncated form of DJ-1 (15 amino acids cleaved at the C terminus, resulting in the removal of helix H8) has much greater protease activity compared to full length DJ-1 [46]. This C-terminally truncated form of DJ-1 (DJ-1Δ15) was found to accumulate in dopaminergic cells exposed to oxidative stress, leading Chen et al. [46] to conclude that full-length WT DJ-1 is in fact a zymogen that becomes activated via a redox-sensitive cleavage mechanism. Importantly, however, it is not known whether DJ-1Δ15 has the ability to form a hexamer, or whether such a hexameric structure is responsible for the observed protease activity. Based on the structural similarity of DJ-1Δ15 and PH1704, we proposed in Chapter 2 that DJ-1Δ15 can form functional hexamers as a result of removal of the C-terminal 15 residues, and this oligomerization could allow for the formation of a new interface necessary for the assembly of a trimer of dimers. In contrast, full length DJ-1 does not form a hexamer because helix H8 occludes this interface. To address

this hypothesis, we purified DJ-1Δ15 from an *E.coli* expression system. The protein was analyzed via a native PAGE and AUC, and a predicted three-dimensional structure of DJ-1Δ15 was examined using PyMOL. Our results showed that DJ-1Δ15 can potentially form high order oligomeric species. Specifically, the results of our Pymol analysis revealed that DJ-1Δ15 has the ability to form a closed hexamer by forming a new interface (patch 1'). In contrast, full-length DJ-1 cannot adopt a hexameric structure due to steric conflicts involving helix 8, as expected. Formation of the DJ-1Δ15 hexamer brings a glutamate residue at position 84 in proximity to the catalytic site to potentially form a catalytic triad with residues C106 and H126. In addition, the results of AUC analyses revealed that the formation of high-order oligomeric species by DJ-1Δ15 is concentration-dependent.

Oxidative stress can cause mitochondrial dysfunction through *S*-glutathionylation of mitochondrial proteins, including F_0F_1 ATP synthase, thus decreasing their activity [228]. Furthermore, glutathione-S-transferases (GSTs) have been shown to protect cells against oxidative stress [229]. In Chapter 3 we reported that high molecular weight (high-MW) species immunoreactive with a DJ-1 antibody are present in our preparations of recombinant, human WT DJ-1 (purified initially as a GST fusion protein prior to removal of the GST tag via proteolytic cleavage). These high-MW species have ATPase activity and appear as ring-like structures when examined by electron microscopy. In contrast, purified GST lacks both ATPase activity and ring-like structures. Interestingly, a proteomics study revealed that DJ-1 interacts with the α- and β-subunits of F_1 ATP synthase in a

rat mesencephalic cell line [205]. The biochemical function of DJ-1 is unknown. Our results show that DJ-1 interacts with *E.coli* F_1 ATP synthase, and that the reduced form of DJ-1 is preferentially involved in this interaction. These results provide new insights into the biochemical mechanism by which DJ-1 preserves mitochondrial function in neurons exposed to PD-related insults – namely, by interacting with F_1 ATPase, a protein complex that is structurally and functionally well conserved between *E. coli* and eukaryotic mitochondria.

ATP13A2 knockdown has been shown to decrease proteolytic processing of lysosomal enzymes, reduce degradation of lysosomal substrates, increase mitochondrial mass, and increase ROS production [175, 176]. Cells lacking DJ-1 exhibit a decrease in mitochondrial clearance (mitophagy), an increase in mitochondrial mass and an increase in ROS levels [144]. In Chapter 4, we examined the functional interplay between ATP13A2 and DJ-1 in neuronal cells exposed to a PD-related stress, METH, a drug that imposes a burden on the autophagy clearance system in dopaminergic neuronal cells [230, 231]. We hypothesized that knockdown of ATP13A2 or DJ-1 in N27 dopaminergic cells would disrupt lysosomal degradation, leading to an increase in LC3-II, an autophagosome marker. Our results showed that ATP13A2 knockdown in N27 cells led to an increase in LC3-II. This increase was further enhanced with the addition of METH in the absence or presence of NH_4Cl, an agent that disrupts lysosomal pH. Because ATP13A2 is a lysosomal ATPase that is known to acidify lysosomes [175], our data suggest that the increase in LC3-II-positive autophagosomes may be due to the disruption of lysosomal pH, a defect that

precludes autophagosome-lysosome fusion [232]. Furthermore, N27 cells depleted of ATP13A2 showed a decrease in red puncta staining using AO, a dye that accumulates in acidic vesicles (pH<4). In addition, overexpression of ATP13A2 interfered with the METH-induced up-regulation of autophagosomes and autolysosomes in SH-SY5Y dopaminergic neuronal cells. These results suggest that ATP13A2 may enhance autophagic clearance and inhibit autophagosome accumulation in METH-treated cells, potentially by enhancing autophagosome-lysosome fusion and/or lysosomal degradation [175]. Likewise, N27 DJ-1 knockdown cells exhibited increased levels of LC3-II. Previous results have shown that cells lacking DJ-1 exhibit a decrease in mitochondrial clearance, an increase in mitochondrial mass, and an increase in ROS levels [144]. ROS accumulation could disrupt the lysosomal membrane [161]. Therefore, our data suggest that N27 DJ-1 knockdown cells have high basal levels of ROS that cause disruption of the lysosomal membrane and hence prevent the fusion of autophagosomes with lysosomes. METH may enhance this disruption of autophagy by triggering additional oxidative stress. In addition, DJ-1 might be enhancing clearance of the autophagosomes.

To analyze the effects of DJ-1 or ATP13A2 knockdown on mitochondrial respiration, the rate of O_2 consumption was measured on in intact cells. Our results showed a decrease in O_2 consumption for N27 cells depleted of either ATP13A2 or DJ-1. Dopaminergic neurons contain high levels of ROS due to the presence of dopamine. Dopamine undergoes auto-oxidation to the *o*-quinone form, a reaction that involves the generation of superoxide radicals [36]. Because

dopaminergic neurons have higher basal levels of oxidative stress than other types of neurons, they are more susceptible to pathogenic mechanisms that further up-regulate ROS, including mitochondrial dysfunction. Interestingly, another group reported that fibroblasts from human patients with an ATP13A2 mutation exhibit increased O_2 consumption rates compared to control fibroblasts. These data suggest that dopamine auto-oxidation may render dopaminergic neuronal cells more vulnerable to a build-up of dysfunctional mitochondria as a result of a loss of ATP13A2 or DJ-1 function. Dopamine auto-oxidation should result in the formation of *o*-quinones that disrupt complex 1 in dopaminergic neuronal cells, and this effect could be enhanced by the accumulation of dysfunctional mitochondria as a result of mitophagy impairment in cells depleted of ATP13A2 or DJ-1. In additional experiments, we sought to determine whether ATP13A2 and DJ-1 interact on a functional level to modulate mitochondrial or/and lysosomal function. We found that ATP13A2 mRNA and protein were down-regulated in N27 DJ-1 knockdown cells, and levels of DJ-1 mRNA were reduced in N27 ATP13A2 knockdown cells. These results suggest that DJ-1 and ATP13A2 are co-regulated in N27 cells. In contrast, ATP13A2 mRNA was increased in rat primary midbrain cultures depleted of DJ-1 via shRNA knockdown. These results suggest that the gene expression patterns of ATP13A2 and DJ-1 in N27 cells versus primary midbrain cultures are overlapping but non-identical, perhaps reflecting differences in N27 gene expression patterns associated with immortalization and/or the fact that primary midbrain cultures consist of a mixture of glial and neuronal cell types. Up-regulation of ATP13A2 in

primary midbrain cultures implies that ATP13A2 may have evolved as a protective mechanism to alleviate toxic effects of DJ-1 down-regulation (e.g. oxidative stress, disrupted autophagy) in neuronal and/or glial cells.

5.2. Future directions

5.2.1 To determine whether E84A is a member of a catalytic triad in hexameric DJ-1Δ15.

In Chapter 2, we reported that hexamer formation by DJ-1Δ15 might bring a glutamate residue 84 from one subunit (E84) into a position suitable for forming a catalytic triad with cysteine 106 (C106) and histidine 126 (H126) form a second subunit. Formation of the catalytic triad could be essential for the ability of DJ-1Δ15 to function as a protease. To determine whether E84 is important for the protease activity of DJ-1Δ15, we have generated a construct with E84 mutated to alanine (DJ-1Δ15-E84A). Future experiments will be aimed at examining the protease activity of this mutant. If E84A shows a loss of protease activity, then we will infer that DJ-1-Δ15 adopts a hexameric structure to enable the assembly of a catalytic triad essential for protease function, similar to PH1704 [112]. If our prediction is incorrect, then we will infer that the formation of a catalytic triad involving E84 is not essential for the protease activity of DJ-1-Δ15. A potential limitation is that DJ-1-Δ15 may fail to form a stable hexamer as a result of C106 over-oxidation. In this case, we will repeat the experiment with DJ-1Δ15-C106A and/or DJ-1Δ15-C106D. The findings from this study will provide more insights into how DJ-1Δ15 carriers out a protease function by revealing information about its active site architecture, how it is regulated, and its optimal substrates.

Ultimately it may be possible to develop inhibitors to test the biological role of this protease.

5.2.2 To determine whether GST modulates interactions of DJ-1 with F_1 ATP synthase.

In Chapter 3, we determined that recombinant; human WT DJ-1 (purified initially as a GST fusion protein prior to removal of the GST tag via proteolytic cleavage) contained high molecular weight (high-MW) species immunoreactive with DJ-1 antibodies. The presence of these high-MW species correlates with (i) the presence of ring-like structures that can be visualized by TEM, and (ii) the presence of ATPase activity in our DJ-1 preparations. We inferred that the high-MW species observed in these preparations consisted of a complex of DJ-1 with F_1 ATP synthase. In contrast, untagged recombinant human WT DJ-1 purified via ion-exchange chromatography did not contain high-MW, DJ-1-immunoreactive species or show ATPase activity (data not shown). Based on these results, a future goal will be to determine the role of GST in modulating the interaction between DJ-1 and F_1 ATP synthase.

To assess whether DJ-1 interacts with GST, a pull-down experiment will be carried out by incubating recombinant untagged DJ-1 with GST bound to a resin with covalently linked glutathione (GSH). The protein material isolated using the pull-down approach will be analyzed via Western blotting using antibodies specific to DJ-1 and GST. To examine whether GST co-purifies with DJ-1 and/or F_1 ATP synthase, GST and untagged DJ-1 will be co-expressed in *E.coli* cells and purified using a GSH resin. The purified protein will be tested for ATPase

activity and for the presence of F_1 ATP synthase subunits, GST, and DJ-1 via Western blotting. Evidence of ATPase activity and of ATP synthase subunits, GST, and DJ-1 in the affinity-purified protein would suggest that DJ-1 and F_1 ATP synthase form a complex with GST. To further address this hypothesis, the purified protein will be analyzed via mass spectrometry. Previous studies have shown that in the presence of oxidative stress, F_1 ATP synthase subunits are glutathionylated, thus decreasing their activity [228]. In addition, cysteine oxidative post-translational modifications (for example, disulfide bond formation within) the ATP synthase complex cause conformational changes that modulate its activity [233]. Furthermore, Drosophila glutathione S-transferase Omega 1 (GSTO) rescued glutathionylated ATP synthase beta subunit, thus enhancing its activity [229]. Glutathionylation, deglutathionylation and other post translational modifications of mitochondrial ATP synthase subunits are important for these proteins to function under oxidative stress conditions. Therefore, results from our studies will shed more light on mechanism for DJ-1 neuroprotection in mitochondria. First, DJ-1 may modulate ATP synthase activity by protecting against glutathionylation through its interaction with ATP synthase, second, in the presence of GST, DJ-1 may deglutathionylate ATP synthase subunits. Third, GST may modulate the DJ-1-F_1 ATP synthase interaction.

5.2.3 To determine the effects of aSyn on F_1 ATPase activity.

A proteomics study revealed that aSyn interacts with the α- and β-subunits of F_1 ATP synthase in a rat mesencephalic cell line [205]. To examine the effects of aSyn on the function of F_1 ATP synthase, purified F_1 ATP synthase complex will

be incubated in the absence or presence of aSyn and tested for ATPase activity. If we find that aSyn inhibits the ATPase function, then the F_1 ATP synthase complex will be pre-incubated with aSyn in the absence or presence of DJ-1 and re-tested for ATPase activity. As a complementary approach, the effects of aSyn on the ATPase activity associated with recombinant DJ-1 (purified as a GST fusion protein prior to removal of the GST tag via proteolytic cleavage) will be examined. These data will provide insight into how aSyn elicits mitochondrial dysfunction and the mechanism by which DJ-1 carries out its neuroprotective function.

5.2.4 To determine the effects of DJ-1 or ATP13A2 expression on LC3-II accumulation and mitochondrial respiration.

Future efforts will be directed towards testing the effects of over-expressing DJ-1 or ATP13A2 in N27 cells depleted of either protein. We predict that DJ-1 or ATP13A2 expression will rescue defects in autophagosome-lysosome fusion in ATP13A2 or DJ-1 knockdown cells, respectively. We also predict that defects in mitochondrial respiration will be rescued by over-expression of DJ-1 in ATP13A2 knockdown cells (and vice versa). If this is true, then we will infer that both proteins act in concert to alleviate mitochondrial dysfunction and/or the accumulation of defective mitochondria triggered by PD-related insults.

5.2.5 To determine the effects of DJ-1 or ATP13A2 expression on aSyn stability.

Aggregated aSyn is eliminated from cells via lysosomal autophagy [164, 175]. In addition, aSyn accumulation induces a buildup of ROS which have been shown

to disrupt lysosomal membrane integrity, ultimately causing cell death [210, 234]. DJ-1 is known to inhibit aSyn aggregation and toxicity, suppress oxidative stress, and stimulate lysosomal autophagy [144, 156, 214]. We predict that DJ-1 and ATP13A2 interact functionally to inhibit aSyn aggregation and neurotoxicity. To address this hypothesis, N27 cells depleted of ATP13A2 will be transduced with an adenovirus encoding DJ-1, whereas DJ-1 knockdown cells will be transduced with an adenovirus encoding ATP13A2 (both sets of cells will be co-transduced with aSyn virus). As controls, cells depleted of ATP13A2 or DJ-1 will be transduced with LacZ virus (instead of virus encoding DJ-1 or ATP13A2). The effects of DJ-1 or ATP13A2 over-expression on aSyn stability, lysosomal membrane integrity, and autophagosome accumulation will be evaluated. We predict that DJ-1 or ATP13A2 over-expression will rescue defects in aSyn stability, lysosomal membrane integrity, and autophagosome-lysosome fusion in ATP13A2 or DJ-1 knockdown cells, respectively. If this is true, then we will infer that DJ-1 and ATP13A2 act as part of a common pathway to preserve lysosomal autophagy and ensure the lysosomal clearance of toxic aSyn aggregates (Fig. 5.1). Preliminary data from an experiment involving ATP13A2 knockdown in dopaminergic neuronal cells suggest that ATP13A2 plays a role in modulating aSyn accumulation (Fig. 5.2). Consistent with this finding, evidence suggests that the *C. elegans* ATP13A2 ortholog inhibits the misfolding of human aSyn [179].

5.2.6 To determine the effects of DJ-1 or ATP13A2 knockdown on aSyn degradation.

We predict that DJ-1 and ATP13A2 cooperate to promote aSyn degradation. To address this hypothesis, lysosomes will be isolated from N27 cells depleted of ATP13A2 or DJ-1 via centrifugation of a mitochondrial-lysosomal fraction through a discontinuous metrizamide density gradient [235]. Lysosomes will be incubated with radiolabeled aSyn and glyceraldehyde 3-phosphate dehydrogenase (GAPDH), a protein that will serve as a positive control [235]. After precipitating the proteins with trichloroacetic acid, the degree of proteolysis will be calculated as the percentage of the initial acid-insoluble radioactivity (protein) transformed into acid-soluble radioactivity (amino acids and small peptides resulting from protein degradation) [236]. The data will indicate whether lysosomes isolated from cells depleted of ATP13A2 or DJ-1 have a reduced ability to degrade aSyn in a cell-free system, which will serve as a model of chaperone-mediated autophagy [237]. We predict that lysosomes isolated from cells depleted of ATP13A2 may be dysfunctional as a result of acidification defects and thus may exhibit a decreased rate of aSyn clearance via autophagy. In addition, we predict that lysosomes isolated from cells depleted of DJ-1 may be damaged by oxidative stress and thus may exhibit a decreased rate of aSyn degradation. If these predictions are validated, then we will infer that the function of ATP13A2 and/or DJ-1 is necessary for aSyn degradation via lysosomal autophagy (i.e. both chaperone-mediated autophagy and macroautophagy).

In addition, the rates of aSyn degradation in N27 cells depleted of ATP13A2 or DJ-1 or in control cells will be assessed via pulse pulse-chase analysis. The cells will be labeled with ^{35}S-methionine (pulse), washed with buffer, and incubated in fresh media with excess unlabeled methionine (chase). The half-life of aSyn will be estimated from exponential decay curves of radioactivity versus time.

Collectively, our findings may support a model in which ATP13A2 and DJ-1 protect against the neurotoxicity of PD-related insults by suppressing the accumulation of dysfunctional mitochondria and ROS production, thereby alleviating defects in lysosomal membrane integrity and autophagy (Fig 5.1)

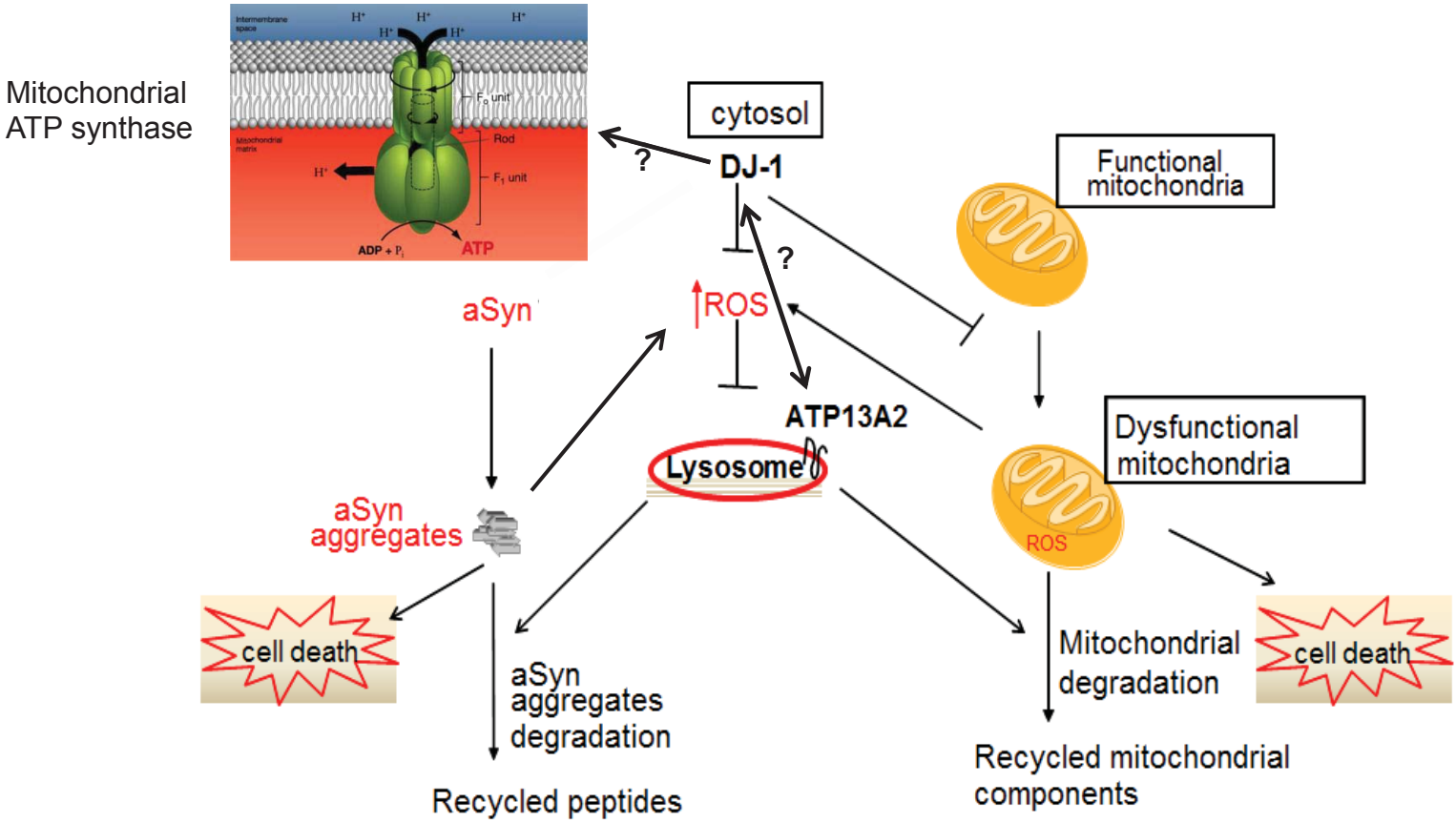

Figure 5.1 Proposed model for DJ-1 and ATP13A2 neuroprotective interplay.

DJ-1 maintains lysosomal membrane integrity by inhibiting mitochondrial dysfunction and ROS accumulation. Expression of ATP13A2 in the lysosomal membrane is predicted to be necessary for the elimination of aSyn aggregates and dysfunctional mitochondria via autophagy. Cells deficient in DJ-1 and/or ATP13A2 will show an increase in ROS and a decreased rate of clearance of aSyn and dysfunctional mitochondria.

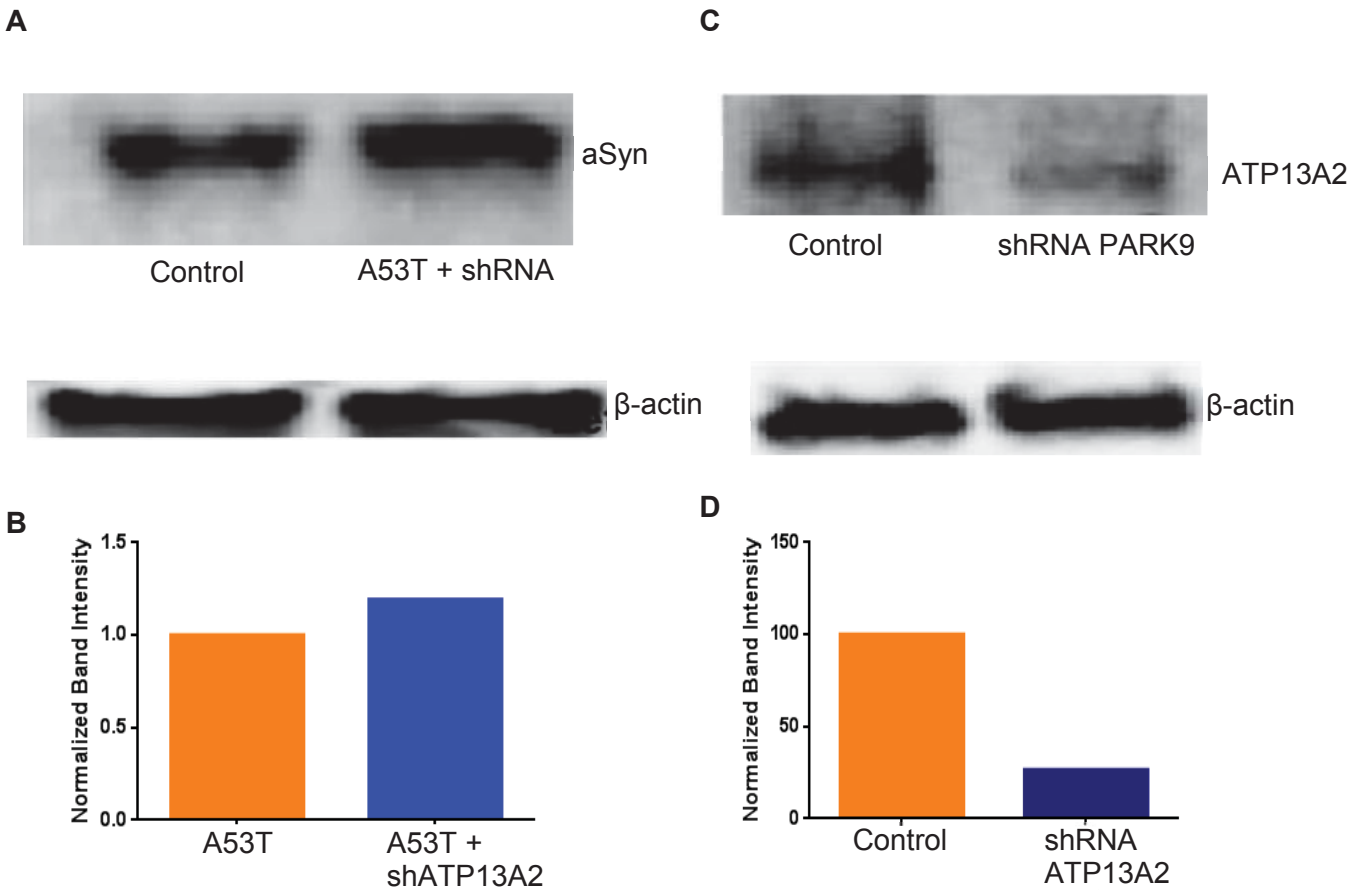

Figure 5.2 Knocking down ATP13A2 increases the accumulation of aSyn A53T in dopaminergic cells.
MES 23.5 cells were transduced with A53T adenovirus +/- ATP13A2 shRNA lentivirus. The cells were harvested after 96 h, and cell lysates were analyzed via Western blotting (15 µg of protein per lane) using a primary antibody specific for aSyn (A, B) or ATP13A2 (C, D). Control MES 23.5 cells were untreated. Beta-actin was used as a loading control.

LIST OF REFERENCES

LIST OF REFERENCES

1. Parkinson, J., *An essay on the shaking palsy. 1817.* J Neuropsychiatry Clin Neurosci, 2002. **14**(2): p. 223-36; discussion 222.
2. Spillantini, M.G., et al., *a-Synuclein in Lewy bodies.* Nature, 1997. **388**: p. 839-840.
3. Moore, D.J., et al., *Molecular pathophysiology of Parkinson's disease.* Annu Rev Neurosci, 2005. **28**: p. 57-87.
4. Lang, A.E. and A.M. Lozano, *Parkinson's disease. First of two parts.* N Engl J Med, 1998. **339**(15): p. 1044-53.
5. de Lau, L.M., et al., *Incidence of parkinsonism and Parkinson disease in a general population: the Rotterdam Study.* Neurology, 2004. **63**(7): p. 1240-4.
6. Kowal, S.L., et al., *The current and projected economic burden of Parkinson's disease in the United States.* Mov Disord, 2013. **28**(3): p. 311-8.
7. Lim, S.Y. and A.E. Lang, *The nonmotor symptoms of Parkinson's disease--an overview.* Mov Disord, 2010. **25 Suppl 1**: p. S123-30.
8. Barone, P., et al., *The PRIAMO study: A multicenter assessment of nonmotor symptoms and their impact on quality of life in Parkinson's disease.* Mov Disord, 2009. **24**(11): p. 1641-9.
9. Martinez-Martin, P., et al., *The impact of non-motor symptoms on health-related quality of life of patients with Parkinson's disease.* Mov Disord, 2011. **26**(3): p. 399-406.
10. Hughes, A.J., et al., *Accuracy of clinical diagnosis of idiopathic Parkinson's disease: a clinico-pathological study of 100 cases.* J Neurol Neurosurg Psychiatry, 1992. **55**(3): p. 181-4.
11. Braak, H., et al., *Staging of brain pathology related to sporadic Parkinson's disease.* Neurobiol Aging, 2003. **24**(2): p. 197-211.
12. Pollanen, M.S., D.W. Dickson, and C. Bergeron, *Pathology and biology of the Lewy body.* J Neuropathol Exp Neurol, 1993. **52**(3): p. 183-91.
13. Baba, M., et al., *Aggregation of alpha-synuclein in Lewy bodies of sporadic Parkinson's disease and dementia with Lewy bodies.* Am J Pathol, 1998. **152**(4): p. 879-84.
14. Spillantini, M.G., et al., *Alpha-synuclein in Lewy bodies.* Nature, 1997. **388**(6645): p. 839-40.
15. Gibb, W.R. and A.J. Lees, *The relevance of the Lewy body to the pathogenesis of idiopathic Parkinson's disease.* J Neurol Neurosurg Psychiatry, 1988. **51**(6): p. 745-52.

16. Rao, G., et al., *Does this patient have Parkinson disease?* JAMA, 2003. **289**(3): p. 347-53.
17. Jankovic, J., *Levodopa strengths and weaknesses.* Neurology, 2002. **58**(4 Suppl 1): p. S19-32.
18. Munoz, P., et al., *Dopamine oxidation and autophagy.* Parkinsons Dis, 2012. **2012**: p. 920953.
19. Jankovic, J. and L.G. Aguilar, *Current approaches to the treatment of Parkinson's disease.* Neuropsychiatr Dis Treat, 2008. **4**(4): p. 743-57.
20. Jankovic, J. and M. Stacy, *Medical management of levodopa-associated motor complications in patients with Parkinson's disease.* CNS Drugs, 2007. **21**(8): p. 677-92.
21. Solla, P., et al., *Therapeutic interventions and adjustments in the management of Parkinson disease: role of combined carbidopa/levodopa/entacapone (Stalevo).* Neuropsychiatr Dis Treat, 2010. **6**: p. 483-90.
22. Hwang, O., *Role of oxidative stress in Parkinson's disease.* Exp Neurobiol, 2013. **22**(1): p. 11-7.
23. Schapira, A.H. and P. Jenner, *Etiology and pathogenesis of Parkinson's disease.* Mov Disord, 2011. **26**(6): p. 1049-55.
24. Obeso, J.A., et al., *Missing pieces in the Parkinson's disease puzzle.* Nat Med, 2010. **16**(6): p. 653-61.
25. Dawson, T.M. and V.L. Dawson, *The role of parkin in familial and sporadic Parkinson's disease.* Mov Disord, 2010. **25 Suppl 1**: p. S32-9.
26. Corti, O., S. Lesage, and A. Brice, *What genetics tells us about the causes and mechanisms of Parkinson's disease.* Physiol Rev, 2011. **91**(4): p. 1161-218.
27. Martin, I., V.L. Dawson, and T.M. Dawson, *Recent advances in the genetics of Parkinson's disease.* Annu Rev Genomics Hum Genet, 2011. **12**: p. 301-25.
28. Shulman, J.M., P.L. De Jager, and M.B. Feany, *Parkinson's disease: genetics and pathogenesis.* Annu Rev Pathol, 2011. **6**: p. 193-222.
29. Schapira, A.H., et al., *Mitochondrial complex I deficiency in Parkinson's disease.* Lancet, 1989. **1**(8649): p. 1269.
30. Parker, W.D., Jr., J.K. Parks, and R.H. Swerdlow, *Complex I deficiency in Parkinson's disease frontal cortex.* Brain Res, 2008. **1189**: p. 215-8.
31. Greenamyre, J.T., et al., *Complex I and Parkinson's disease.* IUBMB Life, 2001. **52**(3-5): p. 135-41.
32. Keeney, P.M., et al., *Parkinson's disease brain mitochondrial complex I has oxidatively damaged subunits and is functionally impaired and misassembled.* J Neurosci, 2006. **26**(19): p. 5256-64.
33. Abou-Sleiman, P.M., M.M. Muqit, and N.W. Wood, *Expanding insights of mitochondrial dysfunction in Parkinson's disease.* Nat Rev Neurosci, 2006. **7**(3): p. 207-19.
34. Lin, M.T. and M.F. Beal, *Mitochondrial dysfunction and oxidative stress in neurodegenerative diseases.* Nature, 2006. **443**(7113): p. 787-95.

35. Henchcliffe, C. and M.F. Beal, *Mitochondrial biology and oxidative stress in Parkinson disease pathogenesis.* Nat Clin Pract Neurol, 2008. **4**(11): p. 600-9.
36. Graham, D.G., et al., *Autoxidation versus covalent binding of quinones as the mechanism of toxicity of dopamine, 6-hydroxydopamine, and related compounds toward C1300 neuroblastoma cells in vitro.* Mol Pharmacol, 1978. **14**(4): p. 644-53.
37. Berman, S.B. and T.G. Hastings, *Dopamine oxidation alters mitochondrial respiration and induces permeability transition in brain mitochondria: implications for Parkinson's disease.* J Neurochem, 1999. **73**(3): p. 1127-37.
38. Xu, Y., et al., *Dopamine, in the presence of tyrosinase, covalently modifies and inactivates tyrosine hydroxylase.* J Neurosci Res, 1998. **54**(5): p. 691-7.
39. Whitehead, R.E., et al., *Reaction of oxidized dopamine with endogenous cysteine residues in the human dopamine transporter.* J Neurochem, 2001. **76**(4): p. 1242-51.
40. LaVoie, M.J., et al., *Dopamine covalently modifies and functionally inactivates parkin.* Nat Med, 2005. **11**(11): p. 1214-21.
41. Dehay, B., et al., *Lysosomal impairment in Parkinson's disease.* Mov Disord, 2013. **28**(6): p. 725-32.
42. Ebrahimi-Fakhari, D., L. Wahlster, and P.J. McLean, *Protein degradation pathways in Parkinson's disease: curse or blessing.* Acta Neuropathol, 2012. **124**(2): p. 153-72.
43. Tofaris, G.K., *Lysosome-dependent pathways as a unifying theme in Parkinson's disease.* Mov Disord, 2012. **27**(11): p. 1364-9.
44. Vila, M., et al., *Lysosomal membrane permeabilization in Parkinson disease.* Autophagy, 2011. **7**(1): p. 98-100.
45. Sidransky, E., et al., *Multicenter analysis of glucocerebrosidase mutations in Parkinson's disease.* N Engl J Med, 2009. **361**(17): p. 1651-61.
46. Chen, J., L. Li, and L.S. Chin, *Parkinson disease protein DJ-1 converts from a zymogen to a protease by carboxyl-terminal cleavage.* Hum Mol Genet, 2010. **19**(12): p. 2395-408.
47. Levine, B. and D.J. Klionsky, *Development by self-digestion: molecular mechanisms and biological functions of autophagy.* Dev Cell, 2004. **6**(4): p. 463-77.
48. Wang, Y., et al., *Macroautophagy and chaperone-mediated autophagy are required for hepatocyte resistance to oxidant stress.* Hepatology, 2010. **52**(1): p. 266-77.
49. Ravikumar, B., et al., *Regulation of mammalian autophagy in physiology and pathophysiology.* Physiol Rev, 2010. **90**(4): p. 1383-435.
50. Tanida, I. and S. Waguri, *Measurement of autophagy in cells and tissues.* Methods Mol Biol, 2010. **648**: p. 193-214.
51. Klionsky, D.J., et al., *A unified nomenclature for yeast autophagy-related genes.* Dev Cell, 2003. **5**(4): p. 539-45.

52. Tanida, I., T. Ueno, and E. Kominami, *LC3 conjugation system in mammalian autophagy.* Int J Biochem Cell Biol, 2004. **36**(12): p. 2503-18.
53. Kabeya, Y., et al., *LC3, GABARAP and GATE16 localize to autophagosomal membrane depending on form-II formation.* J Cell Sci, 2004. **117**(Pt 13): p. 2805-12.
54. Tanida, I., et al., *HsAtg4B/HsApg4B/autophagin-1 cleaves the carboxyl termini of three human Atg8 homologues and delipidates microtubule-associated protein light chain 3- and GABAA receptor-associated protein-phospholipid conjugates.* J Biol Chem, 2004. **279**(35): p. 36268-76.
55. Tanida, I., et al., *Human Apg3p/Aut1p homologue is an authentic E2 enzyme for multiple substrates, GATE-16, GABARAP, and MAP-LC3, and facilitates the conjugation of hApg12p to hApg5p.* Journal of Biological Chemistry, 2002. **277**(16): p. 13739-13744.
56. Kabeya, Y., et al., *LC3, a mammalian homologue of yeast Apg8p, is localized in autophagosome membranes after processing.* Embo Journal, 2000. **19**(21): p. 5720-5728.
57. Banerjee, R., M.F. Beal, and B. Thomas, *Autophagy in neurodegenerative disorders: pathogenic roles and therapeutic implications.* Trends Neurosci, 2010. **33**(12): p. 541-9.
58. Lynch-Day, M.A., et al., *The role of autophagy in Parkinson's disease.* Cold Spring Harb Perspect Med, 2012. **2**(4): p. a009357.
59. Klein, C. and A. Westenberger, *Genetics of Parkinson's disease.* Cold Spring Harb Perspect Med, 2012. **2**(1): p. a008888.
60. Polymeropoulos, M.H., et al., *Mutation in the alpha-synuclein gene identified in families with Parkinson's disease.* Science, 1997. **276**(5321): p. 2045-7.
61. Kruger, R., et al., *Ala30Pro mutation in the gene encoding alpha-synuclein in Parkinson's disease.* Nat Genet, 1998. **18**(2): p. 106-8.
62. Zarranz, J.J., et al., *The new mutation, E46K, of alpha-synuclein causes Parkinson and Lewy body dementia.* Ann Neurol, 2004. **55**(2): p. 164-73.
63. Khalaf, O., et al., *The H50Q Mutation Enhances alpha-Synuclein Aggregation, Secretion, and Toxicity.* J Biol Chem, 2014. **289**(32): p. 21856-76.
64. Fares, M.B., et al., *The novel Parkinson's disease linked mutation G51D attenuates in vitro aggregation and membrane binding of alpha-synuclein, and enhances its secretion and nuclear localization in cells.* Hum Mol Genet, 2014. **23**(17): p. 4491-509.
65. Chartier-Harlin, M.C., et al., *Alpha-synuclein locus duplication as a cause of familial Parkinson's disease.* Lancet, 2004. **364**(9440): p. 1167-9.
66. Singleton, A.B., et al., *alpha-Synuclein locus triplication causes Parkinson's disease.* Science, 2003. **302**(5646): p. 841.
67. Conway, K.A., et al., *Acceleration of oligomerization, not fibrillization, is a shared property of both alpha-synuclein mutations linked to early-onset Parkinson's disease: implications for pathogenesis and therapy.* Proc Natl Acad Sci U S A, 2000. **97**(2): p. 571-6.

68. Rochet, J.C., B.A. Hay, and M. Guo, *Molecular insights into Parkinson's disease.* Prog Mol Biol Transl Sci, 2012. **107**: p. 125-88.
69. Olanow, C.W. and P. Brundin, *Parkinson's disease and alpha synuclein: is Parkinson's disease a prion-like disorder?* Mov Disord, 2013. **28**(1): p. 31-40.
70. George, J.M., *The synucleins.* Genome Biol, 2002. **3**(1): p. REVIEWS3002.
71. Davidson, W.S., et al., *Stabilization of alpha-synuclein secondary structure upon binding to synthetic membranes.* J Biol Chem, 1998. **273**(16): p. 9443-9.
72. Perrin, R.J., et al., *Interaction of human alpha-Synuclein and Parkinson's disease variants with phospholipids. Structural analysis using site-directed mutagenesis.* J Biol Chem, 2000. **275**(44): p. 34393-8.
73. Giasson, B.I., et al., *A hydrophobic stretch of 12 amino acid residues in the middle of alpha-synuclein is essential for filament assembly.* J Biol Chem, 2001. **276**(4): p. 2380-6.
74. Li, W., et al., *Aggregation promoting C-terminal truncation of alpha-synuclein is a normal cellular process and is enhanced by the familial Parkinson's disease-linked mutations.* Proc Natl Acad Sci U S A, 2005. **102**(6): p. 2162-7.
75. Liu, C.W., et al., *A precipitating role for truncated alpha-synuclein and the proteasome in alpha-synuclein aggregation: implications for pathogenesis of Parkinson disease.* J Biol Chem, 2005. **280**(24): p. 22670-8.
76. Murray, I.V., et al., *Role of alpha-synuclein carboxy-terminus on fibril formation in vitro.* Biochemistry, 2003. **42**(28): p. 8530-40.
77. Anderson, J.P., et al., *Phosphorylation of Ser-129 is the dominant pathological modification of alpha-synuclein in familial and sporadic Lewy body disease.* J Biol Chem, 2006. **281**(40): p. 29739-52.
78. Murphy, D.D., et al., *Synucleins are developmentally expressed, and alpha-synuclein regulates the size of the presynaptic vesicular pool in primary hippocampal neurons.* J Neurosci, 2000. **20**(9): p. 3214-20.
79. Cabin, D.E., et al., *Synaptic vesicle depletion correlates with attenuated synaptic responses to prolonged repetitive stimulation in mice lacking alpha-synuclein.* J Neurosci, 2002. **22**(20): p. 8797-807.
80. Larsen, K.E., et al., *Alpha-synuclein overexpression in PC12 and chromaffin cells impairs catecholamine release by interfering with a late step in exocytosis.* J Neurosci, 2006. **26**(46): p. 11915-22.
81. George, J.M., et al., *Characterization of a novel protein regulated during the critical period for song learning in the zebra finch.* Neuron, 1995. **15**(2): p. 361-72.
82. Kholodilov, N.G., et al., *Increased expression of rat synuclein in the substantia nigra pars compacta identified by mRNA differential display in a model of developmental target injury.* J Neurochem, 1999. **73**(6): p. 2586-99.

83. Vila, M., et al., *Alpha-synuclein up-regulation in substantia nigra dopaminergic neurons following administration of the parkinsonian toxin MPTP.* J Neurochem, 2000. **74**(2): p. 721-9.
84. Sidhu, A., C. Wersinger, and P. Vernier, *alpha-Synuclein regulation of the dopaminergic transporter: a possible role in the pathogenesis of Parkinson's disease.* FEBS Lett, 2004. **565**(1-3): p. 1-5.
85. Sidhu, A., C. Wersinger, and P. Vernier, *Does alpha-synuclein modulate dopaminergic synaptic content and tone at the synapse?* FASEB J, 2004. **18**(6): p. 637-47.
86. Chandra, S., et al., *Alpha-synuclein cooperates with CSPalpha in preventing neurodegeneration.* Cell, 2005. **123**(3): p. 383-96.
87. Bennett, M.C., et al., *Degradation of alpha-synuclein by proteasome.* J Biol Chem, 1999. **274**(48): p. 33855-8.
88. Webb, J.L., et al., *Alpha-Synuclein is degraded by both autophagy and the proteasome.* J Biol Chem, 2003. **278**(27): p. 25009-13.
89. Yamada, S., et al., *Archaeal proteasomes effectively degrade aggregation-prone proteins and reduce cellular toxicities in mammalian cells.* J Biol Chem, 2006. **281**(33): p. 23842-51.
90. Yoshimoto, Y., K. Nakaso, and K. Nakashima, *L-dopa and dopamine enhance the formation of aggregates under proteasome inhibition in PC12 cells.* FEBS Lett, 2005. **579**(5): p. 1197-202.
91. Riedel, M., et al., *17-AAG induces cytoplasmic alpha-synuclein aggregate clearance by induction of autophagy.* PLoS ONE, 2010. **5**(1): p. e8753.
92. Sarkar, S., et al., *Trehalose, a novel mTOR-independent autophagy enhancer, accelerates the clearance of mutant huntingtin and alpha-synuclein.* J Biol Chem, 2007. **282**(8): p. 5641-52.
93. Williams, A., et al., *Novel targets for Huntington's disease in an mTOR-independent autophagy pathway.* Nat Chem Biol, 2008. **4**(5): p. 295-305.
94. Yu, W.H., et al., *Metabolic activity determines efficacy of macroautophagic clearance of pathological oligomeric alpha-synuclein.* Am J Pathol, 2009. **175**(2): p. 736-47.
95. Schell, H., et al., *Nuclear and neuritic distribution of serine-129 phosphorylated alpha-synuclein in transgenic mice.* Neuroscience, 2009. **160**(4): p. 796-804.
96. Machiya, Y., et al., *Phosphorylated alpha-synuclein at Ser-129 is targeted to the proteasome pathway in a ubiquitin-independent manner.* J Biol Chem, 2010. **285**(52): p. 40732-44.
97. Ebrahimi-Fakhari, D., et al., *Distinct roles in vivo for the ubiquitin-proteasome system and the autophagy-lysosomal pathway in the degradation of alpha-synuclein.* J Neurosci, 2011. **31**(41): p. 14508-20.
98. Winslow, A.R., et al., *alpha-Synuclein impairs macroautophagy: implications for Parkinson's disease.* J Cell Biol, 2010. **190**(6): p. 1023-37.
99. Bonifati, V., et al., *Mutations in the DJ-1 gene associated with autosomal recessive early-onset parkinsonism.* Science, 2003. **299**(5604): p. 256-9.

100. Abou-Sleiman, P.M., et al., *The role of pathogenic DJ-1 mutations in Parkinson's disease.* Ann Neurol, 2003. **54**(3): p. 283-6.
101. Hering, R., et al., *Novel homozygous p.E64D mutation in DJ1 in early onset Parkinson disease (PARK7).* Hum Mutat, 2004. **24**(4): p. 321-9.
102. Annesi, G., et al., *DJ-1 mutations and parkinsonism-dementia-amyotrophic lateral sclerosis complex.* Ann Neurol, 2005. **58**(5): p. 803-7.
103. Clark, L.N., et al., *Analysis of an early-onset Parkinson's disease cohort for DJ-1 mutations.* Mov Disord, 2004. **19**(7): p. 796-800.
104. Tao, X. and L. Tong, *Crystal structure of human DJ-1, a protein associated with early onset Parkinson's disease.* J Biol Chem, 2003. **278**(33): p. 31372-9.
105. Honbou, K., et al., *The crystal structure of DJ-1, a protein related to male fertility and Parkinson's disease.* J Biol Chem, 2003. **278**(33): p. 31380-4.
106. Wilson, M.A., et al., *The 1.1-A resolution crystal structure of DJ-1, the protein mutated in autosomal recessive early onset Parkinson's disease.* Proc Natl Acad Sci U S A, 2003. **100**(16): p. 9256-61.
107. Huai, Q., et al., *Crystal structure of DJ-1/RS and implication on familial Parkinson's disease.* FEBS Lett, 2003. **549**(1-3): p. 171-5.
108. Lee, S.J., et al., *Crystal structures of human DJ-1 and Escherichia coli Hsp31, which share an evolutionarily conserved domain.* J Biol Chem, 2003. **278**(45): p. 44552-9.
109. Lev, N., et al., *Role of DJ-1 in Parkinson's disease.* J Mol Neurosci, 2006. **29**(3): p. 215-25.
110. Bandyopadhyay, S. and M.R. Cookson, *Evolutionary and functional relationships within the DJ1 superfamily.* BMC Evol Biol, 2004. **4**(1): p. 6.
111. Lucas, J.I. and I. Marin, *A new evolutionary paradigm for the Parkinson disease gene DJ-1.* Mol Biol Evol, 2007. **24**(2): p. 551-61.
112. Du, X., et al., *Crystal structure of an intracellular protease from Pyrococcus horikoshii at 2-A resolution.* Proc Natl Acad Sci U S A, 2000. **97**(26): p. 14079-84.
113. Jung, H.J., et al., *Dissection of the dimerization modes in the DJ-1 superfamily.* Mol Cells, 2012. **33**(2): p. 163-71.
114. Nagakubo, D., et al., *DJ-1, a novel oncogene which transforms mouse NIH3T3 cells in cooperation with ras.* Biochem Biophys Res Commun, 1997. **231**(2): p. 509-13.
115. Abeliovich, A. and M. Flint Beal, *Parkinsonism genes: culprits and clues.* J Neurochem, 2006. **99**(4): p. 1062-72.
116. Kubo, S., N. Hattori, and Y. Mizuno, *Recessive Parkinson's disease.* Mov Disord, 2006. **21**(7): p. 885-93.
117. Lev, N., et al., *Oxidative insults induce DJ-1 upregulation and redistribution: implications for neuroprotection.* Neurotoxicology, 2008. **29**(3): p. 397-405.
118. Canet-Aviles, R.M., et al., *The Parkinson's disease protein DJ-1 is neuroprotective due to cysteine-sulfinic acid-driven mitochondrial localization.* Proc Natl Acad Sci U S A, 2004. **101**(24): p. 9103-8.

119. Im, J.Y., et al., *DJ-1 protects against oxidative damage by regulating the thioredoxin/ASK1 complex.* Neurosci Res, 2010. **67**(3): p. 203-8.
120. Kim, Y.C., et al., *Oxidation of DJ-1-dependent cell transformation through direct binding of DJ-1 to PTEN.* Int J Oncol, 2009. **35**(6): p. 1331-41.
121. Waak, J., et al., *Oxidizable residues mediating protein stability and cytoprotective interaction of DJ-1 with apoptosis signal-regulating kinase 1.* J Biol Chem, 2009. **284**(21): p. 14245-57.
122. Mo, J.S., et al., *DJ-1 modulates the p38 mitogen-activated protein kinase pathway through physical interaction with apoptosis signal-regulating kinase 1.* J Cell Biochem, 2010. **110**(1): p. 229-37.
123. Takahashi-Niki, K., et al., *Reduced anti-oxidative stress activities of DJ-1 mutants found in Parkinson's disease patients.* Biochem Biophys Res Commun, 2004. **320**(2): p. 389-97.
124. Martinat, C., et al., *Sensitivity to oxidative stress in DJ-1-deficient dopamine neurons: an ES- derived cell model of primary Parkinsonism.* PLoS Biol, 2004. **2**(11): p. e327.
125. Zhou, W. and C.R. Freed, *DJ-1 up-regulates glutathione synthesis during oxidative stress and inhibits A53T alpha-synuclein toxicity.* J Biol Chem, 2005. **280**(52): p. 43150-8.
126. Liu, F., et al., *Mechanisms of DJ-1 neuroprotection in a cellular model of Parkinson's disease.* J Neurochem, 2008. **105**(6): p. 2435-53.
127. Nishinaga, H., et al., *Expression profiles of genes in DJ-1-knockdown and L 166 P DJ-1 mutant cells.* Neurosci Lett, 2005. **390**(1): p. 54-9.
128. Yamaguchi, S., et al., *Transcriptional activation of low-density lipoprotein receptor gene by DJ-1 and effect of DJ-1 on cholesterol homeostasis.* PLoS ONE, 2012. **7**(5): p. e38144.
129. Takahashi, K., et al., *DJ-1 positively regulates the androgen receptor by impairing the binding of PIASx alpha to the receptor.* J Biol Chem, 2001. **276**(40): p. 37556-63.
130. Niki, T., et al., *DJBP: a novel DJ-1-binding protein, negatively regulates the androgen receptor by recruiting histone deacetylase complex, and DJ-1 antagonizes this inhibition by abrogation of this complex.* Mol Cancer Res, 2003. **1**(4): p. 247-61.
131. Tillman, J.E., et al., *DJ-1 binds androgen receptor directly and mediates its activity in hormonally treated prostate cancer cells.* Cancer Res, 2007. **67**(10): p. 4630-7.
132. Ishii, T., et al., *Transcription factor Nrf2 coordinately regulates a group of oxidative stress-inducible genes in macrophages.* J Biol Chem, 2000. **275**(21): p. 16023-9.
133. Zhang, D.D. and M. Hannink, *Distinct cysteine residues in Keap1 are required for Keap1-dependent ubiquitination of Nrf2 and for stabilization of Nrf2 by chemopreventive agents and oxidative stress.* Mol Cell Biol, 2003. **23**(22): p. 8137-51.

134. Clements, C.M., et al., *DJ-1, a cancer- and Parkinson's disease-associated protein, stabilizes the antioxidant transcriptional master regulator Nrf2.* Proc Natl Acad Sci U S A, 2006. **103**(41): p. 15091-6.
135. Gan, L., D.A. Johnson, and J.A. Johnson, *Keap1-Nrf2 activation in the presence and absence of DJ-1.* Eur J Neurosci, 2010. **31**(6): p. 967-77.
136. Shinbo, Y., et al., *DJ-1 restores p53 transcription activity inhibited by Topors/p53BP3.* Int J Oncol, 2005. **26**(3): p. 641-8.
137. Fan, J., et al., *DJ-1 decreases Bax expression through repressing p53 transcriptional activity.* J Biol Chem, 2008. **283**(7): p. 4022-30.
138. Kato, I., et al., *Oxidized DJ-1 inhibits p53 by sequestering p53 from promoters in a DNA-binding affinity-dependent manner.* Mol Cell Biol, 2013. **33**(2): p. 340-59.
139. McNally, R.S., et al., *DJ-1 enhances cell survival through the binding of Cezanne, a negative regulator of NF-kappaB.* J Biol Chem, 2011. **286**(6): p. 4098-106.
140. Chang, C.P., et al., *TLR2-dependent selective autophagy regulates NF-kappaB lysosomal degradation in hepatoma-derived M2 macrophage differentiation.* Cell Death Differ, 2013. **20**(3): p. 515-23.
141. Shendelman, S., et al., *DJ-1 is a redox-dependent molecular chaperone that inhibits alpha-synuclein aggregate formation.* PLoS Biol, 2004. **2**(11): p. e362.
142. Zhou, W., et al., *The oxidation state of DJ-1 regulates its chaperone activity toward alpha-synuclein.* J Mol Biol, 2006. **356**(4): p. 1036-48.
143. Zondler, L., et al., *DJ-1 interactions with alpha-synuclein attenuate aggregation and cellular toxicity in models of Parkinson's disease.* Cell Death Dis, 2014. **5**: p. e1350.
144. Krebiehl, G., et al., *Reduced basal autophagy and impaired mitochondrial dynamics due to loss of Parkinson's disease-associated protein DJ-1.* PLoS ONE, 2010. **5**(2): p. e9367.
145. Shimura, H., et al., *Familial Parkinson disease gene product, parkin, is a ubiquitin-protein ligase.* Nat Genet, 2000. **25**(3): p. 302-5.
146. Zhang, Y., et al., *Parkin functions as an E2-dependent ubiquitin- protein ligase and promotes the degradation of the synaptic vesicle-associated protein, CDCrel-1.* Proc Natl Acad Sci U S A, 2000. **97**(24): p. 13354-9.
147. Exner, N., et al., *Mitochondrial dysfunction in Parkinson's disease: molecular mechanisms and pathophysiological consequences.* Embo Journal, 2012. **31**(14): p. 3038-62.
148. Narendra, D., et al., *Parkin is recruited selectively to impaired mitochondria and promotes their autophagy.* J Cell Biol, 2008. **183**(5): p. 795-803.
149. Shin, J.H., et al., *PARIS (ZNF746) repression of PGC-1alpha contributes to neurodegeneration in Parkinson's disease.* Cell, 2011. **144**(5): p. 689-702.

150. Plun-Favreau, H., et al., *The mitochondrial protease HtrA2 is regulated by Parkinson's disease-associated kinase PINK1.* Nat Cell Biol, 2007. **9**(11): p. 1243-52.
151. Poole, A.C., et al., *The PINK1/Parkin pathway regulates mitochondrial morphology.* Proc Natl Acad Sci U S A, 2008. **105**(5): p. 1638-43.
152. Geisler, S., et al., *PINK1/Parkin-mediated mitophagy is dependent on VDAC1 and p62/SQSTM1.* Nat Cell Biol, 2010. **12**(2): p. 119-31.
153. Matsuda, N., et al., *PINK1 stabilized by mitochondrial depolarization recruits Parkin to damaged mitochondria and activates latent Parkin for mitophagy.* J Cell Biol, 2010. **189**(2): p. 211-21.
154. Narendra, D.P., et al., *PINK1 is selectively stabilized on impaired mitochondria to activate Parkin.* PLoS Biol, 2010. **8**(1): p. e1000298.
155. Kim, R.H., et al., *Hypersensitivity of DJ-1-deficient mice to 1-methyl-4-phenyl-1,2,3,6-tetrahydropyrindine (MPTP) and oxidative stress.* Proc Natl Acad Sci U S A, 2005. **102**: p. 5215-5220.
156. Liu, F., et al., *Mechanisms of DJ-1 neuroprotection in a cellular model of Parkinson's disease.* J. Neurochem., 2008. **105**: p. 2435-2453.
157. Zhang, L., et al., *Mitochondrial localization of the Parkinson's disease related protein DJ-1: implications for pathogenesis.* Hum Mol Genet, 2005. **14**(14): p. 2063-73.
158. Thomas, K.J., et al., *DJ-1 acts in parallel to the PINK1/parkin pathway to control mitochondrial function and autophagy.* Hum Mol Genet, 2011. **20**(1): p. 40-50.
159. Kamp, F., et al., *Inhibition of mitochondrial fusion by alpha-synuclein is rescued by PINK1, Parkin and DJ-1.* Embo Journal, 2010. **29**(20): p. 3571-89.
160. Joselin, A.P., et al., *ROS-dependent regulation of Parkin and DJ-1 localization during oxidative stress in neurons.* Hum Mol Genet, 2012. **21**(22): p. 4888-903.
161. Dehay, B., et al., *Pathogenic lysosomal depletion in Parkinson's disease.* J Neurosci, 2010. **30**(37): p. 12535-44.
162. Gao, H., et al., *DJ-1 protects dopaminergic neurons against rotenone-induced apoptosis by enhancing ERK-dependent mitophagy.* J Mol Biol, 2012. **423**(2): p. 232-48.
163. Hampshire, D.J., et al., *Kufor-Rakeb syndrome, pallido-pyramidal degeneration with supranuclear upgaze paresis and dementia, maps to 1p36.* J Med Genet, 2001. **38**(10): p. 680-2.
164. Ramirez, A., et al., *Hereditary parkinsonism with dementia is caused by mutations in ATP13A2, encoding a lysosomal type 5 P-type ATPase.* Nat Genet, 2006. **38**(10): p. 1184-91.
165. Kuhlbrandt, W., *Biology, structure and mechanism of P-type ATPases.* Nat Rev Mol Cell Biol, 2004. **5**(4): p. 282-95.
166. Biskup, S., et al., *Genes associated with Parkinson syndrome.* J Neurol, 2008. **255 Suppl 5**: p. 8-17.

167. Belin, A.C. and M. Westerlund, *Parkinson's disease: a genetic perspective.* FEBS J, 2008. **275**(7): p. 1377-83.
168. Di Fonzo, A., et al., *ATP13A2 missense mutations in juvenile parkinsonism and young onset Parkinson disease.* Neurology, 2007. **68**(19): p. 1557-62.
169. Weingarten, L.S., et al., *Developmental expression of P5 ATPase mRNA in the mouse.* Cell Mol Biol Lett, 2012. **17**(1): p. 153-70.
170. Xu, Q., et al., *Hypoxia regulation of ATP13A2 (PARK9) gene transcription.* J Neurochem, 2012. **122**(2): p. 251-9.
171. Tan, J., et al., *Regulation of intracellular manganese homeostasis by Kufor-Rakeb syndrome-associated ATP13A2 protein.* J Biol Chem, 2011. **286**(34): p. 29654-62.
172. Tsunemi, T. and D. Krainc, *Zn(2)(+) dyshomeostasis caused by loss of ATP13A2/PARK9 leads to lysosomal dysfunction and alpha-synuclein accumulation.* Hum Mol Genet, 2014. **23**(11): p. 2791-801.
173. Ugolino, J., et al., *Mutant Atp13a2 proteins involved in parkinsonism are degraded by ER-associated degradation and sensitize cells to ER-stress induced cell death.* Hum Mol Genet, 2011. **20**(18): p. 3565-77.
174. Kong, S.M., et al., *Parkinson's disease-linked human PARK9/ATP13A2 maintains zinc homeostasis and promotes alpha-Synuclein externalization via exosomes.* Hum Mol Genet, 2014. **23**(11): p. 2816-33.
175. Dehay, B., et al., *Loss of P-type ATPase ATP13A2/PARK9 function induces general lysosomal deficiency and leads to Parkinson disease neurodegeneration.* Proc Natl Acad Sci U S A, 2012. **109**(24): p. 9611-6.
176. Gusdon, A.M., et al., *ATP13A2 regulates mitochondrial bioenergetics through macroautophagy.* Neurobiol Dis, 2012. **45**(3): p. 962-72.
177. Covy, J.P., E.A. Waxman, and B.I. Giasson, *Characterization of cellular protective effects of ATP13A2/PARK9 expression and alterations resulting from pathogenic mutants.* J Neurosci Res, 2012. **90**(12): p. 2306-16.
178. Grunewald, A., et al., *ATP13A2 mutations impair mitochondrial function in fibroblasts from patients with Kufor-Rakeb syndrome.* Neurobiol Aging, 2012. **33**(8): p. 1843 e1-7.
179. Gitler, A.D., et al., *Alpha-synuclein is part of a diverse and highly conserved interaction network that includes PARK9 and manganese toxicity.* Nat Genet, 2009. **41**(3): p. 308-15.
180. Chesi, A., et al., *The role of the Parkinson's disease gene PARK9 in essential cellular pathways and the manganese homeostasis network in yeast.* PLoS ONE, 2012. **7**(3): p. e34178.
181. Usenovic, M. and D. Krainc, *Lysosomal dysfunction in neurodegeneration: the role of ATP13A2/PARK9.* Autophagy, 2012. **8**(6): p. 987-8.
182. Tsunemi, T. and D. Krainc, *Zn2+ dyshomeostasis caused by loss of ATP13A2/PARK9 leads to lysosomal dysfunction and alpha-synuclein accumulation.* Hum Mol Genet, 2014. **23**(11): p. 2791-801.

183. Park, J.S., et al., *Parkinson's disease-associated human ATP13A2 (PARK9) deficiency causes zinc dyshomeostasis and mitochondrial dysfunction.* Hum Mol Genet, 2014. **23**(11): p. 2802-15.
184. Choi, J., et al., *Oxidative damage of DJ-1 is linked to sporadic Parkinson and Alzheimer diseases.* J Biol Chem, 2006. **281**(16): p. 10816-24.
185. Anderson, P.C. and V. Daggett, *Molecular basis for the structural instability of human DJ-1 induced by the L166P mutation associated with Parkinson's disease.* Biochemistry, 2008. **47**(36): p. 9380-93.
186. Narayanan, A., et al., *Structure-function studies of DNA binding domain of response regulator KdpE reveals equal affinity interactions at DNA half-sites.* PLoS ONE, 2012. **7**(1): p. e30102.
187. Schuck, P., *Size-distribution analysis of macromolecules by sedimentation velocity ultracentrifugation and lamm equation modeling.* Biophys J, 2000. **78**(3): p. 1606-19.
188. Polgar, L., *The catalytic triad of serine peptidases.* Cell Mol Life Sci, 2005. **62**(19-20): p. 2161-72.
189. Wang, J., et al., *Crystal structures of enterovirus 71 3C protease complexed with rupintrivir reveal the roles of catalytically important residues.* J Virol, 2011. **85**(19): p. 10021-30.
190. Andres-Mateos, E., et al., *DJ-1 gene deletion reveals that DJ-1 is an atypical peroxiredoxin-like peroxidase.* Proc Natl Acad Sci U S A, 2007. **104**(37): p. 14807-12.
191. Hartl, F.U., *Molecular chaperones in cellular protein folding.* Nature, 1996. **381**(6583): p. 571-9.
192. Gething, M.J. and J. Sambrook, *Protein folding in the cell.* Nature, 1992. **355**(6355): p. 33-45.
193. Chae, H.Z., S.J. Chung, and S.G. Rhee, *Thioredoxin-dependent peroxide reductase from yeast.* J Biol Chem, 1994. **269**(44): p. 27670-8.
194. Schroder, E., et al., *Crystal structure of decameric 2-Cys peroxiredoxin from human erythrocytes at 1.7 A resolution.* Structure, 2000. **8**(6): p. 605-15.
195. Jang, H.H., et al., *Two enzymes in one; two yeast peroxiredoxins display oxidative stress-dependent switching from a peroxidase to a molecular chaperone function.* Cell, 2004. **117**(5): p. 625-35.
196. Jacob, C., et al., *Sulfur and selenium: the role of oxidation state in protein structure and function.* Angew Chem Int Ed Engl, 2003. **42**(39): p. 4742-58.
197. Kiley, P.J. and G. Storz, *Exploiting thiol modifications.* PLoS Biol, 2004. **2**(11): p. e400.
198. Poole, L.B., *Formation and functions of protein sulfenic acids.* Curr Protoc Toxicol, 2004. **Chapter 17**: p. Unit17 1.
199. Jacob, C., A.L. Holme, and F.H. Fry, *The sulfinic acid switch in proteins.* Org Biomol Chem, 2004. **2**(14): p. 1953-6.
200. Jonsson, T.J., L.C. Johnson, and W.T. Lowther, *Protein engineering of the quaternary sulfiredoxin.peroxiredoxin enzyme.substrate complex reveals*

the molecular basis for cysteine sulfinic acid phosphorylation. J Biol Chem, 2009. **284**(48): p. 33305-10.
201. Banik, U. and S. Roy, *A continuous fluorimetric assay for ATPase activity.* Biochem J, 1990. **266**(2): p. 611-4.
202. Ackerman, S.H. and A. Tzagoloff, *Function, structure, and biogenesis of mitochondrial ATP synthase.* Prog Nucleic Acid Res Mol Biol, 2005. **80**: p. 95-133.
203. Burwick, N.R., et al., *An Inhibitor of the F1 subunit of ATP synthase (IF1) modulates the activity of angiostatin on the endothelial cell surface.* J Biol Chem, 2005. **280**(3): p. 1740-5.
204. Hausrath, A.C., et al., *Structural features of the gamma subunit of the Escherichia coli F(1) ATPase revealed by a 4.4-A resolution map obtained by x-ray crystallography.* Proc Natl Acad Sci U S A, 1999. **96**(24): p. 13697-702.
205. Jin, J., et al., *Identification of novel proteins associated with both alpha-synuclein and DJ-1.* Mol Cell Proteomics, 2007. **6**(5): p. 845-59.
206. Hyndman, D.J., et al., *Nucleotide-binding sites on Escherichia coli F1-ATPase. Specificity of noncatalytic sites and inhibition at catalytic sites by MgADP.* J Biol Chem, 1994. **269**(46): p. 28871-7.
207. Fontanesi, F., *Mechanisms of mitochondrial translational regulation.* IUBMB Life, 2013. **65**(5): p. 397-408.
208. Kinumi, T., et al., *Cysteine-106 of DJ-1 is the most sensitive cysteine residue to hydrogen peroxide-mediated oxidation in vivo in human umbilical vein endothelial cells.* Biochem Biophys Res Commun, 2004. **317**(3): p. 722-8.
209. Hao, L.Y., B.I. Giasson, and N.M. Bonini, *DJ-1 is critical for mitochondrial function and rescues PINK1 loss of function.* Proc Natl Acad Sci U S A, 2010. **107**(21): p. 9747-52.
210. Hsu, L.J., et al., *a-synuclein promotes mitochondrial deficit and oxidative stress.* Am. J. Pathol., 2000. **157**(2): p. 401-410.
211. Kubota, C., et al., *Constitutive reactive oxygen species generation from autophagosome/lysosome in neuronal oxidative toxicity.* J Biol Chem, 2010. **285**(1): p. 667-74.
212. Cubells, J.F., et al., *Methamphetamine neurotoxicity involves vacuolation of endocytic organelles and dopamine-dependent intracellular oxidative stress.* J Neurosci, 1994. **14**(4): p. 2260-71.
213. Castino, R., et al., *Suppression of autophagy precipitates neuronal cell death following low doses of methamphetamine.* J Neurochem, 2008. **106**(3): p. 1426-39.
214. Shendelman, S., et al., *DJ-1 Is a redox-dependent molecular chaperone that inhibits a-synuclein aggregate formation.* PLoS Biol, 2004. **2**(11): p. e362.
215. Yokota, T., et al., *Down regulation of DJ-1 enhances cell death by oxidative stress, ER stress, and proteasome inhibition.* Biochem Biophys Res Commun, 2003. **312**(4): p. 1342-8.

216. Wang, I.I. and I.I. Huang, *Adenovirus technology for gene manipulation and functional studies.* Drug Discov Today, 2000. **5**(1): p. 10-16.
217. Lores-Arnaiz, S., et al., *Brain mitochondrial nitric oxide synthase: in vitro and in vivo inhibition by chlorpromazine.* Arch Biochem Biophys, 2004. **430**(2): p. 170-7.
218. Yuan, K., et al., *Autophagy plays an essential role in the clearance of Pseudomonas aeruginosa by alveolar macrophages.* J Cell Sci, 2012. **125**(Pt 2): p. 507-15.
219. Lau, J.W., S. Senok, and A. Stadlin, *Methamphetamine-induced oxidative stress in cultured mouse astrocytes.* Ann N Y Acad Sci, 2000. **914**: p. 146-56.
220. Larsen, K.E., et al., *Methamphetamine-induced degeneration of dopaminergic neurons involves autophagy and upregulation of dopamine synthesis.* J Neurosci, 2002. **22**(20): p. 8951-60.
221. Boya, P. and G. Kroemer, *Lysosomal membrane permeabilization in cell death.* Oncogene, 2008. **27**(50): p. 6434-51.
222. Pandey, U.B., et al., *HDAC6 rescues neurodegeneration and provides an essential link between autophagy and the UPS.* Nature, 2007. **447**(7146): p. 859-63.
223. Iwata, A., et al., *HDAC6 and microtubules are required for autophagic degradation of aggregated huntingtin.* J Biol Chem, 2005. **280**(48): p. 40282-92.
224. Funakoshi-Hirose, I., et al., *Distinct effects of methamphetamine on autophagy-lysosome and ubiquitin-proteasome systems in HL-1 cultured mouse atrial cardiomyocytes.* Toxicology, 2013. **312**: p. 74-82.
225. Nara, A., et al., *Hyperstimulation of macropinocytosis leads to lysosomal dysfunction during exposure to methamphetamine in SH-SY5Y cells.* Brain Res, 2012. **1466**: p. 1-14.
226. Segura-Aguilar, J., et al., *Protective and toxic roles of dopamine in Parkinson's disease.* J Neurochem, 2014. **129**(6): p. 898-915.
227. Khan, F.H., et al., *Inhibition of rat brain mitochondrial electron transport chain activity by dopamine oxidation products during extended in vitro incubation: implications for Parkinson's disease.* Biochim Biophys Acta, 2005. **1741**(1-2): p. 65-74.
228. Garcia, J., et al., *Regulation of mitochondrial glutathione redox status and protein glutathionylation by respiratory substrates.* J Biol Chem, 2010. **285**(51): p. 39646-54.
229. Kim, K., et al., *Glutathione s-transferase omega 1 activity is sufficient to suppress neurodegeneration in a Drosophila model of Parkinson disease.* J Biol Chem, 2012. **287**(9): p. 6628-41.
230. Appel, L.J., et al., *Comparative effectiveness of weight-loss interventions in clinical practice.* N Engl J Med, 2011. **365**(21): p. 1959-68.
231. Funk, K.L., et al., *Development and Implementation of a Tailored Self-assessment Tool in an Internet-based Weight Loss Maintenance Program.* Clin Pract Epidemiol Ment Health, 2011. **7**: p. 67-73.

232. Mizushima, N., T. Yoshimori, and B. Levine, *Methods in mammalian autophagy research.* Cell, 2010. **140**(3): p. 313-26.
233. Wang, S.B., et al., *Redox regulation of mitochondrial ATP synthase.* Trends Cardiovasc Med, 2013. **23**(1): p. 14-8.
234. Glasgow, R.E., et al., *Applying the PRECIS criteria to describe three effectiveness trials of weight loss in obese patients with comorbid conditions.* Health Serv Res, 2012. **47**(3 Pt 1): p. 1051-67.
235. Martinez-Vicente, M., et al., *Dopamine-modified alpha-synuclein blocks chaperone-mediated autophagy.* J Clin Invest, 2008. **118**(2): p. 777-88.
236. Aniento, F., et al., *Uptake and degradation of glyceraldehyde-3-phosphate dehydrogenase by rat liver lysosomes.* J Biol Chem, 1993. **268**(14): p. 10463-70.
237. Cuervo, A.M., et al., *Impaired degradation of mutant alpha-synuclein by chaperone-mediated autophagy.* Science, 2004. **305**(5688): p. 1292-5.

APPENDIX

APPENDIX: LIST OF PRIMERS

Primers used to generate DJ-1Δ15 variants in Chapter 2 and Chapter 3

Human DJ-1 (Forward primer)

5’CGAGCTCTCTCTAGAAATAATTTTGTTTAACTTTAAGAAGGAGATATACATA
TG GCTTCCAAAAGAGCTCTGGT 3’

Human DJ-1Δ15 (Reverse primer)
5’ CGAGCTCTCCTCGAGCTAGCCATTCAGGGCTTCAACAATTG 3’

Primers used for qRT PCR in Chapter 4

Rat Park9 (Forward primer)

5’ GCGTACACAGGGCATCTT 3’

Rat Park9 (Reverse primer)

5’ GACCAGTGGCAGCAACAT 3’

Rat Park7 (Forward primer)

5' GGAGAACAGGAAGGGCCTCATA 3'

Rat Park7 (Reverse primer)

5' GGGTGCGATGTAACCTTGCAT 3'

Rat GAPDH (Forward primer)

5' GAACATCATCCCTGCATCCA 3'

Rat GAPDH (Reverse primer)

5' CCAGTGAGCTTCCCGTTCA 3'

VITA

VITA

Josephat Mogaka Asiago was born in Kisii, Kenya, to Zachariah Asiago Ogoti and Josephine Nyanchama Asiago. He is the fifth of the six children, two sisters and three brothers.

Josephat attended Ngonyek primary school in Kitale, Kenya from standard one to standard eight. He then joined Chebara high school in Marakwet, Kenya where he graduated from high school in 1998. He later joined Tracom College in Nakuru, Kenya where he completed level one of Kenya Certified Public Accounts (CPA). He later got admitted to Moi University in Eldoret to pursue a degree in Economics. He did not graduate because he had to relocate to United States of America (USA).

While in USA, he lived in the state of Delaware from 2001 to 2006. While in Delaware, he attended Cecil College, Northeast, Maryland, to pursue an associate degree in nursing and biology. He later dropped out of the nursing program and graduated with an associate degree in biology in May 2006. He later moved to the state of Tennessee and joined East Tennessee State University (ETSU) where he graduated with a bachelor degree in biology in May 2008. At ETSU, he got an opportunity to participate in undergraduate research in

the lab of Dr. Cecilia McIntosh. In summer, 2008, he applied and got accepted in a Summer Research Program at Purdue (SROP), Purdue University in West Lafayette, Indiana. Under the SROP, he did research in the lab of Dr. Jean-Christophe Rochet in department of Medicinal Chemistry and Molecular Pharmacology (MCMP). These experiences greatly increased his interest in research, he applied to graduate schools.

In August 2008, Josephat started his doctoral studies at Purdue University, in Purdue Life Sciences program (PULSe). After four lab rotations (eight weeks each), he joined the lab of Dr. Jean-Christophe Rochet in MCMP. Under Dr. Rochet's mentorship, Josephat studies focused on elucidating mechanistic details accounting for the functional overlap between two familial Parkinson's disease (PD) proteins, DJ-1 and ATP13A2. The goal of my research is to provide insight into cellular mechanisms underlying the neuroprotective functions of ATP13A2 and DJ-1 and suggest new strategies to slow PD pathogenesis. While at Purdue, Josephat was a third author on two publications and currently working on three first-author manuscripts.

PUBLICATIONS

PUBLICATIONS

1. Krasnoslobodtsev AV, Volkov IL, **Asiago JM**, Hindupur J, Rochet J-C, Lyubchenko YL. (2013) Alpha-synuclein misfolding assessed with single molecule AFM force spectroscopy: Effect of pathogenic mutations. *Biochemistry,* 52 (42), pp 7377–7386

2. Krasnoslobodtsev AV, Peng J, **Asiago JM**, Hindupur J, Rochet J-C, Lyubchenko YL. (2012) Effect of Spermidine on Misfolding and Interactions of Alpha-Synuclein. *PLoS ONE 7(5):* e38099. doi:10.1371/journal.pone.0038099